INFORMATION TO USERS

This manuscript has been reproduced from the microfilm master. UMI films the text directly from the original or copy submitted. Thus, some thesis and dissertation copies are in typewriter face, while others may be from any type of computer printer.

The quality of this reproduction is dependent upon the quality of the copy submitted. Broken or indistinct print, colored or poor quality illustrations and photographs, print bleedthrough, substandard margins, and improper alignment can adversely affect reproduction.

In the unlikely event that the author did not send UMI a complete manuscript and there are missing pages, these will be noted. Also, if unauthorized copyright material had to be removed, a note will indicate the deletion.

Oversize materials (e.g., maps, drawings, charts) are reproduced by sectioning the original, beginning at the upper left-hand corner and continuing from left to right in equal sections with small overlaps.

Photographs included in the original manuscript have been reproduced xerographically in this copy. Higher quality 6" x 9" black and white photographic prints are available for any photographs or illustrations appearing in this copy for an additional charge. Contact UMI directly to order.

Bell & Howell Information and Learning
300 North Zeeb Road, Ann Arbor, MI 48106-1346 USA
800-521-0600

Interfacial Properties and Aggregation of Surfactants

by

Joann H. Mathias

A dissertation submitted to the Graduate Faculty in Chemistry
in partial fulfillment of the requirements for the degree of

Doctor of Philosophy

The City University of New York

2000

Approval Page

This manuscript has been read and accepted for the Graduate Faculty in Chemistry in satisfaction of the dissertation requirement for the degree of Doctor of Philosophy.

5/23/00
Date

Prof. Milton J. Rosen

6/9/2000
Date

Prof. G. Koeppl, Executive Officer
The Graduate School and University Center

Prof. Lesley Davenport

Prof. Gary Mennitt

Prof. Ruth Stark

THE CITY UNIVERSITY OF NEW YORK

Abstract

Interaction and Aggregation of Surfactants

by

Joann H. Mathias

Adviser: Professor Milton J. Rosen

Bis(quaternary ammonium halide) surfactants (gemini surfactants) having, variously, diethylether, p-dimethylene phenylene, monohydroxypropyl and di-hydroxybutyl spacer groups have been investigated by surface tension, interfacial tension and steady-state and dynamic fluorescence techniques. The critical micelle concentration (CMC) and area per molecule (A_{min}) are shown to deviate from the expected patterns of behavior as the number of carbon atoms in the alkyl chain (n) increases beyond a certain maximum. This aberrant behavior is observed at the hydrocarbon/water as well as the aqueous/air interface. The unexpected values of the physico-chemical parameters at long alkyl chain length have been interpreted on the basis of a concentration region in which sub-micellar or multi-layer structures are forming. Fluorescence measurements provide confirmation of CMC values by an alternative technique. Comparison of the fluorescence emission maxima profiles of the gemini surfactants with those of their mono-quaternary analogues demonstrates that there is a continuously changing shape with change in n for the geminis; whereas, the profiles for non-geminis are invariant. Long-chain geminis exhibit a gradually sloping sigmoidal profile indicating a variety of environments experienced by the probe between the totally aqueous environment at low surfactant concentration and the hydrophobic

(entirely micellar) environment at high surfactant concentration. The large variation in the polarity of the probe environment between these two extremes may be attributed to the formation of sub-micellar structures.

Dynamic fluorescence measurements using the time-resolved single photon counting technique provided aggregation numbers for conventional and cationic gemini surfactants. Aggregation numbers of 2 (gemini molecules per micelle) were found in the surfactant concentration region between the expected and observed cmc values for long chain geminis, regardless of the chemical nature of the spacer, indicating dimer formation. Evidence of two observable cmc values was obtained by surface tension and steady state fluorescence measurements. Dimer formation below the first cmc is followed by normal aggregation growth until reaching the second cmc at which concentration dimers are again observed. The aggregation process for long chain geminis appears to be a dynamic process involving: dimer formation → growth → reformation.

In view of the considerable interest in these cost-effective and environmentally sound gemini surfactants, full understanding of their physico-chemical properties and aggregation behavior is highly desirable.

To my mother and to the memory of my father

Acknowledgments

I wish to thank the members of my committee, Professor Gary Mennitt, Professor Ruth Stark and Dr. E.D. Goddard for their professional guidance during the course of my doctoral studies. Professor Irwin Cohen deserves thanks for his excellent computer help as well as his continuous support.

Professor Lesley Davenport played a major role in the completion of these studies through contribution of her time, expertise and use of her fluorescence laboratory.

Professor Milton J. Rosen served as my mentor and taught me innumerable lessons, both scientific and philosophic. I thank him for many hours of enlightening conversation, directing my path towards becoming a research scientist.

Table of Contents

Tables

Figures

Schemes

Chapter I.

Introduction

I.1 Aqueous Surfactant Systems

Surfactants are a group of chemical substances one of whose properties is the reduction of the surface tension of H_2O or other solvent. The surface tension, defined as the tension of the surface film that makes it contract to minimum area, is measured in terms of force per unit length (1). The physical basis of this phenomenon was demonstrated by Traube (1891) who showed that fatty acids, alcohols, and amides migrate to the surface of an aqueous solution with a resulting decrease in surface tension (2). Although the amphipathic nature of these molecules, i.e., a hydrophobic hydrocarbon chain and hydrophilic head group, was soon recognized as the reason for the migration to the surface (3), the thermodynamic interpretation was a source of debate for nearly a century. Tanford (1979) has shown that, rather than the attraction between the hydrocarbon chains of the molecules, it is the free energy of attraction of water for itself which leads to removal of the surfactant molecules from the bulk of the solution and migration to the surface (4).

As the bulk surfactant concentration is increased, surface tension reduction reaches a point at which it levels off and the surface tension of the solution becomes constant. This behavior was first explained by McBain (1914) who suggested that it was the result of surfactant aggregation above a critical micelle concentration (cmc) (5). McBain's conclusions were based on

anomalous osmotic pressure data of soap solutions. It is now recognized that many physico-chemical properties, including conductivity, solubilisation, magnetic resonance and self-diffusion, change abruptly at the cmc, and these changes are readily interpreted on the basis of aggregate formation (6).

The morphology of these aggregates has been the subject of vigorous debates from the time of their discovery, until the present day. Menger (7) notes that over 2800 publications on the subject of micelles were published between 1970 and 1978 alone. Topics include: shape of micelles; number of surfactant molecules per micelle (aggregation number) and the statistical distribution of these aggregation numbers; effect of additives such as salt or alcohols; and effect of counter-ions and degree of ionization in ionic micelles.

This dissertation is concerned with the shape and aggregation number of surfactants, specifically gemini surfactants, containing two hydrophobic and two hydrophilic groups. Their aggregation behavior, as the chemical structure of the surfactant is modified, is observed using surface tension, interfacial tension, steady-state and dynamic fluorescence methods. Fundamental interfacial properties of geminis are also studied using these methods. An understanding of both structure/aggregation relationship and basic interfacial properties is vital to the intelligent use of these surfactants in industrial processes, as well as to the development of improved, more effective surfactants.

I.2 Morphology of Surfactant Micelles

The earliest theories concerning the shape of micelles formed from conventional surfactants, i.e., those with one hydrophobic and one hydrophilic component, were roughly divided into two groups. McBain (8,9) proposed a lamellar structure, while Hartley (10,11) favored a spherical micelle. In the 1950's, new models describing prolate and oblate ellipsoids (12-14) and cylinders (15) began to appear. In general, these models are based on geometric considerations, which were later reviewed in the light of experimental evidence, often of a spectroscopic nature, e.g. laser Raman spectroscopy (16) and neutron scattering (17).

I.2.1 Conventional Surfactant Micelles

Tartar (12) and Tanford (14) have presented expressions for the length (l_c) of a hydrocarbon chain in a surfactant monomer and volume (V_H) occupied by the hydrophobic groups in the micellar core. Israelachvili (18) proposed a packing parameter (V_H/a_0l_c), where a_0 is the cross-sectional area occupied by the hydrophilic group at the micelle-solution interface. This parameter provides a convenient, albeit rough, guide to the shape of a normal surfactant aggregate. Its increase parallels the change in shape from spherical→ cylindrical→lamellar. This transition is shown in Scheme I.1.

Scheme I.1. Morphology of surfactant micelles in aqueous phase

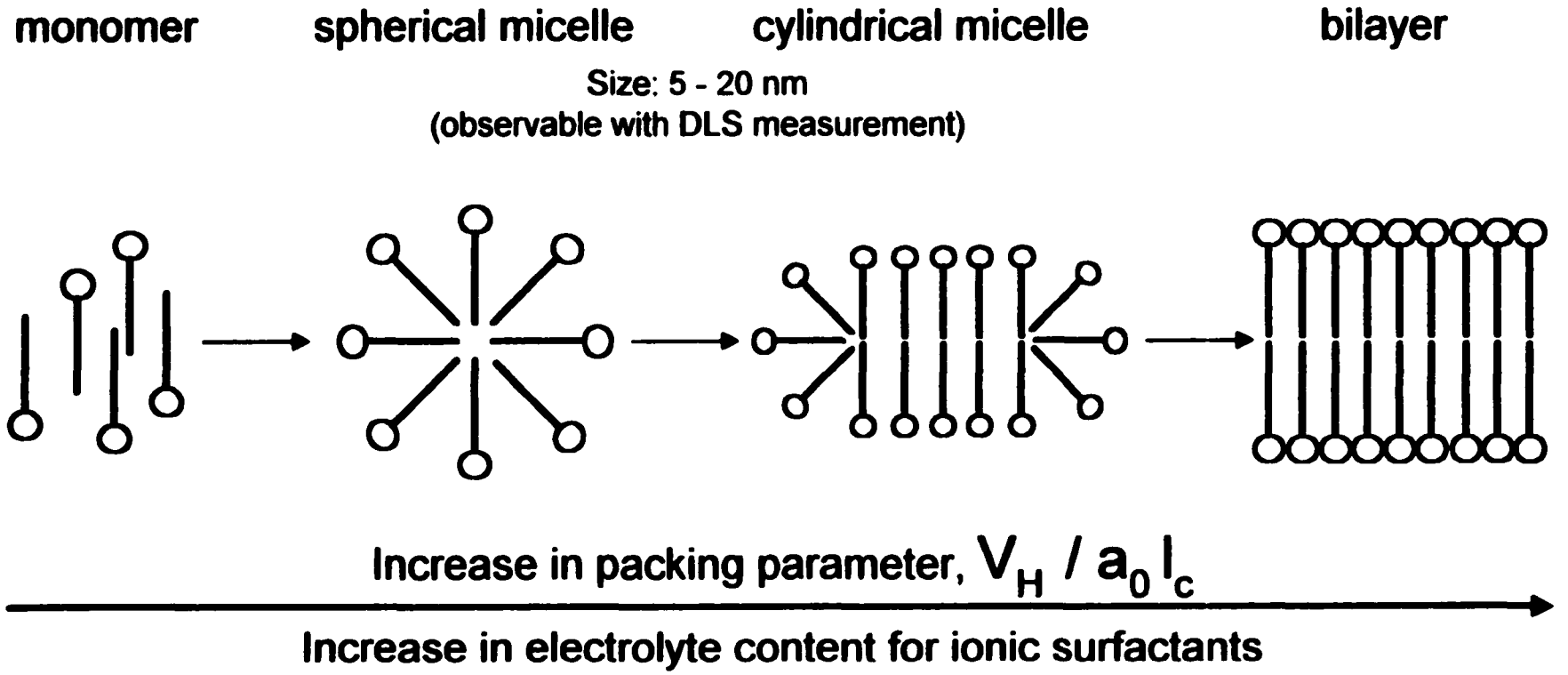

I.2.2. Gemini Surfactant Micelles

Surfactants having two hydrophobic and two hydrophilic groups in the molecule (gemini surfactants) are known to exhibit enhanced surface-active properties (19-22). The greater efficiency and effectiveness of geminis over comparable conventional surfactants make them more cost-effective as well as environmentally desirable.

Bis(quaternary ammonium halides) geminis were first synthesized and studied for their superior performance, relative to monoquaternary ammonium halides, as catalysts in organic reactions (23). Later they came to be studied for their bactericidal capabilities (24) and for their unusual physicochemical properties. Although this class of cationic surfactants has been studied for over two decades (25) the details of their structure-performance relationship remain elusive. Aberrant behavior, particularly in those members of a homologous series of compounds containing long alkyl chains as the hydrophobic moiety, has been cited by several investigators (26-28).

Pursuant to continued research in this area, we have recently synthesized a series of α,ω-bis(N,N-dimethylalkylammonium bromide)diethylether surfactants codified as $(C_nN)_2O$ where n = 10 to 20. Three series of cationic geminis previously synthesized (27,28) are included in this dissertation. These compounds contain one or two hydroxyl groups in the chemical spacer which joins the hydrophilic head groups and are codified as $(C_nN)_2OH$ and$(C_nN)_2(OH)_2$ respectively, and a series containing a rigid phenyl spacer codified as $(C_nN)_2Ar$. The structures of these compounds are shown in Scheme I.2.

Scheme I.2 Chemical structures of cationic gemini surfactants.

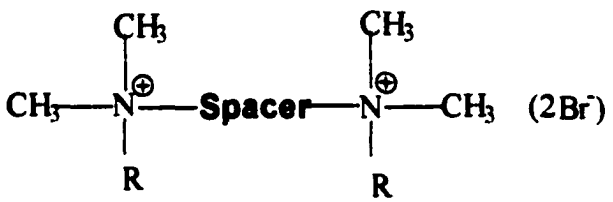

Spacer	Abbreviation
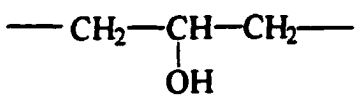	$(CnN)_2OH$
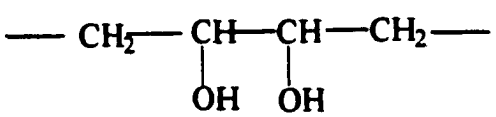	$(CnN)_2(OH)_2$
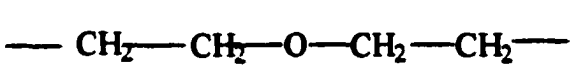	$(CnN)_2O$
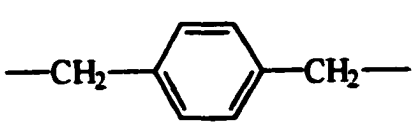	$(CnN)_2Ar$

Understanding of the morphology of gemini micelles is in a relatively early stage of development. Our fluorescence studies and those of others (29) , as well as cyro-transmission electron microscopy (29-31) indicate that, at surfactant concentrations just above the cmc, for surfactant monomers with short alkyl chain length, micelles are spherical and monodisperse. However, an increase in surfactant concentration often results in unusual growth patterns, which depend on length of the spacer and the alkyl chain length. Zana et al.(29) have documented that for concentrated solutions of the $(C_{12}N)_2(CH_2)_s$ series, an increase in spacer carbon number (s) leads to the sequence:

thread-like → spheroidal micelles → vesicles.

Evidence of lamellar phase fragments was found to be added to the sequence for solutions of $(C_{16}N)_2(CH_2)_s$ for short spacer length.

As noted earlier, the value of the packing parameter (V_H/a_0l_c) controls the shape of the aggregate. The size of the aggregate, however, is a thermodynamic balance between energy and entropy factors. For amphiphilic structures, the repulsive energy between head-groups is at a minimum when the head-group area attains an optimal value a_0 (32). Entropy factors dictate the smallest possible aggregates; yet, very small structures are energetically unfavorable as they force the surface area to increase above its optimal value to satisfy the packing constraints. The observation of dimers in a surfactant system would therefore indicate an overwhelming entropy consideration.

Scheme I.3. Morphology of gemini surfactant micelles in aqueous phase

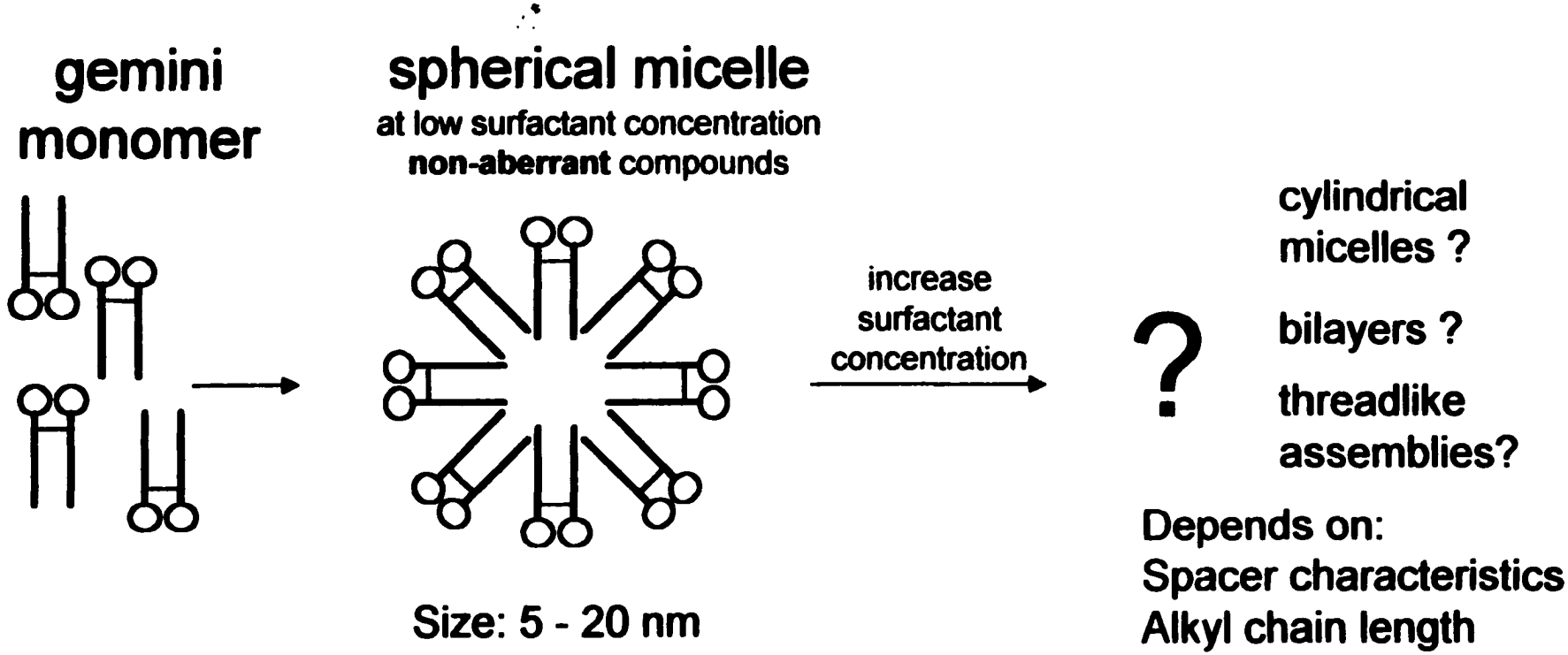

Scheme I.4. Morphology of aberrant gemini surfactant micelles in aqueous phase

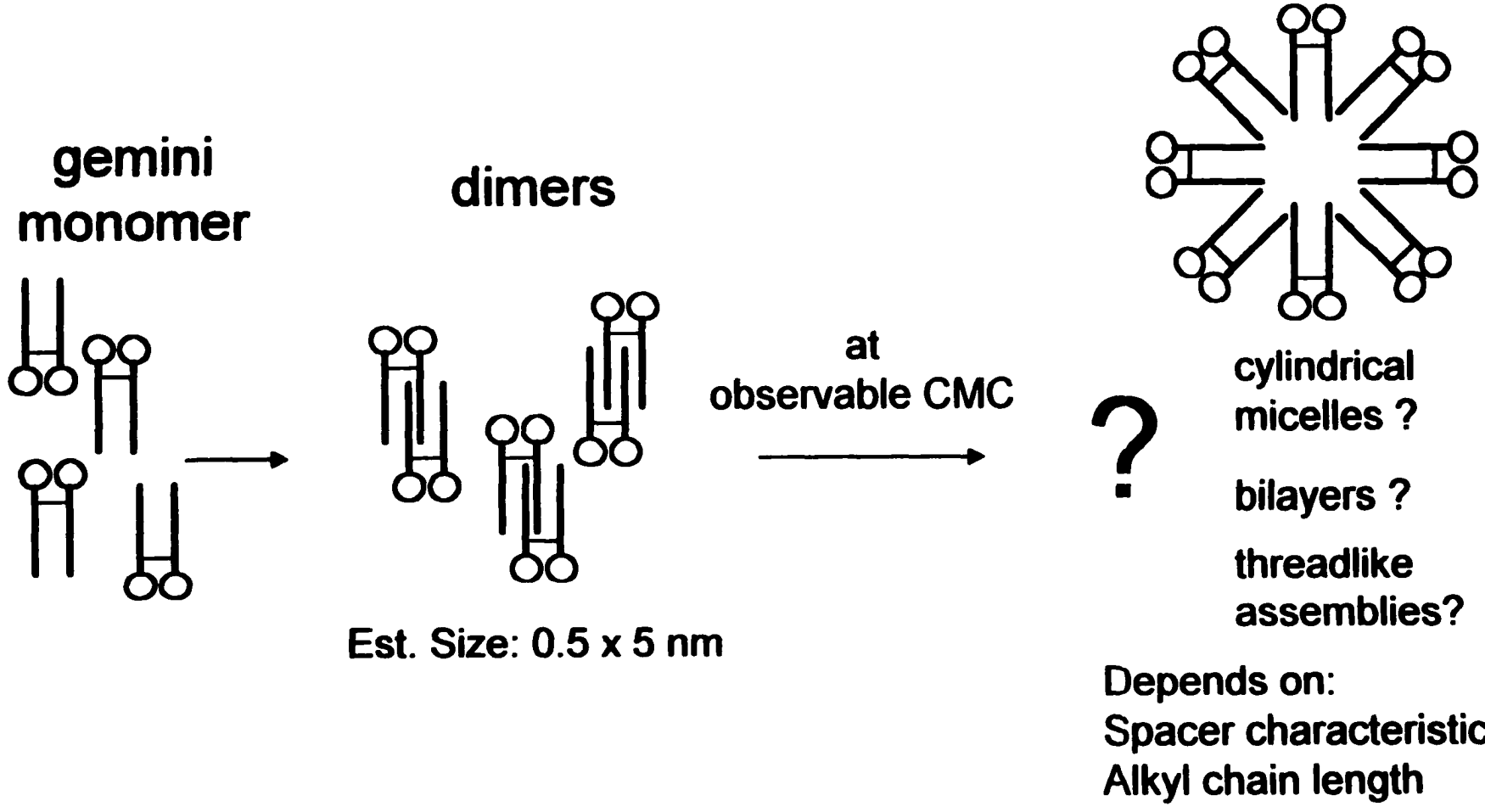

I.3 Interfacial Properties

Reduction of interfacial tension of the solvent is only one of many surfactant properties. Increase in the solubilizing capacity of solutions upon addition of surfactant, at concentrations above the cmc, has applications in drug delivery systems, catalysis of organic reactions and detergency. Emulsification, the dispersion of one liquid phase in another, is also accomplished by addition of a surfactant. Emulsifying agents are used extensively in the food industry and in paints, polishing agents and insecticides. Inhibitory effects in biological systems, e.g. bacterial systems, are important for cationic surfactants. Other properties include modification of wetting, foaming and dispersing ability of solutions. Synergism in mixtures of surfactants , described in quantitative terms, is based on individual properties (33-36).

All of these properties can be explained by the adsorption of the surfactant at an interface and by its tendency to aggregate above a critical concentration.

I.3.1. Interfacial Properties at the aqueous solution/air interface

Dissolution of a surfactant, at low concentrations, in an aqueous solution disrupts the structure of the water and raises the free energy of the system. Migration of the surfactant to the interface partially restores this structure and lowers the free energy of the system. The maximum surface excess concentration of surfactant at the interface is calculated using the Gibbs equation (37) as follows:

$$\Gamma_{max} = -\frac{1}{2.303nRT}\left(\frac{\partial\gamma}{\partial \log C}\right)_T \qquad [1]$$

The minimum area per molecule at the interface (A_{min}) is calculated from the relationship (38):

$$A_{min} = \left(N_A\ \Gamma\right)^{-1} x\ 10^{16} \qquad [2]$$

where R = 8.31 J-mol^{-1}K^{-1}, N = Avogadro's number, Γ_{max} is in mol/cm^2 and A_{min} is in (nm^2/molecule) x 10^2. The parameter *n* represents the number of species at the interface whose concentration changes with surfactant concentration. For cationic surfactants, its value is unambiguous only in the presence of a swamping amount of electrolyte. Under these conditions *n* = 1. In aqueous solution it has been set at two or three by various investigators. We chose to use *n* = 3 with the understanding that we are merely comparing A_{min} values within a series of compounds. Comparison with literature values must be made with caution, particularly for older data where *n* is not explicitly defined.

Once maximum saturation of the interface is achieved, continued increase in surfactant concentration results in an alternate method of reducing the free energy of the system, i.e. aggregation. In this case, decrease in free energy is accompanied by increase in entropy of the system with release of water molecules from the hydrocarbon tails of the surfactant molecules.

Interfacial tension and steady-state fluorescence methods can be used to detect micelle (or aggregate) formation. The break point in a plot of interfacial

tension versus log of surfactant concentration (C_s) is defined as the critical micelle concentration, cmc.

Two steady-state fluorescence methods, employing pyrene and pyrenecarboxaldehyde as probes, were used for cmc determination.

In the first case, the emission spectra of pyrene taken with an excitation wavelength of 338 nm were observed as a function of surfactant concentration. The ratio of the intensity of the first vibronic band to that of the third (I_1/I_3) is a measure of the polarity of the probe's environment. The initial break in a plot of I_1/I_3 versus log C_s is taken as the cmc. The curves tend to exhibit a sigmoidal shape, with a rapid decrease in I_1/I_3 just above the cmc and level off at high C_s. There is some disagreement in the literature as to whether it is the first break point or the intercept of the rapidly decreasing part of the plot and the nearly horizontal part at high C_s which corresponds to the cmc. Our data, and that of investigators also comparing values with those obtained from surface tension measurements (39), define the first break point as the cmc. Ultrasonic absorption and electrical conductivity determinations of cmc values (40) agree more closely with those obtained by fluorescence when the intercept with the horizontal region is defined as the cmc.

The fluorescence probe pyrene-3-carboxaldehyde is known to measure the polarity of the micelle-water interface (41) and, hence, may be used to determine cmc's. The choice of this probe follows from its proven ability to accurately predict cmc values; and, its documented lack of effect on the surface tension behavior for all classes of surfactant (39). Fluorescence emission

spectra taken with an excitation wavelength of 400 nm exhibit a single peak, the position of which correlates with solvent polarity (41, 42). The maxima are blue-shifted as solvent polarity decreases. A plot of maximum wavelength (λ_{max}) versus log surfactant concentration displays a break at the cmc.

I.3.2. Interfacial Properties at the aqueous solution/hydrocarbon interface

When the gaseous phase (air) is replaced by a hydrocarbon phase, disruption of the hydrocarbon structure occurs via the hydrophilic groups in the surfactant and disruption of the aqueous phase via the hydrophobic groups. Movement of surfactant molecules to the interface once again lowers the free energy of the system.

Equations [1] and [2] apply equally well to aqueous/hydrocarbon as to aqueous/air systems. For aqueous/hydrocarbon systems, however, partitioning of the hydrocarbon into the bulk surfactant phase must be considered. For a homologous series of compounds of increasing alkyl chain length, the A_{min} value at the aqueous solution/air interface decreases as the number of carbon atoms, n, in the chain increases. This is due to tighter packing at the interface due to increased attraction between the hydrocarbon chains. Conversely, in hydrocarbon systems there is increased intercalation of the hydrocarbon at the hydrocarbon/water interface as the alkyl chain length increases (43,44) resulting in an increase in the A_{min} value as n increases.

Another difference lies in the parameter designated as a measure of surfactant efficiency, the pC_x value. This is defined as the negative log of the

concentration of surfactant in the aqueous phase at interfacial pressure of x mN/m. In hydrocarbon/water systems, pC_{30} values, rather than the pC_{20} values used for air/water systems, are used as a measure of surfactant efficiency because saturation is usually achieved at an interfacial pressure of 30 dyne/cm (43).

In order to determine whether partitioning is significant in any system, it is possible to estimate a partition coefficient as:

$$K = \frac{(CMC_T - CMC)}{CMC} x \frac{1}{\Phi} \qquad [3]$$

where Φ is the volume ratio of hydrocarbon to aqueous phases, CMC refers to the actual critical micelle concentration in the aqueous phase and CMC_T refers to the total concentration of surfactant added to the system required to reach an apparent critical micelle concentration in the aqueous phase in the presence of hydrocarbon. CMC_T is assumed different due to partitioning of surfactant into the hydrocarbon phase.

I.3.3. Dynamic Interfacial Properties at the aqueous/hydrocarbon interface

The interfacial properties discussed thus far have been equilibrium properties. For processes involving emulsification or foaming, it is more relevant to have a description of the interfacial tension as a function of time, i.e., dynamic interfacial tension. The maximum bubble pressure method has been used to

investigate the dynamic surface tension of cationic and anionic gemini surfactants (45-47). The data were well-described by mathematical equations previously published by the same group (48-50). Dynamic interfacial tension data of anionic gemini surfactants, obtained by the drop volume method, are here shown to also be described by these equations. The values of parameters having physical significance can be equally well determined by this method as by the maximum bubble pressure method. Both the maximum bubble pressure method and the drop volume method will return equilibrium values comparable to those obtained by the Wilhemy plate method if the rate for establishment of equilibrium is much faster than the formation of the drop or bubble (51).

The anionic gemini surfactants studied by this method are presented in Scheme I.5.

Scheme I.5. Chemical structures of anionic gemini surfactants.

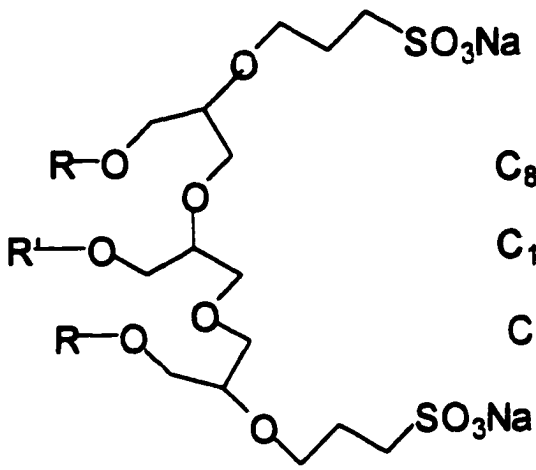

$C_8C_1C_8$ R=C_8H_{17} ; R'=CH_3

$C_{10}C_1C_{10}$ R=$C_{10}H_{21}$; R'=CH_3

$C_{10}C_8C_{10}$ R=$C_{10}H_{21}$; R'=C_8H_{17}

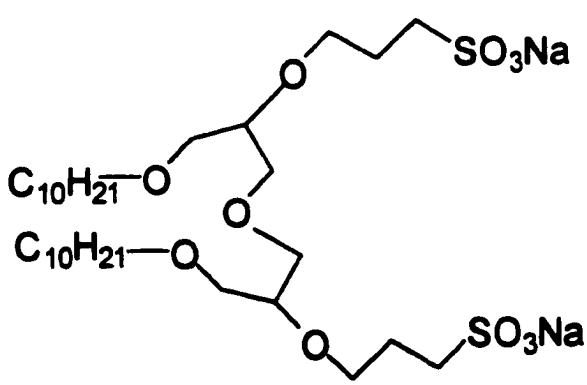

$C_{10}OC_{10}$

I.4 Aggregation of Surfactants

Aggregate size and shape determine function; hence, prediction of these factors based on chemical structure is a fundamental research goal. The similarity of surfactant aggregates to biochemical systems such as globular proteins and cell membranes has long been recognized. This opens the possibility of use of surfactant systems for modeling of the more complex biological systems. Possibilities for kinetic studies stem from the analogy between micellar and enzymatic catalysis (52). In the field of engineering, understanding of surfactant aggregation is important in microemulsion systems. It has been found that a bicontinuous microstructure results in the ultralow interfacial tensions necessary in enhanced oil recovery (53).

While the morphology of gemini micelles is of equal importance, the primary focus of this research concerns the number of gemini molecules per surfactant aggregate, i.e., the aggregation number, N. Aggregation numbers may be determined by a variety of methods including: conventional (54) and dynamic (55) light scattering; small-angle neutron scattering (SANS) (56,57); sedimentation (58) and various spectroscopic probe techniques. One of the most widely used spectroscopic methods involves fluorescence measurements. Turro and Yekta (59) first proposed a steady-state fluorescence quenching method in 1978 wherein the aggregation number is calculated from the following:

$$\ln\left(\frac{I_0}{I}\right) = \frac{N[Q]}{(C_S - cmc)} \qquad [4]$$

where I and I_0 are the fluorescence intensity in the presence and absence of quencher respectively, [Q] is the concentration of quencher, C_s is the total concentration of surfactant and the cmc is assumed equal to the monomer concentration for a pure surfactant. The aggregation number, N, is determined from the slope of a plot of $\ln(I_0/I)$ versus [Q]. This method must be used with caution as the derivation of equation [4] involves a number of assumptions as pointed out by numerous reviewers (60-63). Chief among these assumptions is that of static quenching, i.e., a drop in fluorescence intensity occurs with increasing [Q] without change in fluorescence lifetime. Further, the probe and quencher molecules are assumed to have a Poisson distribution among the aggregates, which is frozen on the fluorescence timescale. It is necessary to choose the probe/quencher pair with care, and to check the dependence of lifetime as a function of [Q] by dynamic methods before aggregation numbers obtained by steady-state methods may be assumed valid.

Time-resolved fluorescence quenching (dynamic quenching) involves measurement of the decay of fluorescence intensity as a function of time following a brief excitation pulse. Application of this method to the determination of aggregation numbers was initiated at the same time as the steady-state method (64). This method is more versatile than steady-state as it provides kinetic information on the dynamics of micelles (65,66) as well as aggregation numbers. Finally, this method enables the distribution in aggregation numbers for polydisperse micellar systems to be determined (67,68).

Chapter II

Theory

II.1 Equilibrium Interfacial Properties

The elegantly simple Gibbs equation [1] provides access to a number of useful parameters, which characterize surfactant systems at equilibrium. The slope of a plot of interfacial tension versus log aqueous surfactant concentration (γ versus log C) is directly proportional to the maximum surface excess concentration of surfactant at the interface, Γ_{max}. This parameter represents the effectiveness of adsorption (69) of the surfactant at that interface, i.e., its concentration at surface saturation. Γ_{max} is inversely proportional to A_{min} [2], which value is a direct reflection of the size and shape of the molecule at the interface. The ability of a surfactant to produce a desired effect, the efficiency of adsorption parameter (70), may also be derived from plotting γ versus log C. We define this as the concentration of surfactant needed to reduce to interfacial tension of the solvent by 20 mN/m in aqueous solution /air systems and by 30 mN/m in aqueous solution/hydrocarbon systems. The negative log of this concentration, pC_{20} or pC_{30}, is an alternate description.

Standard thermodynamic parameters, such as the standard free energy of adsorption at the aqueous/air and aqueous/hydrocarbon interface, $\Delta G°_{ad}$, may be calculated directly from the efficiency and effectiveness parameter (71):

$$\Delta G^{\circ}_{ad} = -(2.303RT)pC_{20} - 6.023 \times 20A_{min} - 2.303RT \log\omega \quad [5]$$

where ω is the number of moles of water per liter of water and other quantities are as previously defined. The larger the value of the efficiency parameter, the more negative ΔG°_{ad} becomes.

The ratio of the critical micelle concentration to the efficiency parameter, cmc/C_{20} or cmc/C_{30}, measures the relative importance of adsorption to micellization in a surfactant system. Higher ratios indicate inhibition of micellization relative to adsorption due to changes in surfactant structure or in its environment.

Variation of critical micelle concentration with surfactant structure is a crucial part of this research. Aberrant behavior is defined, for homologous straight-chain ionic surfactants, as deviation from the equation (72):

$$\log cmc = A - Bn \quad [6]$$

where A and B are constants for a particular ionic head group at a given temperature and n is the number of carbons in the alkyl chain. Using this equation, it is possible to determine the expected cmc for a compound with a larger value of n from the linear relationship between the shorter chain compounds.

II.2 Dynamic Interfacial Properties

Dynamic interfacial tension measures change in the aqueous solution/hydrocarbon interface while new interfacial area is being formed. In the drop volume method, the hydrocarbon phase is introduced into an aqueous surfactant solution as a drop forced through a capillary at a constant flow rate. Time between subsequent drops is measured and converted to the volume of each drop. This non-equilibrium situation allows diffusion and orientation rates of surfactants to be studied. Clearly, it is most useful in moderately rapid processes where the surfactant does not attain equilibrium.

The interfacial tension as a function of time, $\gamma_I(t)$, is calculated by a balance of forces method. The separation force on the drop at the tip of the capillary is equal to the adherence force leading to the following (73,74):

$$\gamma_I(t) = \frac{Vg(\rho_H - \rho_L)}{\pi d} \qquad [7]$$

where V is the volume of the drop (flow rate x time between subsequent drops), g is the acceleration of gravity, d is the inner diameter of the capillary, and $(\rho_H - \rho_L)$ is the difference in density between the hydrocarbon and aqueous phases.

Dynamic surface tension data, at the aqueous solution/air interface, obtained by the maximum bubble pressure method (45-50) are described by the empirical equation (48):

$$(\gamma_o - \gamma_t)/(\gamma_t - \gamma_m) = (t/t^*)^n \qquad [8]$$

where γ_0 = interfacial tension of the pure solvent

γ_t = interfacial tension of the surfactant solution at time, t

γ_m = mesoequilibrium interfacial tension value.

t* is defined as the time mid-way between pure solvent interfacial tension and equilibrium interfacial tension.

Transforming the equation to linear form:

$$\log [(\gamma_o - \gamma_t)/(\gamma_t - \gamma_m)] = n\log t - n\log t^* \qquad [9]$$

Transforming the equation to exponential form (46):

$$\pi_t = \pi_m/[1 + (1/a)\exp(-n\ln t)] \qquad [10]$$

where $\pi_t = (\gamma_o - \gamma_t)$ surface pressure at time, t

$\pi_m = (\gamma_o - \gamma_m)$ meso-equilibrium surface pressure

$a = (1/t^*)^n$

$t_i = (0.268/a)^{1/n}$

A generalized surface tension versus log time curve (Scheme II.1) exhibits a sigmoidal shape that may be characterized by four regions (48): induction (I), rapid fall (II), meso-equilibrium (III), equilibrium (IV). t_i is defined as the time at the end of the induction region and was later (50) shown to be related to the molecular structure of the surfactant; this parameter increases with the tightness of packing at the interface (46). The parameter, n, is also related to molecular structure in that it increases with the hydrophobic character of the surfactant (46).

We here apply the linear and exponential forms of these equations to dynamic interfacial tension data obtained by the drop volume method.

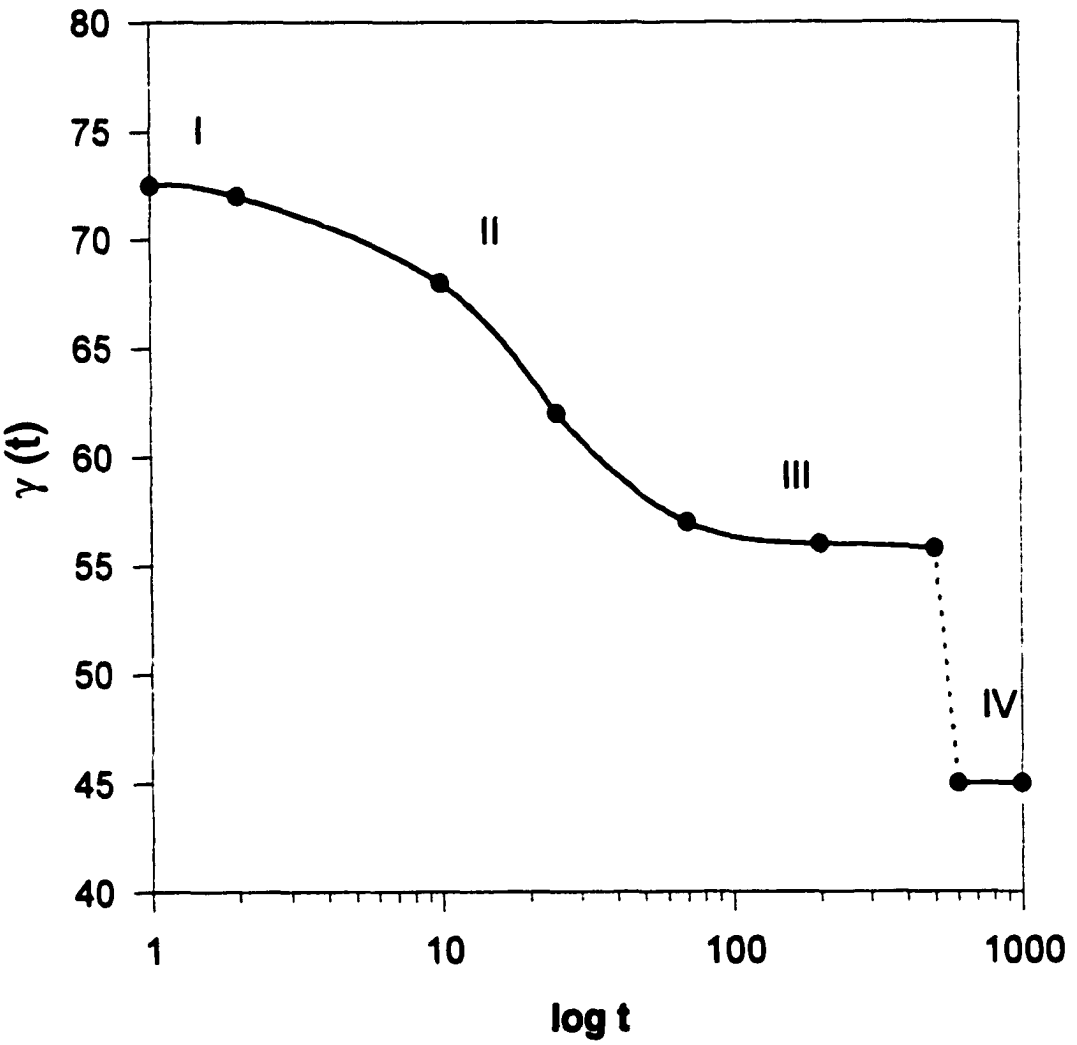

Scheme II.1 Generalized dynamic surface tension curve.

II.3 Fluorescence

Luminescence is the emission of photons from electronically excited states(75). Examples of luminescent probes include: atomic ions, e.g., Eu^{3+}(aq), neutral organic molecules, e.g., pyrene, and charged organic molecules, e.g. TMA-DPH.

Fluorescence involves those transitions arising from the decay of singlet excited states and occurs on a nanosecond timescale. Phosphorescence requires a change of spin orientation during the electronic transition from the excited to ground state; it is a much slower process than fluorescence. Emission of light by luminescence probes is sensitive to the probe environment. This sensitivity can be used to investigate surfactant solutions.

The first use of fluorescence in surfactant research was for cmc determination. Hartley used the color change of organic dyes upon solubilization into micelles as an indication of the cmc (76).

We have used fluorescence as a method of determining cmc and aggregation numbers. Fluorescence methods also provide information on micropolarity (41), microviscosity (77), partition coefficients (78,79) and micelle kinetics (65,66).

II.3.1 General Theory

Absorption of photons of light of a proper wavelength by a fluorescent probe results in electronic excitation of the probe. The rapid absorption process (10^{-15}s) takes place from the ground state, S_0, to vibrationally excited states of higher singlet electronic states. Following excitation, two radiationless processes, vibrational relaxation and internal conversion, return the electron to lower energy states within 10^{-12} s. The emission of fluorescent light corresponds only to the transition from S_1^0 to various levels of the ground state S_0. (Scheme II.2)

Fluorescence emission spectra provide the most useful type of steady state experiment for surfactant solution research (80). Such experiments involve excitation of the sample at a constant wavelength, followed by analysis of the emitted light from the sample as a function of wavelength. In steady state fluorescence experiments, the exciting light is derived from a continuous source, such as a xenon arc lamp, and a monochromator is used to select a single wavelength of light. This discrete excitation wavelength, λ_{ex}, is chosen on the basis of the probe's absorption spectrum. The emitted light passes through an emission monochromator that is scanned over a range of wavelengths, and detected using a photomultiplier tube. The resulting profile of fluorescence intensity as a function of wavelength of emitted light is analyzed for peak intensity and peak position which are directly related to the probe's environment and,

hence, the nature of the surfactant system. Additional information may be obtained from the fine structure of the spectrum. The emission spectra of many probes, including pyrene, reflect the vibrational levels of the ground state. In the same way, the absorption spectrum reflects the vibrational levels of the excited singlet states. This results in a mirror image relationship between a fluorescence emission and ultraviolet absorption spectrum. That the emission spectrum is shifted to longer wavelength, i.e. the Stoke's shift, is the result of loss of energy through vibrational relaxation before emission of light occurs.

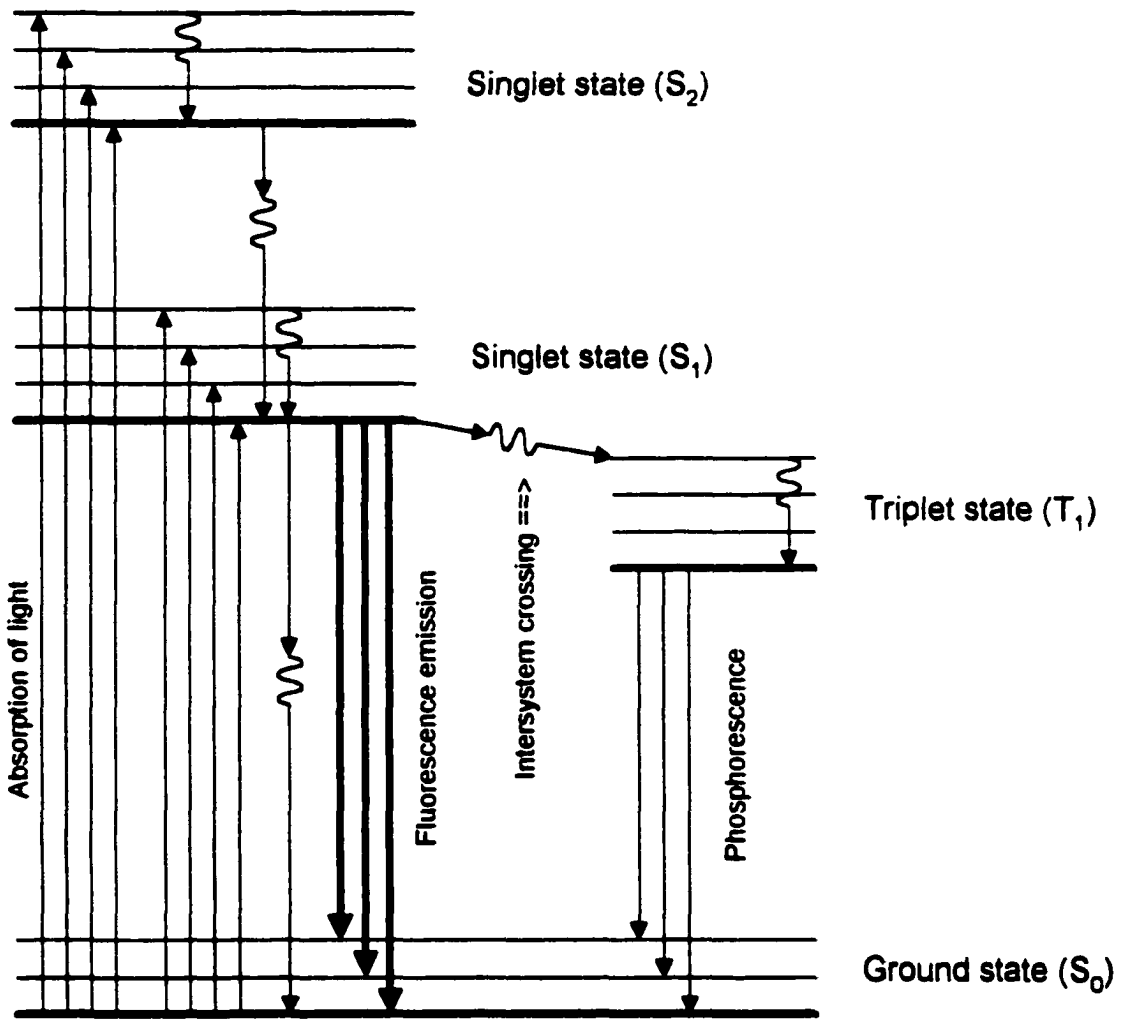

Scheme II.2 Jablonski Diagram

A steady state excitation spectrum follows the fluorescence intensity at a constant emission wavelength, λ_{em}, as the exciting light wavelength is continuously varied. Though of less interest in surfactant research than emission spectra, excitation spectra provide additional information about the probe environment, e.g. concerning the possibility of excited state reactions. In the absence of such reactions, the excitation and uv spectra should overlap as they both correspond to excited state vibrational levels. Deviation from the mirror image rule mentioned above is also an indication of excited state reactions.

In dynamic experiments, the sample is exposed to a brief pulse of light from a flash-lamp or laser, and the decay of fluorescence intensity is followed as a function of time. In this case, both the excitation and emission wavelengths are fixed. The measured fluorescence lifetime, τ_F, is an average value of the time spent by the fluorophore in the excited state. Since deactivation of excited states can occur by nonradiative as well as radiative processes, the measured lifetime is shorter than the intrinsic lifetime, τ_0. The quantum yield of fluorescence is easily determined by lifetime measurements:

$$\Phi_F = \tau_F/\tau_0 \qquad [11]$$

The value of τ_F is of interest in that many probes have lifetimes that are dependent on the polarity of their environment (80).

II.3.2 Steady State Fluorescence Experiments

The fluorescence probes pyrene and pyrene-3-carboxaldehyde have been shown to be reliable probes for cmc determination of cationic and anionic surfactants when used in trace amounts ($<10^{-6}$M). Comparison with surface tension results show that neither surface tension, nor the surface tension derived cmc value is affected at these levels (39).

II.3.2.1 Pyrene-3-carboxaldehye Studies of Surfactant Solutions

The emission spectrum of pyrene-3-carboxaldehyde in water exhibits a single peak at 470nm when excited at 400nm. The position of the maximum of this peak correlates with solvent polarity (41,42). As the environment of the probe becomes more hydrophobic, i.e. as the concentration of added surfactant increases, the fluorescence maxima is blue-shifted until the probe is solubilized inside the micelle. The magnitude of the blue-shift is dependent on the chemical structure of the surfactant. Scheme II.3 shows normalized spectra to illustrate this effect. Each curve represents a specific surfactant concentration.

Proton nmr studies (83,84) have confirmed that pyrene-3-carboxaldehyde is solubilized with the aromatic moiety in the micellar core and the aldehyde group at the micelle-water interface.

The fluorescence emission from the pyrene-3-carboxaldehyde solubilized inside the micelle is due to an n-π^* transition with a small quantum yield, Φ_F <0.001. Increase in the polarity of the environment causes the π-π^* state to become the emitting state; it is now lower in energy due to solvent relaxation and the fluorescence emission is shifted to longer wavelength (41). The red-shift in polar solvents is accompanied by an increase in the quantum yield (Φ_F in methanol = 0.15).

Following the quantum yield, or the fluorescence intensity, as a function of surfactant concentration is an alternate method of monitoring the system.

II.3.2.2 Pyrene Fluorescence and Steady State Application

In pyrene monomer fluorescence, the emission spectrum exhibits five major peaks which represent vibrational transitions. The I_1 peak at 372 nm corresponds to the 0-0 band. The intensity of the band is enhanced in the presence of polar solvents at the expense of the others (85). The I_1/I_3 ratio, with I_3 at 384 nm, is a convenient measure of the polarity of the pyrene environment.

When the concentration of pyrene is increased beyond that used in these experiments, i.e. at $C_{py} \cong 5 \times 10^{-6}$ M, the steady state emission spectra begin to show a broad peak at 480 nm due to excimer formation. The ratio of intensity of excimer to monomer, E/M, may be used as a measure of microviscosity of the the system (77). In this case, monomer fluorescence emission is measured at the fifth vibronic peak, I_5 (395 nm).

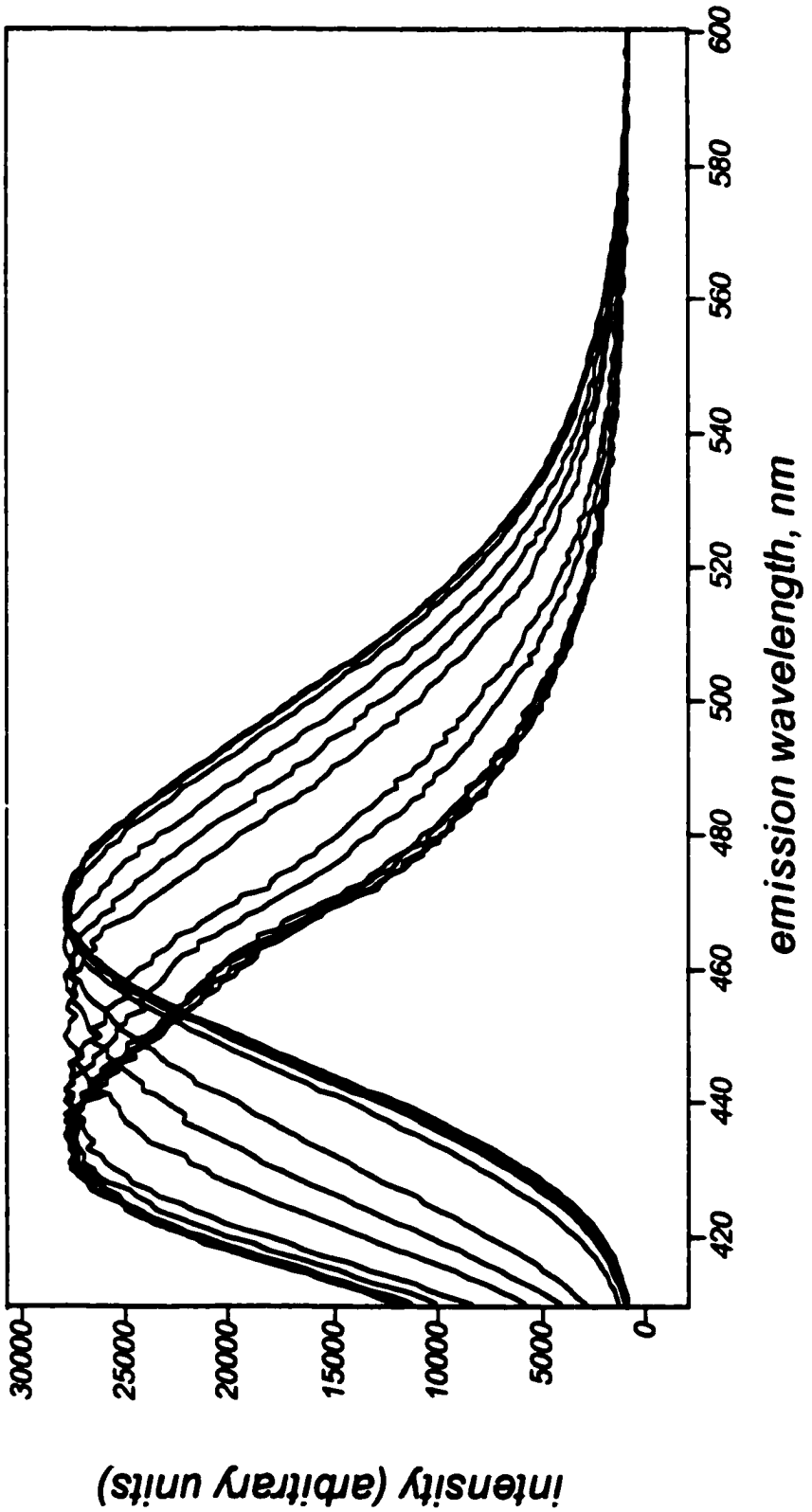

Scheme II.3. Solvent dependent shift of pyrene-3-carboxaldehyde with surfactant concentration.

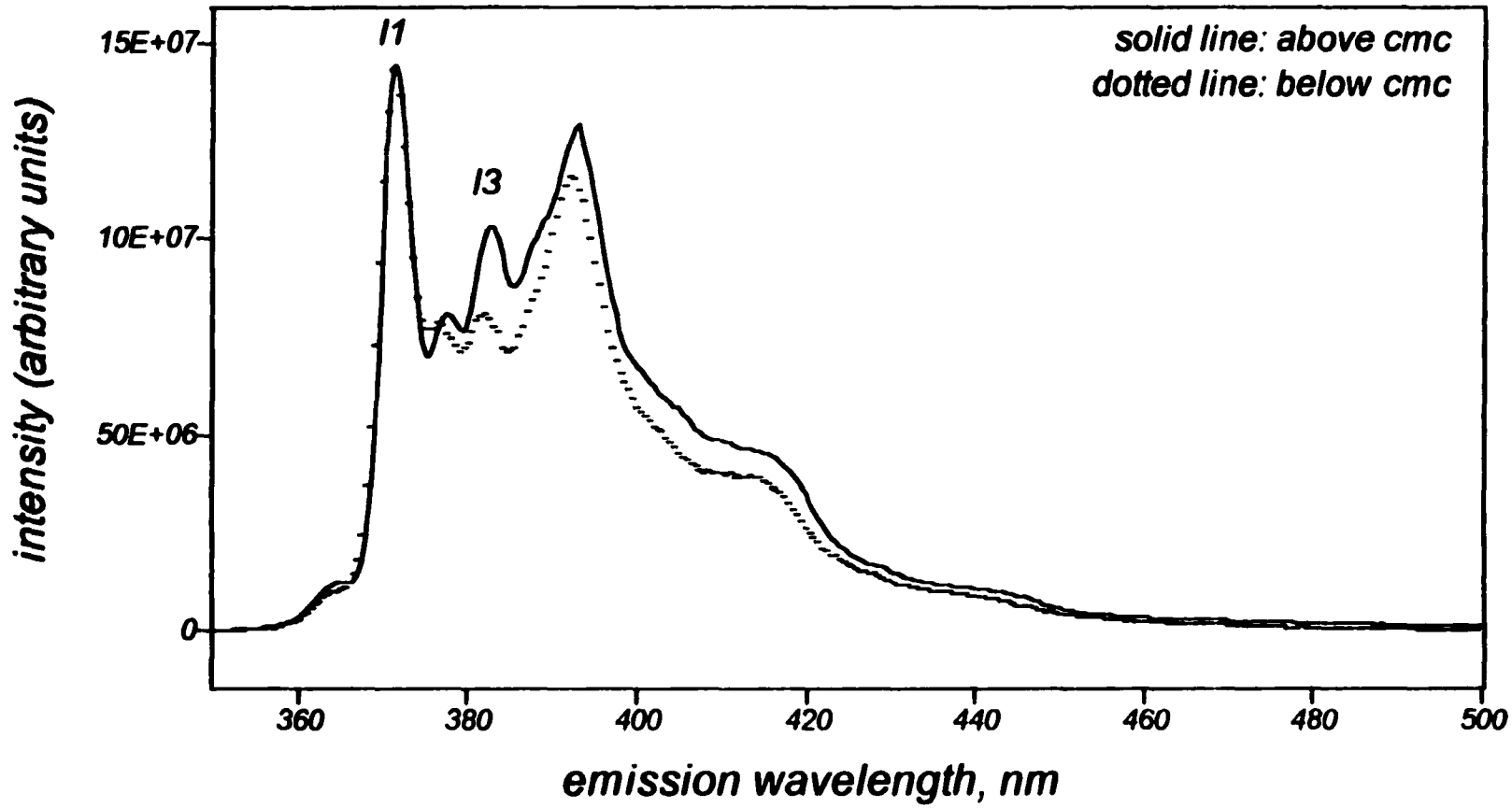

Scheme II.4 Emission spectra of pyrene in surfactant solutions above and below the cmc. Note the difference in the I_1 / I_3 ratio at surfactant concentrations above and below the cmc. (Spectra are normalized on I_1 band intensity).

II.3.3 Dynamic Fluorescence Experiments

The time-correlated single photon counting method was employed, using pyrene as the fluorescent probe, for recovery of lifetimes as well as determination of aggregation numbers.

II.3.3.1 *Time-Correlated Single Photon Counting (TCSPC)*

In the photon-counting method, the sample is excited with a 2-3 ns pulse from the flashlamp. The time interval between the pulse and detection of the first photon by the photomultiplier tube is measured. In order to ensure that only a single photon arrives for each pulse, the light intensity is adjusted so that the count rate is less than 3% of the repetition rate (kHz). This time interval (or Start/Stop interval) is measured for a large number of times, approximately 10^6. The distribution of arrival times forms a histogram that represents the decay curve (86).

The time-resolved decay of fluorescence is fit to a sum of exponentials:

$$I(t) = \Sigma_i \alpha_i e^{\frac{-t}{\tau_i}} \qquad [12]$$

where α_i represents the fractional contribution to the decay of a component with lifetime τ_i.

The fractional intensity of each species is given by:

$$f_i = \frac{\alpha_i \tau_i}{\Sigma_i \alpha_i \tau_i} \qquad [13]$$

It is important to stress (86) that the fitted parameters do not necessarily represent unique species of fluophores. A multi-exponential fit may be the result of one fluorphore in different environments, as it is with pyrene in surfactant solutions. It is often convenient to represent the average lifetime as:

$$\langle \tau \rangle = \frac{\Sigma_i \alpha_i \tau_i^2}{\Sigma_i \alpha_i \tau_i} \qquad [14]$$

Since the flash-lamp does not provide an infinitely short δ pulse, it is necessary to correct for the time-profile of the pulse. The lamp pulse, L(t), is collected at the same time as the sample using a scattering solution of Ludox. The mathematical process of recovering the true decay from the measured decay, R(t), is known as convolution.

Software used in this laboratory is based on a nonlinear least-squares method of analysis (87). Using assumed values of α_i and τ_i, along with the measured lamp pulse, a calculated value of the decay, $R_c(t)$, is obtained from the convolution integral. The goodness of fit parameter is calculated as:

$$\chi^2 = \Sigma_{i=1}^{n} \omega_i [R(t) - R_c(t)]^2 \qquad [15]$$

where ω is a statistical weighting factor. A χ^2 value of one means that each data point is one standard deviation away from the model. According to Lakowicz (88), χ^2 values larger than 2 indicate a poor fit, and χ^2 values less than 1.2 indicate a good fit.

The residuals, $[R_c(t) - R(t)]$ are an indication of closeness of fit of the calculated and observed data. Random distribution of the residuals about zero indicates a good fit. Scheme II.5 illustrates a single and double exponential fit for pyrene in a solution of SDS. The single exponential fit shows a large deviation between the calculated (solid line) and experimental (dotted) points. The double exponential fit is an excellent fit and the residuals are randomly distributed about the zero point.

The autocorrelation function also tests the goodness of fit. This function detects systematic deviations, i.e.; it is a specific test of randomness. The autocorrelation plot allows visualization of the positive and negative correlations. A flat autocorrelation plot indicates the absence of systematic errors.

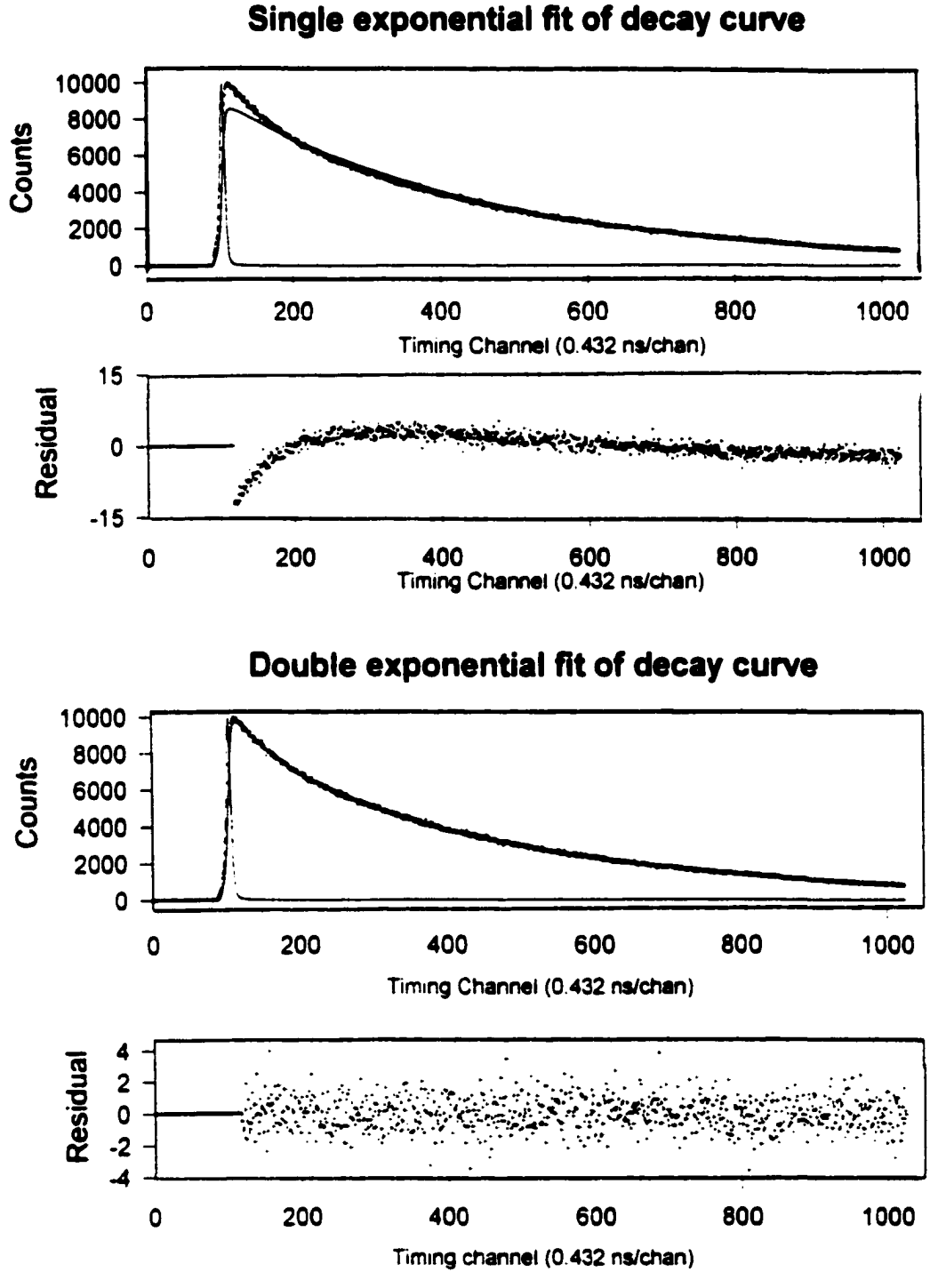

Scheme II.5 Single and double exponential fit of pyrene in a solution of SDS.

II.3.3.2 Aggregation Numbers

Infelta et al. (79) and Tachiya (89) published the original treatments of the kinetics of the quenching of luminescent probes in micelles. The prediction that probe and quencher molecules are distributed among micelles according to Poisson statistics, quickly led to applications, especially the determination of aggregation number (62,90,91).

Studies using pyrene alone (90,91) are based on the ability of pyrene monomer to form an association complex or excimer. In this case, it is the excimer that acts as a quencher of fluorescence:

Excitation of pyrene monomer: $P + h\nu \rightarrow P^*$

Excimer formation: $P + P^* \leftrightarrow PP^*$

If excimer is present, the fluorescence decay curve will show two components: a fast one associated with micelles having solubilized two or more pyrene molecules; a slow one corresponding to decay of pyrene monomer.

Quenching is assumed to follow a first-order rate process (62), and the time dependence of fluorescence intensity is:

$$I(t) = I(0) \exp[-k_1 t - n\{1 - \exp(-k_q t)\}] \qquad [16]$$

where I(0) is the fluorescence intensity at zero time, k_1 is the first-order rate constant for unquenched fluorescence, n is the average number of quenchers per micelle and k_q is the first-order quenching rate constant. Rewriting [16] in logarithmic form:

$$\ln[I(t)/I(0)] = -k_1 t - n\{1 - \exp(-k_q t)\} \qquad [17]$$

For very long times, when all excimer has decayed, [17] reduces to:

$$\ln[I(t)/I(0)] = -k_1 t - n \qquad [18]$$

The limiting slope of a plot of ln[I(t)/I(0)] versus t is $-k_1$. Extrapolation of the linear region to t = 0 is –n.

A series of curves with varying quencher (excimer) concentration will produce parallel, linear tails in the logarithmic representation. This shows that no migration of the quencher has occurred, an assumption inherent in equation [16].

From the value of n, the surfactant aggregation number,N, is calculated:

$$N = n[C_s - \text{cmc}]/C_{py} \qquad [19]$$

where C_s is the total surfactant concentration and C_{py} is the concentration of pyrene. An effective aggregation number can be determined as long as a well-developed tail, characterized by k_1, can be identified (63).

Scheme II.6 illustrates typical plot of pyrene decay characterized by an initial fast decay due to excimer, and a well-developed tail due to monomer decay. Decays were shifted to t = 0, assumed to be at the maximum of fluorescence intensity I(0). Linear regression analysis at long times provides the slope, $-k_1$ and intercept, $-n$. The reciprocal of k_1 is equal to the monomer decay constant, τ_2.

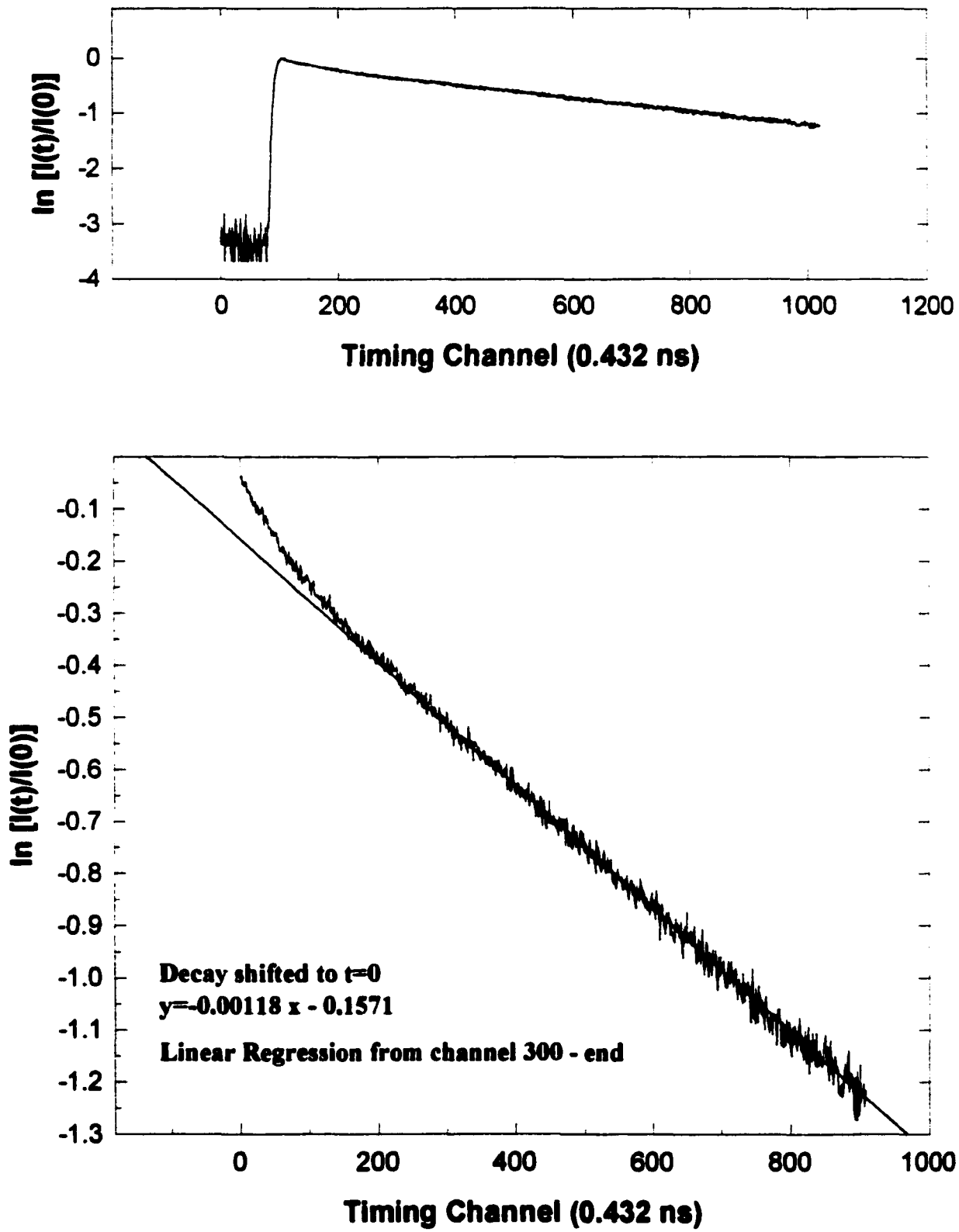

Scheme II.6 Time-resolved Fluorescence Decay of Pyrene in SDS Micelles

Chapter III

Materials and Methods

III.1 Materials

The $(C_nN)_2OH$ and $(C_nN)_2(OH)_2$ surfactants were synthesized as in previous investigations (27,28). The $(C_nN)_2O$ series was synthesized by reaction of 2-bromoethylether with an excess of alkyl-N,N-dimethylamine. Recrystallization from a mixture of tetrahydrofuran and isopropyl alcohol led to a reaction yield over 80%. Purity of the compounds was checked by elemental analysis. For $(C_{12}N)_2O$, Theory: C, 58.35; H, 10.71; N, 4.25. Found: C, 58.63; H, 10.81; N, 4.30. Structures are shown in Scheme I.2.

III.2 Surface Tension Measurements

The surface tensions were measured with a Kruss K12 tensiometer by the Wilhelmy plate technique. Measurements were taken at 25 ± 0.1°C until successive values agreed to within 0.1 mN/m. Solutions were prepared with deionized, doubly-distilled water; NaCl was baked for 5 hours to remove organic impurities. NaCl is preferred over NaBr as the electrolyte for all experiments, because bromide ion is a known fluorescence quencher .

III.3 Interfacial Tension Measurements

Measurements were made by the spinning drop technique using a model 500 interfacial tensiometer (University of Texas). As with surface tension measurements, equilibrium was considered to be obtained when successive

values agreed to within 0.1 mN/m; again at 25 ± 0.1°C. Calculation of interfacial tension is based on the Vonnegut (82) equation:

$$\gamma_I = \left(\frac{5.21x105(\Delta\rho)(D^3)}{p^2} \right) \qquad [20]$$

where γ_I is interfacial tension in mN/m, $\Delta\rho$ is the density difference of water and hydrocarbon in g/cm^3, D is the diameter of the oil droplet in cm, and P is the time of the rotation in msec/rev. The density of water was taken as 0.997g/cm^3 and that of hexadecane as 0.773g/cm^3. Hexadecane (Aldrich) was >99% pure. UV scans using a Hewlett Packard Diode Array spectrophotometer confirmed no absorbance above 250 nm.

III.4 Dynamic Interfacial Measurements

Dynamic interfacial tension measurements were made by the drop volume technique using a Kruss Drop Volume Tensiometer DVT-10. Measurements were taken at room temperature using hexadecane (Aldrich) as the hydrocarbon phase, i.e., the drop. The leading edge of a drop is detected with an IR-LED and photodiode; time between subsequent drops is measured with a timer. The computer program calculates the volume as flow rate times time per drop; conversion of drop volume to interfacial tension is through equation [7].

Generally 5 to 10 drops are collected until the relative standard deviation of the data is less than 1%.

A limitation of this particular instrumental system is that the maximum flow rate of hydrocarbon through the capillary is 45 mL/hr. In some systems, it is not possible to observe γ_t approach γ_0 at the beginning of the induction period. Using very slow flow rates (long drop time) one can approach equilibrium.

III.5 Steady State Fluorescence Measurements

Steady-state fluorescence measurements involving pyrene-3-carboxaldehyde were carried out on a SPEX Fluorolog Tau3 spectrofluorometer (Model FL3-21 Tau3; Instruments SA, Inc. Edison, N.J. 08820) operated in the photon-counting mode. Samples were placed in quartz cuvettes of 1 cm pathlength. All samples showed maximum UV absorbance of <0.1 at 400 nm to obviate inner filter effects (81). Right-angle collection geometry was used. Pyrene-3-carboxaldehyde (Aldrich) was 99% pure. The probe concentration in all cases was $<10^{-6}$ M as determined by UV. No emission bands due to excimers were evident. All solvents were of spectral grade purity. Emission spectra were taken at an excitation wavelength of 400 nm with a bandpass of 1.7 nm. Excitation spectra taken at an emission wavelength of 470 nm showed overlap with UV absorption spectra to within 1 nm, indicating lack of complications due to excited state reactions. Raman emission and blank fluorescence of the solvent

were judged insignificant under these conditions, as the position of the emission peak remained unchanged by blank subtraction.

Steady-state measurements involving pyrene were carried out using a Perkin-Elmer model LS-50B instrument. Pyrene (Aldrich) was 99.9% pure. Emission spectra were taken using an excitation wavelength of 338 nm with a slit width of 4 nm.

III.6 Dynamic Fluorescence Measurements

Time-resolved fluorescence measurements were carried out using a time-correlated single photon counting system constructed in the laboratory of Professor L. Davenport, Fluorescence Institute of Brooklyn College, CUNY. Samples were excited at 340 nm using a thyratron-gated nanosecond flashlamp filled with nitrogen. Emission was monitored at 372 nm using a monochromator and detected with a photomultiplier tube. The timing system was set at 0.432ns/channel, appropriate for the lifetime of pyrene. A scatter solution of aqueous Ludox (colloidal silica, DuPont) was used to collect the lamp response function needed for recovery of the decay parameters. Additionally, a solution of anthracene in methanol was used as a standard to determine the color shift parameter (Q-shift) as well as judge the success of the experiment based on the ability to recover a single exponential lifetime with a good statistical fit.

Chapter IV

Results and Discussion

IV.1 Interfacial Properties

IV.1.1 Equilibrium Surface Properties of Cationic Gemini Surfactants

Equilibrium surface tension, γ_s, versus log bulk surfactant concentration for the $(C_nN)_2O$ series in water at 25°C is plotted in Figure 1. The $(C_{12}N)_2O$, $(C_{14}N)_2O$ and $(C_{16}N)_2O$ members display the expected behavior for a series in which the alkyl chain length is regularly increased, i.e.,the cmc decreases in a linear fashion due to increased tendency towards micellization (92). Also, there is a slight decrease in the surface tension at the cmc, γ_{cmc}, resulting from closer, thus more efficient, packing of the longer alkyl chains at the interface.

Deviation from this pattern begins when the alkyl length reaches 18 carbons. This is apparent from visual inspection of the plot; however, a more precise depiction of the expected (theoretical) $(C_{18}N)_2O$ curve is obtained as follows. Both the log cmc and the pC_{20} (negative log of the surfactant concentration required for a 20 dyne/cm reduction of the solvent surface tension) values are linear functions of the number of carbon atoms in the alkyl chain,n (93). Extrapolation to n = 18 along the straight lines (Figure 2) provides two points for the expected $(C_{18}N)_2O$ γ_s versus log C curve. The γ_{cmc} is estimated as the surface tension at the cmc. The curve for the $(C_{20}N)_2O$ is highly displaced having a cmc nearly three times higher than the $(C_{18}N)_2O$ as well as an

extremely high γ_{cmc} equal to 55 dyne/cm. The molar solubility of $(C_{20}N)_2O$ in water at 25°C is greater than 6 times the cmc value. All experiments were done within the solubility range. This type of aberrant behavior in gemini molecules with long alkyl chains has been observed by other investigators and sometimes explained on the basis of formation of premicellar aggregates (26-28). Assuming that only the monomer contributes to reduction of surface tension, such aggregates would account for the increased γ_{cmc} seen in the $(C_{18}N)_2O$ and $(C_{20}N)_2O$ compounds. The increase in the cmc values may result from the secondary pathway towards small aggregate formation before true micelles are formed. It is important to clarify the dynamics of this non-stoichiometric situation if we are to understand the properties derived from that stoichiometry.

It should be noted that these compounds can be difficult to work with, and may provide skewed results if certain pitfalls are not avoided. Since they are di-cations, they will adsorb onto negatively-charged glass surfaces. All glassware was thoroughly soaked with the solution to be measured; soaking solutions were then discarded and replaced with fresh solution. For the longer chain compounds it was necessary to age the fresh solution for up to twelve hours before measuring. Even then, it sometimes took several hours for equilibrium to be reached. Most of these experiments were repeated several times.

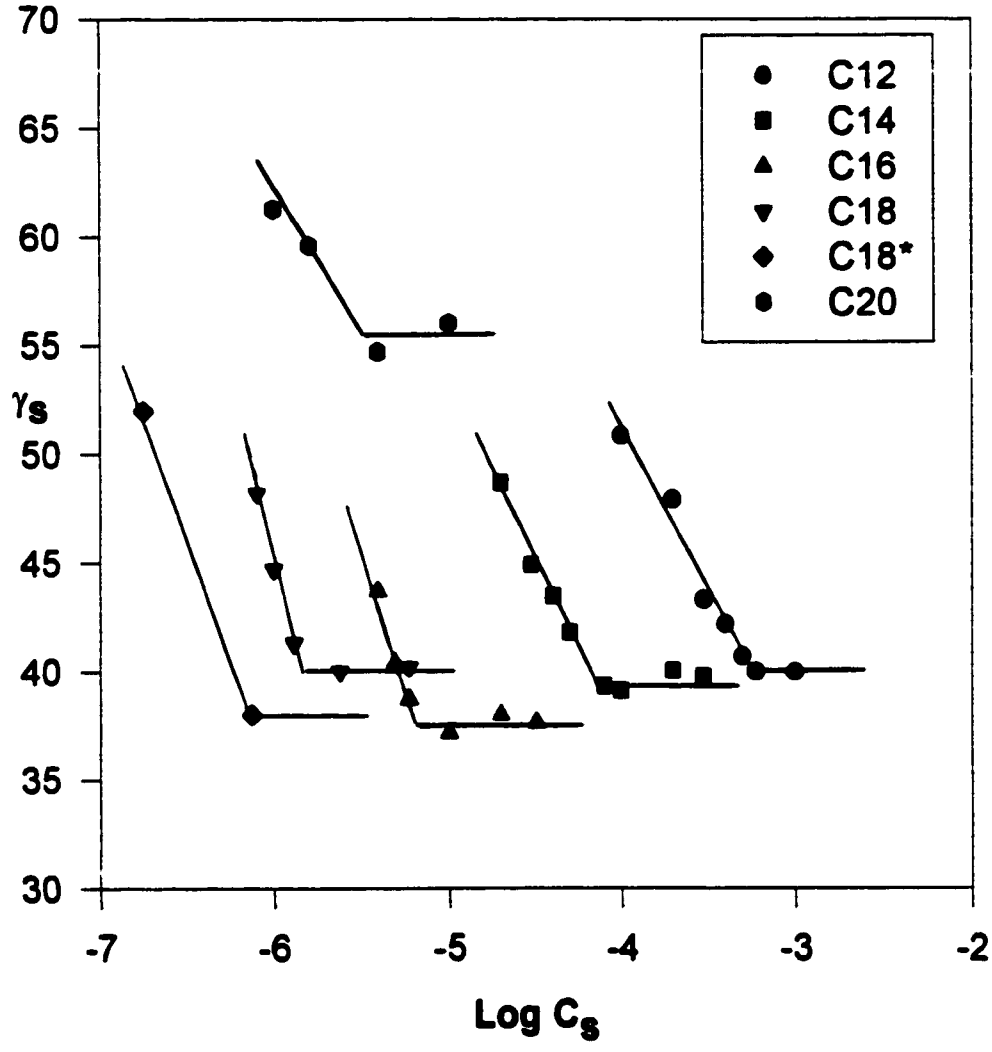

Figure 1. Equilibrium surface tension vs Log C_s of $(C_nN)_2O$ in water at 25°C. C18* is a theoretical curve.

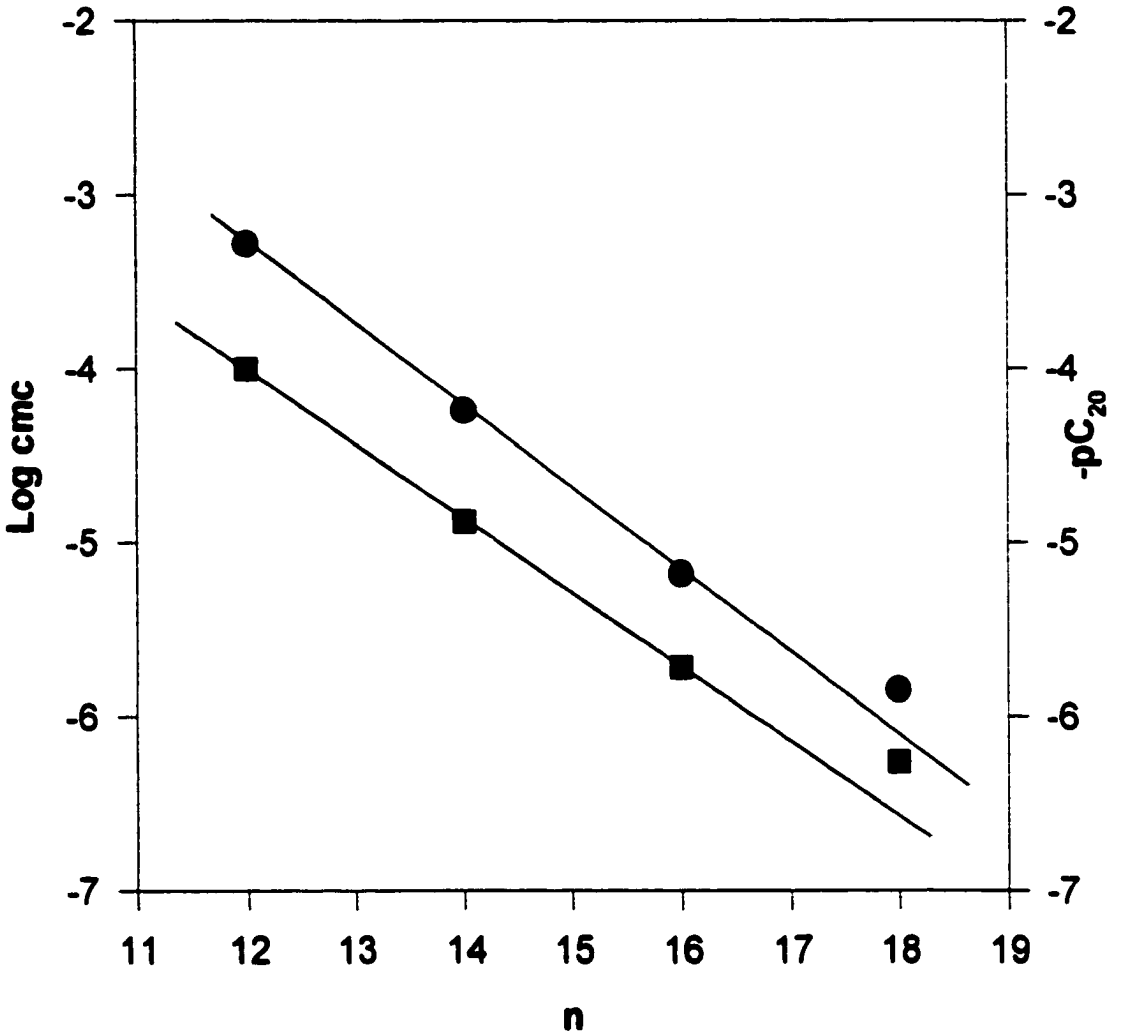

Figure 2. Calculation of theoretical surface tension curve for $(C_{18}N)_2O$ in H_2O at 25^0 in H_2O at 25^0C

Surface properties of $(C_nN)_2O$ compounds in water at 25°C are listed in Table 1, which includes monoquaternary ammonium bromides for comparison in those cases where non-aberrant gemini behavior is observed. The gemini cmc values are roughly two orders of magnitude lower than the conventional surfactant cmc's. This pattern is frequently cited in the literature and explained as resulting simply from the number of hydrophobic (alkyl) carbon atoms being doubled in the geminis (19,94). The γ_{cmc} values are approximately the same for conventional and gemini surfactants; another pattern previously cited (95). The gemini pC_{20} values are two orders of magnitude higher than the conventional values, again because of the greater number of hydrophobic carbon atoms in the molecule.

The A_{min} values (per gemini molecule) for $(C_nN)_2O$ compounds in water show a regular decrease with increasing alkyl chain length; this is expected behavior due to tighter packing of the longer chains at the interface. Comparison of the A_{min} value for $(C_{14}N)_2O$, on a per chain basis, with the literature value (96) for the C14 monoquaternary bromide (TTAB) shows good agreement. We have not reported an A_{min} value for the $(C_{20}N)_2O$ compound. because instrumental limitations at extremely high surface tension values render the slope value uncertain.

Table 1 : Surface Properties of $(C_nN)_2O$ and Trimethylammonium Bromide Surfactants[a] in H_2O at 25°C

COMPOUND	CMC (mol/L)	γ_{CMC} (mN/m)	pC_{20}	$10^{10}\Gamma_{MAX}$ (mol/cm^2)	A_{MIN}[b] (10^2 nm^2)	CMC/C_{20}
$(C_{12}N)_2O$	5.2×10^{-4}	40	4.00	0.97	170	5.2
$C_{12}N^+(CH_3)_3Br^-$	1.6×10^{-2}	39	2.10			2.4
$(C_{14}N)_2O$	5.8×10^{-5}	39	4.88	1.1	156	4.5
$C_{14}N^+(CH_3)_3Br$	3.6×10^{-3}	38	2.8	2.7	61	2.1
$(C_{16}N)_2O$	6.6×10^{-6}	37	5.72	1.6	102	3.5
$C_{16}N^+(CH_3)_3Br$	9.2×10^{-4}	<40				
$(C_{18}N)_2O$	1.4×10^{-6}	40	6.26	2.0	84	2.5
$(C_{20}N)_2O$	4.0×10^{-6}	55				

[a]Data from ref (97).

[b]Values for Γ_{max} and A_{min} were determined using n=3 in the Gibbs equation.

Devinsky et al (98) have investigated the $(C_nN)_2O$ series in water for alkyl chain lengths of 8 to 16 carbons using surface tension and conductivity methods. While cmc values for the lower chain compounds are in good agreement, there is increasing discrepancy between the methods as the alkyl chain length increases. As will be discussed, we have seen excellent agreement between cmc values determined by surface tension and fluorescence methods through 16 carbons. Parreira et al (25) have also studied these compounds by surface tension and conductivity methods. Their reported value of 4.8×10^{-4} M for the cmc of $(C_{12}N)_2O$ agrees closely with our value of 5.2×10^{-4} M obtained by surface tension. However, beginning with $(C_{14}N)_2O$, they reported difficulty in obtaining cmc values, and for $(C_{18}N)_2O$ the cmc was noted as "not apparent".

Figure 3 shows equilibrium surface tension curves for the $(C_nN)_2O$ series in 0.1 M NaCl at 25°C. The corresponding surface properties are listed in Table 2. The presence of the electrolyte decreases the cmc's for the $(C_{12}N)_2O$ and $(C_{14}N)_2O$ as expected, due to the reduction of electrostatic repulsion between the head groups. The $(C_{16}N)_2O$ and $(C_{18}N)_2O$, however, show abnormally high cmc values suggesting that premicellar aggregates, or other submicellar structures, form at shorter alkyl chain length than in aqueous solution. This is reasonably explained, again, on the basis of reduction of electrostatic repulsion, as are the smaller A_{min} values in.0.1 M NaCl solution versus those in water. However, the A_{min} values for $(C_{16}N)_2O$ and $(C_{18}N)_2O$ are abnormally low.

We can only suggest the possibility that, under these conditions, the longer chain compounds are forming some type of multi-layer structure. Nagarajan (99) describes the formation of bilayer vesicles from dialkyl sodium sulfate at an ionic strength of 0.01 M, and postulates that this formation is conditional upon the presence of two long alkyl chains and significant solution ionic strength.

The cmc/C_{20} values, a measure of the surfactant preference for adsorption relative to micellization, decreases as alkyl chain length, n, increases in both aqueous and NaCl solutions.The discontinuously large decrease when n reaches 16 in NaCl solution is a reflection of the large slopes seen in the $(C_{16}N)_2O$ and $(C_{18}N)_2O$ curves, which may themselves reflect multi-layer formation.

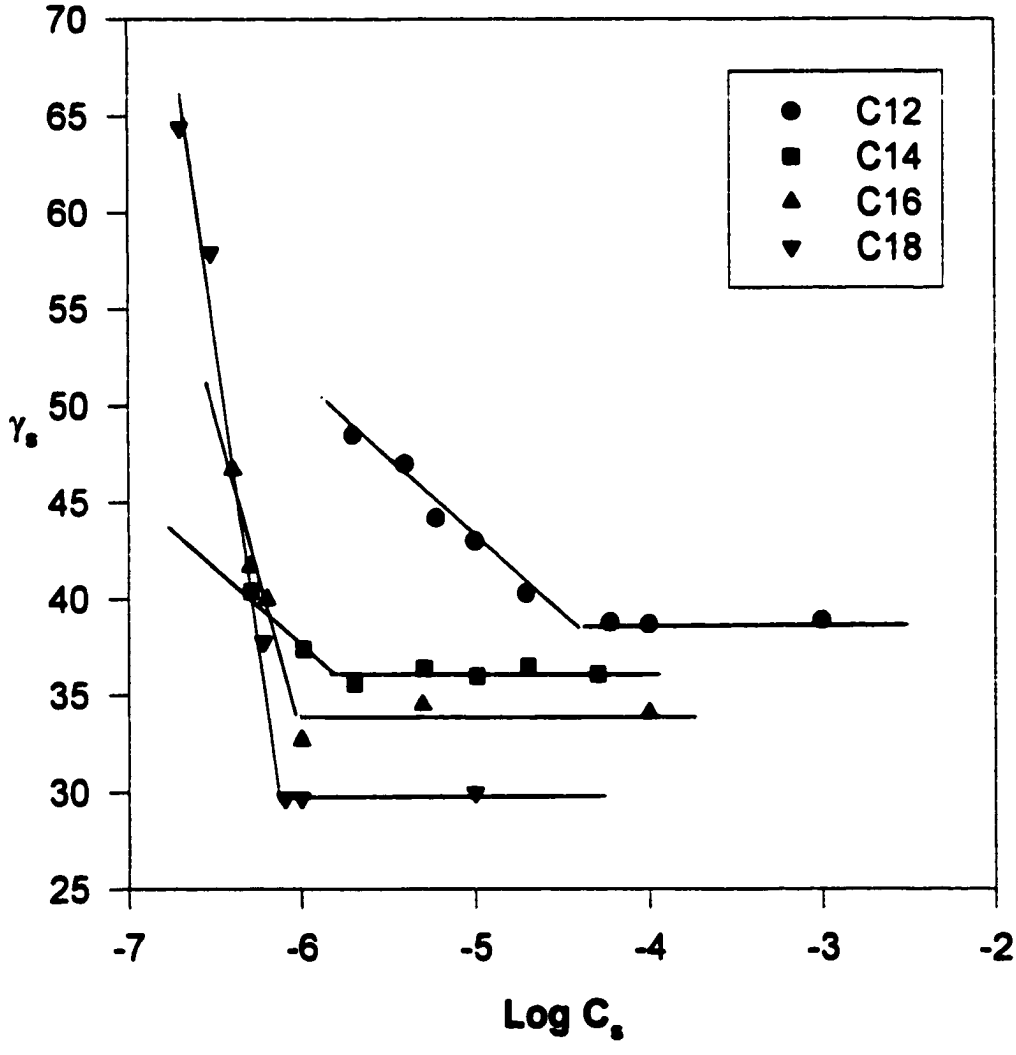

Figure 3. Surface tension vs Log C_s of $(C_nN)_2O$ in 0.1 M NaCl at 25°C.

Table 2 : Surface Properties of $(C_nN)_2O$ in 0.1M NaCl at 25°C

COMPOUND	CMC (mol/L)	γ_{CMC} (mN/m)	pC_{20}	$10^{10}\Gamma_{MAX}$ (mol/cm^2)	A_{MIN} (10^2 nm^2)	CMC/C_{20}
$(C_{12}N)_2O$	3.0×10^{-5}	39	5.96	1.7	95	27
$(C_{14}N)_2O$	1.2×10^{-6}	36	7.30	2.1	79	24
$(C_{16}N)_2O$	9.5×10^{-7}	34	6.5	6.9	24	3.0
$(C_{18}N)_2O$	7.1×10^{-7}	30	6.4	12	14	1.8

IV.1.2 Equilibrium Interfacial Properties of Cationic Gemini Surfactants

Equilibrium interfacial tension curves for the $(C_nN)_2O$, $(C_nN)_2(OH)_2$ and $(C_nN)_2OH$ series, using hexadecane as the hydrocarbon phase, are plotted in Figures 4, 5 and 6. The interfacial properties of the three series of compounds, having different spacer groups between the ionic heads, i.e., ether, hydroxy and dihydroxy linkages are presented in Table 3. Values in parentheses are for the corresponding aqueous solution/air interface. For the hexadecane/water systems, the log cmc versus n functions for the $(C_nN)_2O$ and $(C_nN)_2(OH)_2$ systems are linear until n reaches 18; this parallels the situation in the aqueous system in contact with air (100). For the $(C_nN)_2OH$ compounds in hexadecane/0.1 M NaCl, aberrant behavior begins at n = 14 as it does in the 0.1 M NaCl system in contact with air (27). (Figure 7)

For interfacial data, partitioning of the hexadecane into the bulk surfactant phase must be considered. Approximate partition coefficients (K) for the $(C_nN)_2O$ series, calculated using equation [3], are listed in section IV.1.5. The cmc_t values listed in Table 3 are all greater than the corresponding cmc values in the aqueous/air system due to partitioning. The concentration in the aqueous phase after partitioning is equal to the cmc values in Table 2.

The $(C_{12}N)_2O$, $(C_{14}N)_2O$ and $(C_{16}N)_2O$ compounds have much lower partition coefficient values than the $(C_{18}N)_2O$ compound. The highly displaced $(C_{18}N)_2O$ interfacial curve, in comparison with the only slightly displaced surface tension curve, is due, in part, to partitioning.

However, since K itself may be influenced by sub-micellar structures, it is not possible to separate the effects of partitioning from those of pre-micellar aggregation in this case.

In contrast to the situation at the air/water interface, however, in each of the three series of compounds, A_{min} increases as the number of carbons in the alkyl chain increases, until the point where unusual CMC values are encountered, i.e., at n = 18 in an aqueous system, and n = 14 in 0.1 M NaCl. This increase in A_{min} (for cases where the CMC behaves as expected) reflects the increased intercalation of the hexadecane at the hydrocarbon/water interface as the alkyl chain length increases (43,44). The decrease in A_{min} for the longer chain compounds (also noted in the $(C_nN)_2O$ air/0.1 M NaCl system beginning at n = 14) again suggests the possibility of multi-layer formation.

In hydrocarbon/water systems, pC_{30} values, rather than the pC_{20} values used for air/water systems, are used as a measure of surfactant efficiency because saturation is usually achieved at a surface pressure of 30 dyne/cm (43). For all three series of compounds, the pC_{30} values increase linearly with n, decreasing, however, when the aberrant behavior in area begins, i.e.,A_{min} begins to decrease.

This pattern is repeated for the CMC/C_{30} ratios.The presence of the hydrocarbon phase should reverse the trend seen in air/water systems for the ratio, i.e., it should increase as the alkyl chain length increases. Due to thermodynamic considerations, adsorption is preferred to micellization in hydrocarbon systems (44). An increase in the CMC/C_{30} ratio is seen for the

three systems until it decreases at the point where the parameters mentioned above also begin to decrease. The low CMC/C_{30} ratios for $(C_{18}N)_2O$, $(C_{14}N)_2OH$, and $(C_{16}N)_2OH$, in spite of the abnormally high CMC values for these compounds, indicate a drastic reduction in adsorption efficiency. This, too, is consistent with multi-layer formation.

Table 3 contains interfacial data on two non-aberrant compounds, $(C_{10}N)_2(OH)_2$ and $(C_{12}N)_2(OH)_2$ For both compounds the area per molecule and the cmc values decrease sharply with the addition of an electrolyte, 0.1 M NaBr. Reduction of electrostatic repulsion between head groups is responsible, as it is at an aqueous solution/air interface.

pC_{30} values are shown with pC_{20} values in parentheses for comparison. The values are within experimental error for any particular surfactant system. There appears to be no difference in this efficiency parameter between the aqueous/air and aqueous/hexadecane interface.

cmc_T values, compared to cmc values in parentheses, are approximately the same or slightly higher. This indicates relatively little partitioning into the hexadecane as would be expected for these cationic (polar) compounds.

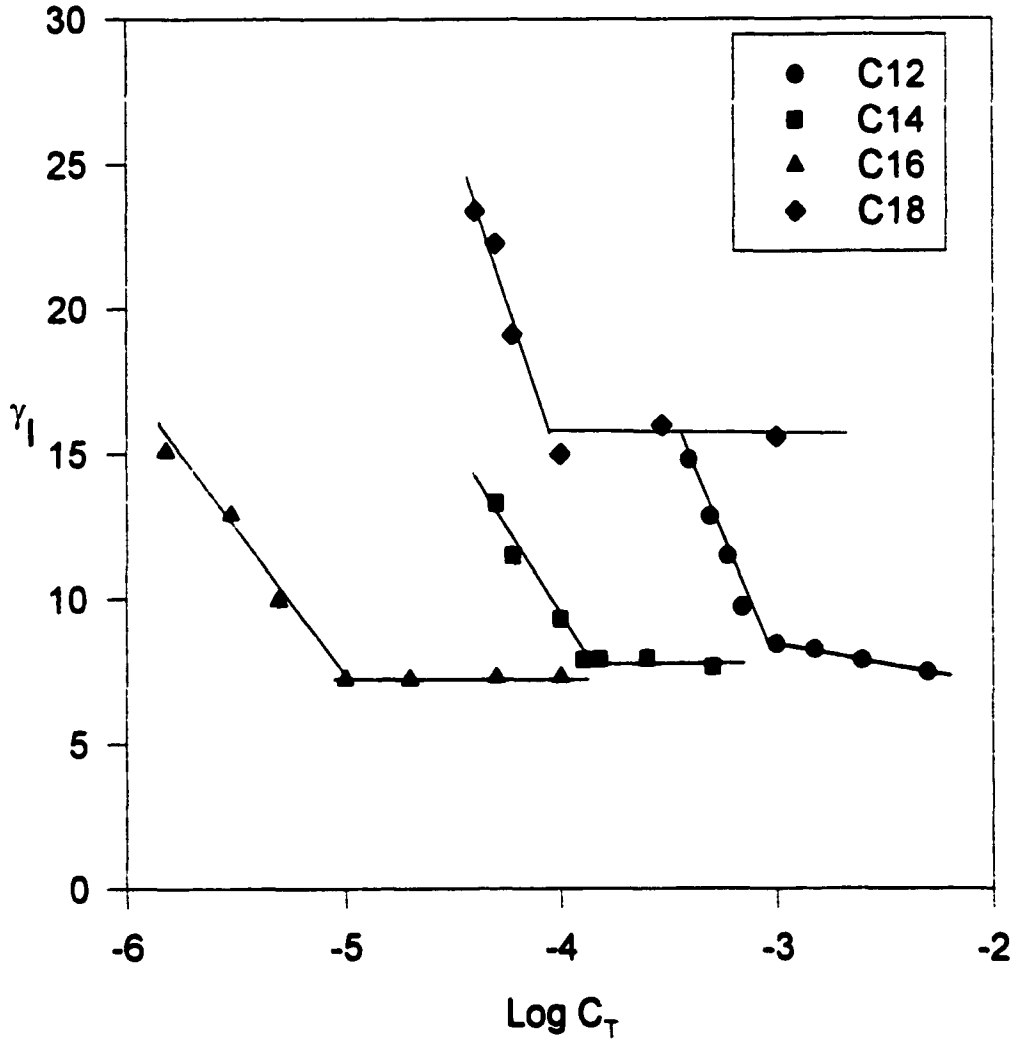

Figure 4. Equilibrium Interfacial tension vs Log C_T of $(C_nN)_2O$ in hexadecane/H_2O system at 25°C.

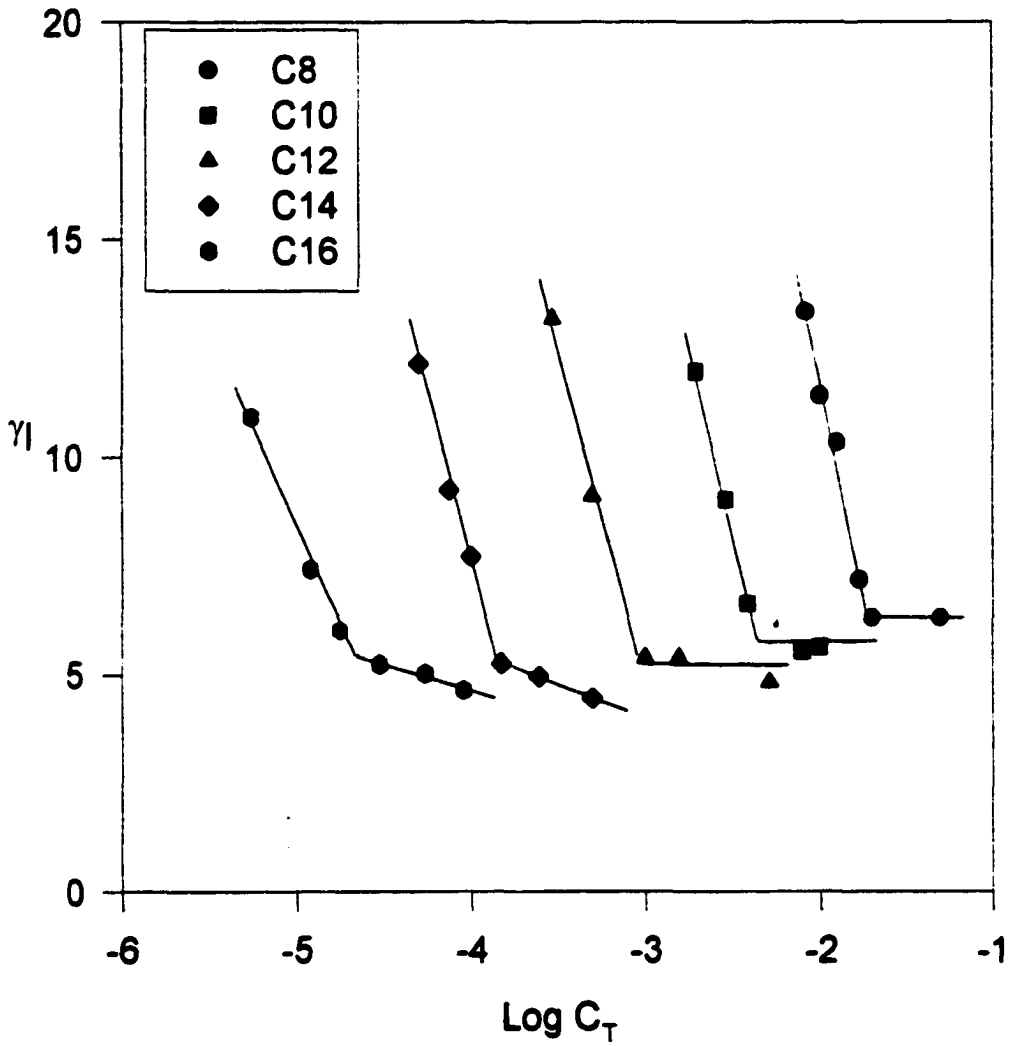

Figure 5. Equilibrium interfacial tension vs Log C_T of $(C_nN)_2(OH)_2$ in hexadecane/H_2O system at 25°C.

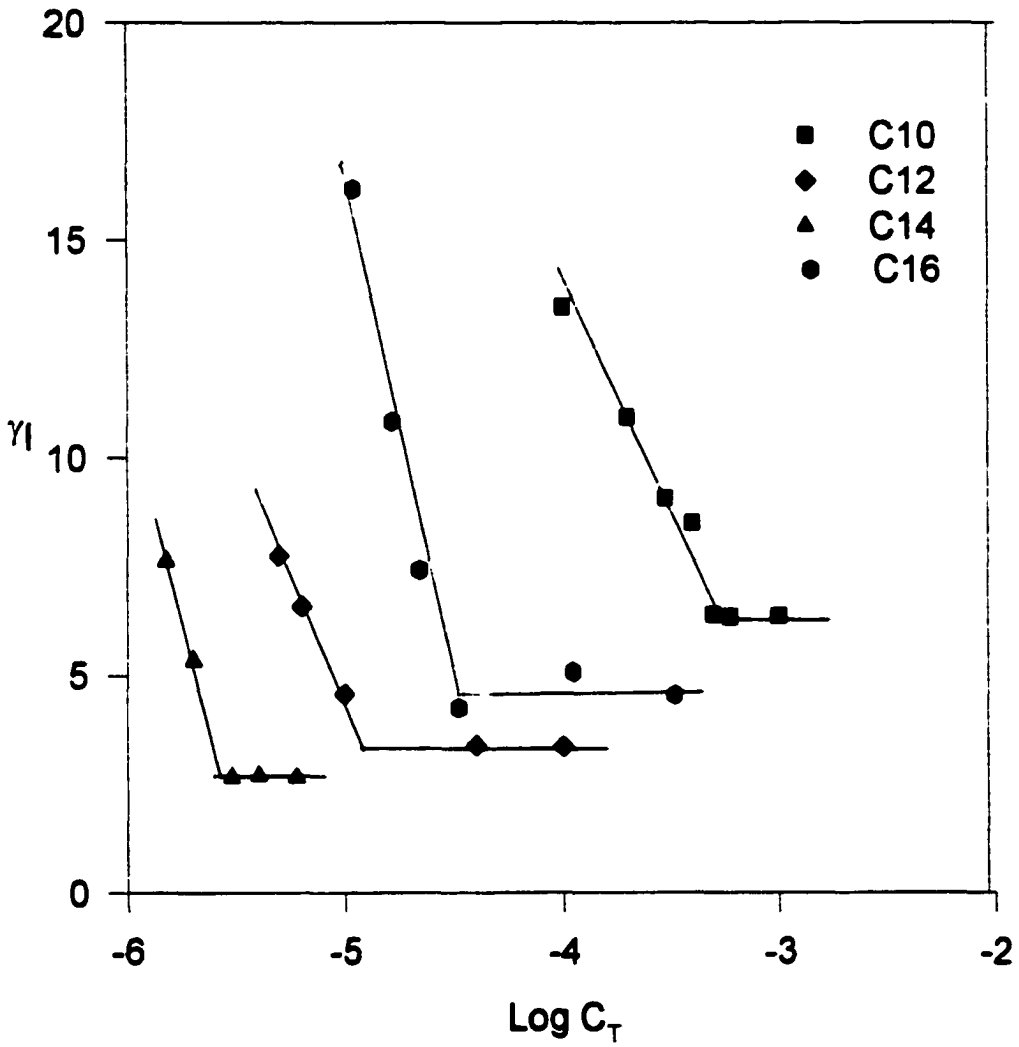

Figure 6. Equilibrium interfacial tension vs Log C_T of $(C_nN)_2OH$ in hexadecane/0.1 M NaCl system at 25°C.

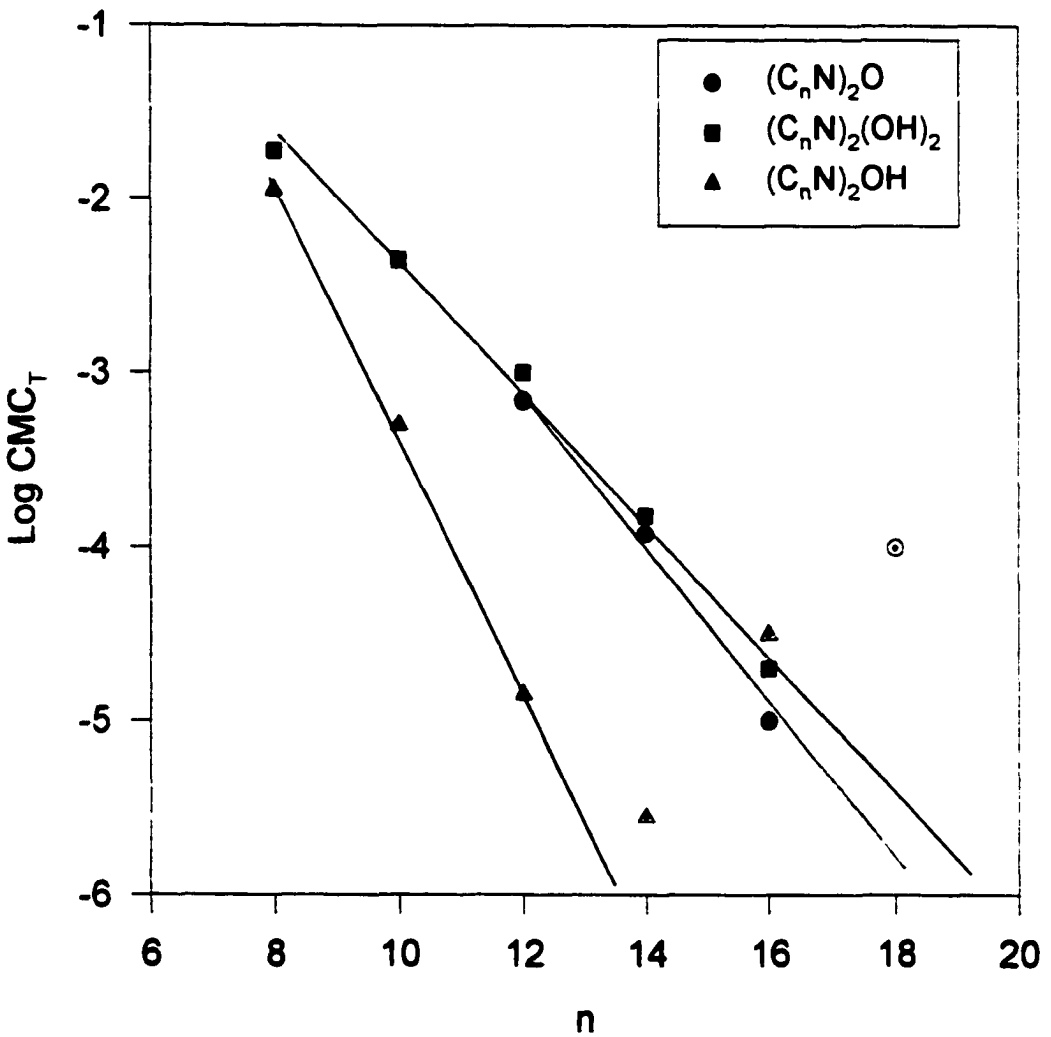

Figure 7. Log CMC_T vs alkyl chain carbon number (n) of cationic gemini surfactants in hexadecane/aqueous systems at 25°C. Aberrant values denoted by open symbols.

Table 3: Interfacial Properties of Cationic Gemini Surfactants at 25°C[a]

COMPOUND	SYSTEM	$CMC_T X10^4$ (mol/L)	γ_{CMC} (mN/m)	pC_{30}	$A_{MIN}{}^b X10^2$ (nm^2)	CMC_T/C_{30}
$(C_{12}N)_2O$	Hexadecane/H_2O	6.9	<8.0	3.72	124	3.6
$(C_{14}N)_2O$	Hexadecane/H_2O	1.2	8.0	5.04	227	13
$(C_{16}N)_2O$	Hexadecane/H_2O	0.10	7.3	6.52	298	33
$(C_{18}N)_2O$	Hexadecane/H_2O	0.91	15	4.12	114	1.2
$(C_8N)_2(OH)_2$	Hexadecane/H_2O	190	6.3	2.52	142	6.3
$(C_{10}N)_2(OH)_2$	Hexadecane/H_2O	45 (37[c])	5.6	3.26 (3.24[c])	179	8.2
$(C_{10}N)_2(OH)_2$	Hexadecane/0.1M NaBr	2.9 (3.3[c])	5.6	4.90 (5.17[c])	87 (75[c])	23
$(C_{12}N)_2(OH)_2$	Hexadecane/H_2O	10 (7.0[c])	5.4	4.16 (3.89[c])	199	14
$(C_{12}N)_2(OH)_2$	Hexadecane/0.1M NaBr	0.042 (0.060[c])	9.2	6.20 (6.47[c])	71 (64[c])	6.7
$(C_{14}N)_2(OH)_2$	Hexadecane/H_2O	1.5 (0.85[c])	<5.0	5.00 (5.50[c])	209	15
$(C_{16}N)_2(OH)_2$	Hexadecane/H_2O	0.20 (0.24)	<4.5	6.20	322	32
$(C_{10}N)_2OH$	Hexadecane/0.1M NaCl	5.0 (4.0[d])	6.4	4.60 (4.60[d])	80 (73[d])	20
$(C_{12}N)_2OH$	Hexadecane/0.1M NaCl	0.14 (0.096[d])	3.4	6.64 (6.04[d])	95 (51[d])	61
$(C_{14}N)_2OH$	Hexadecane/0.1M NaCl	0.028 (0.10[d])	2.7	6.84 (6.22[d])	63 (55[d])	19
$(C_{16}N)_2OH$	Hexadecane/0.1M NaCl	0.32 (0.32[d])	4.7	5.28 (5.10[d])	41 (47[d])	6.1

[a]Values in parentheses are for the corresponding air/aqueous solution systems.

[b]Values for A_{min} were determined using n=3 in the Gibbs equation for the hexadecane/water systems; n=1 for the NaCl systems.

[c] Data from ref (28). [d]Data from ref (27)

IV.1.3 Equilibrium Interfacial Properties of Anionic Gemini Surfactants

Sodium salts of sulfonic acid are the most widely used surfactants in industrial and household detergents (101). Incorporation of additional hydrophilic groups improves solubility in hard water but is accompanied by depression of surface-active properties (102). Surfactants with two or three long-chain alkyl groups and two sulfonate groups have been found to have higher hydrophilicity and enhanced surface properties relative to their conventional analogues (21,94,103).

Anionic gemini surfactants containing three hydrophobic groups and two hydrophilic sulfonate groups are shown in Scheme I.5. Interfacial tension data for $C_8C_1C_8$, $C_{10}C_1C_{10}$ and $C_{10}C_8C_{10}$ are plotted in Figure 8 with interfacial properties tabulated in Table 4. The cmc_T value for $C_{10}C_1C_{10}$ is considerably lower than that of $C_8C_1C_8$ indicating a much greater tendency towards micellization in the former, longer-chain, compound as expected. The degree of difference ($\approx$35 times) is greater than the order of magnitude difference with increase in alkyl chain length for non-aberrant cationic geminis with two alkyl chains. The cmc_T value for the $C_{10}C_8C_{10}$ and $C_{10}C_1C_{10}$ compounds are virtually the same, although the $C_{10}C_8C_{10}$ is the more effective surfactant as indicated by its much lower value of γ_{cmc}. Interestingly, this pattern is directly borne out for the corresponding air/aqueous system. (Values, in parentheses in Table 4 are from reference 104).

cmc_T values in all cases are only slightly higher than the corresponding cmc values for aqueous systems, indicating very little partitioning of the surfactant into the hydrocarbon.

There is a linear increase in pC_{30} value with increased number of carbons in the alkyl chain ,n, as expected. A_{min} increases with n due to increased intercalation of the hydrocarbon; however, the increase in area going from $C_{10}C_1C_{10}$ to $C_{10}C_8C_{10}$ is small. Apparently, increasing the length of the central alkyl chain length from 1 to 8 has little effect on either the area per molecule or the cmc_T.

cmc_T/C_{30} increases because of preference for adsorption relative to micellization. This is the expected pattern in hydrocarbon systems (44).

For purposes of comparison, the most commonly used conventional sulfonic acid salt, $C_{12}H_{25}SO_3^-Na^+$ in 0.1 M NaCl at 25°C has a cmc value of 2.5×10^{-3}; pC_{20} value of 3.4 and A_{min} value of 44 (105).

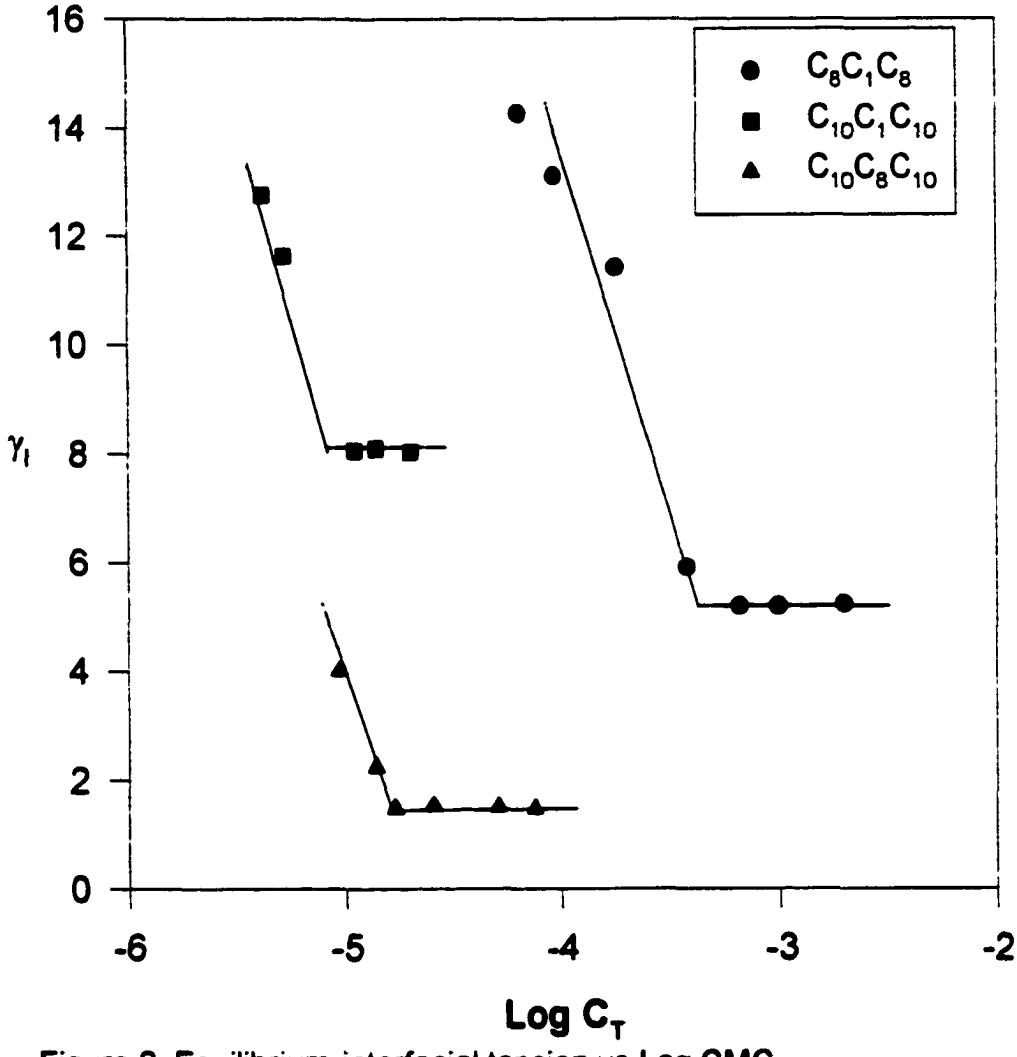

Figure 8. Equilibrium interfacial tension vs Log CMC_T of anionic gemini surfatants in hexadecane/0.1 M NaCl systems at 25°C.

Table 4: Interfacial Properties of Anionic Gemini Surfactants In Hexadecane/0.1 M NaCl at 25°C[a]

COMPOUND	cmc_T X 10^4 (mol/L)	γ_{CMC} (mN/M)	pC_{30}	A_{MIN} X 10^2 (nm^2)	cmc_T/C_{30}
$C_8C_1C_8$	4.0 (2.2[b])	5.2 (31[b])	4.5 (4.8[b])	68 (54[b])	12.6 (15.5[b])
$C_{10}C_1C_{10}$	0.11 (0.072[b])	8.1 (39[b])	6.0 (6.3[b])	82 (85[b])	11.0 (14.4[b])
$C_{10}C_8C_{10}$	0.16 (0.063b)	1.6 (28[b])	6.5 (8.3[b])	86 (111[b])	50 (126[b])

[a]Values in parentheses are for the corresponding air/aqueous solution systems.
[b]Data from *ref* (104)

IV.1.4 Equilibrium Interfacial Properties of Conventional Surfactants

Nonionic surfactants of the type, C_nEO_x where n is the number of carbons in the alkyl chain and x is the number of ethlyene oxide groups, are widely used as emulsifying agents. Consequently, their behavior at the aqueous solution/hydrocarbon interface is of fundamental interest.

The amine oxide, $C_{14}N(CH_3)_2O$, is a zwitterionic surfactant of interest for its anti-microbial activity which is dependent on its ability to form aggregates(24).

Interfacial tension data are plotted in Figure 9. Interfacial properties are listed in Table 5.

For the nonionic C_nEO_x compounds, partitioning of the surfactant into the hydrocarbon phase is a significant factor, in contrast to the situation for the anionic or cationic geminis discussed thusfar. cmc_T values in Table 5 represent apparent (or uncorrected) critical micelle concentrations. Corrected values would require calculation of the partition coefficient by an independent method, as by UV absorption studies in alkyl pyrrolidones (106).

The length of the ethylene oxide group is the major factor in determining degree of partitioning. When the hydrophilic EO group is very short, e.g. x = 2, the partition coefficient is several orders of magnitude greater than for x = 7-8, for the same number of alkyl carbon atoms. For the compounds shown in Figure 9, it is important to compare only curves representing the same aqueous system: pure water or 0.1 M NaCl.

For $C_{12}EO_7$ and $C_{12}EO_8$ in hexadecane/0.1 M NaCl, cmc_T and A_{min} values are virtually the same. In hexadecane/H_2O (43) there is no change in either

parameter indicating lack of partitioning and lack of intercalation of hydrocarbon. The $C_{12}EO_7$ in hexadecane/0.1 M NaCl appears to be a more effective surfactant than the $C_{12}EO_8$ in the same system, having a lower value of γ_{cmc}.

The $C_{12}EO_2$ and $C_{16}EO_8$ in hexadecane/H_2O have cmc's which are highly displaced due to partitioning. Partitioning is the result of small number of EO groups in the first case and large number of alkyl carbons in the second. That the $C_{12}EO_2$ is highly soluble in the hexadecane can be seen from the much larger value of A_{min} in this system versus that for the aqueous solution/air interface. The smaller increase in A_{min} at the hydrocarbon interface for $C_{16}EO_8$ reflects its smaller partition coefficient.

There is no partitioning of the amine oxide into the hydrocarbon phase, and the A_{min} values at the aqueous solution/air and aqueous solution/hexadecane interface are equal

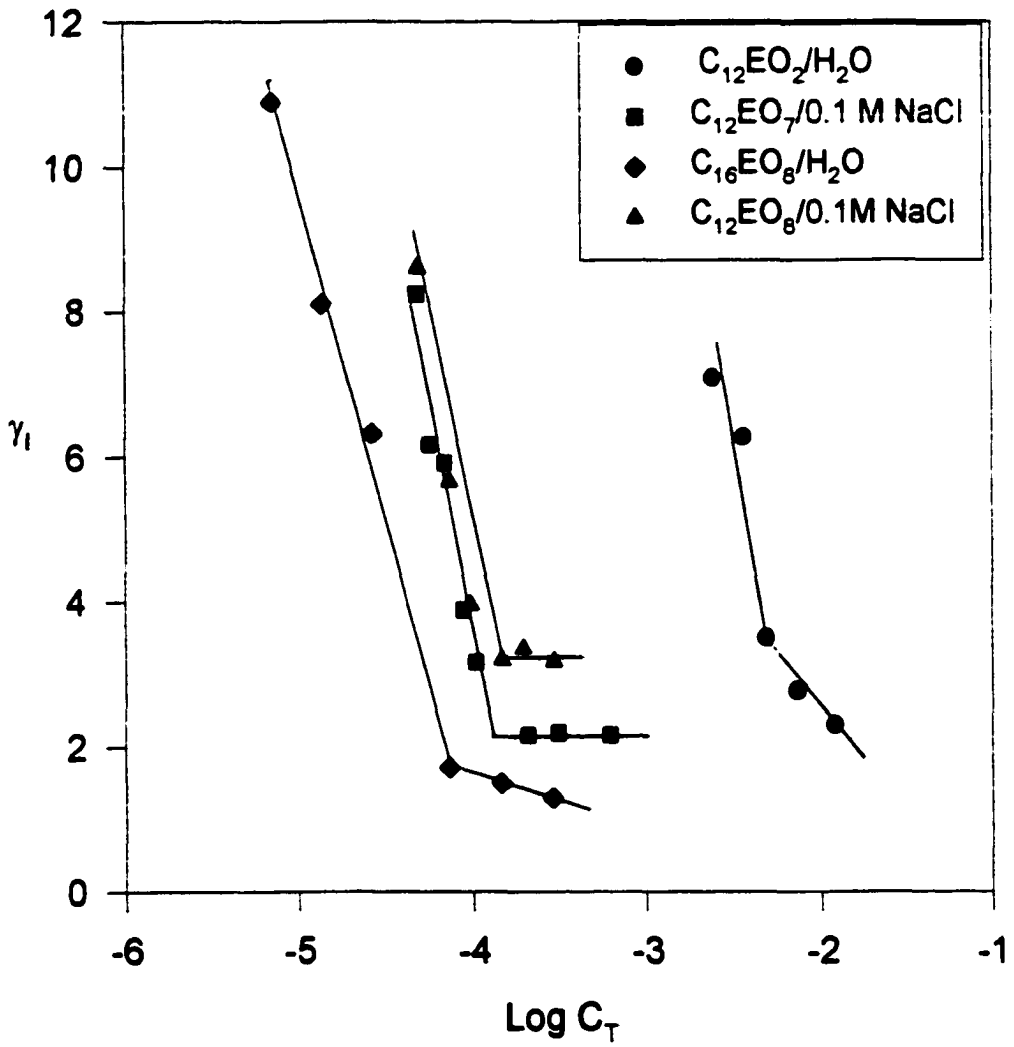

Figure 9. Equilibrium interfacial tension vs Log C_T of C_nEO surfactants in hexadecane at 25°C.

Table 5: Interfacial Properties of Conventional Surfactants at 25°C[a]

COMPOUND	SYSTEM	CMC_T X 10^4 (mol/L)	γ_{CMC} (mN/m)	pC_{30}	A_{MIN} X 10^2 (nm^2)	CMC_T/C_{30}
$C_{12}EO_2$	Hexadecane/H_2O	47 (0.33[b])	3.5	3.3	53 (35[b])	9.4 (4.2[b])
$C_{12}EO_7$	Hexadecane/0.1 M NaCl	1.1 (0.87[c])	2.2	5.2 (5.3[c])	66 (63[c])	17 (19[c])
$C_{12}EO_8$	Hexadecane/H_2O	1.0[d] (1.1[b])	3.4[d]	5.2[d] (4.5[b])	63[d] (66[b])	16[d] (3.3[b])
$C_{12}EO_8$	Hexadecane/0.1 M NaCl	1.1 (1.0[c])	3.6	5.1 (5.2[c])	63 (64[c])	14 (18[c])
$C_{16}EO_8$	Hexadecane/H_2O	0.40 (0.035[b])	2.0	5.4	55 (48[e])	10
$C_{14}N(CH_3)_2O$ pH = 5.8	Hexadecane/0.1 M NaCl	0.89 (1.0[c])	2.2	5.0 (5.2[c])	48 (50[c])	8.9 (16[c])

[a]Values in parentheses are for the corresponding air/aqueous solution systems.
[b]Data from ref (107)
[c]Data from ref (104)
[d]Data from ref (43)
[e]Data from ref (108)

IV.1.5 Partition Coefficients

Approximate partition coefficients (K) for gemini and conventional surfactants are listed in Table 6.

One condition for disregarding partition coefficient values is that $K\Phi < 1$ where Φ is the volume ratio of hydrocarbon to aqueous phase (43). For these systems, $\Phi = 0.01$ for cationic geminis and 0.025 for all other surfactants. The value of $K\Phi$ is less than 1 for all geminis except $(C_{18}N)_2O$, and partitioning is insignificant. In the case of $(C_{18}N)_2O$ it is not possible to separate the effects of partitioning and pre-micellar aggregation on the displacement of the cmc. For non-ionic compounds, only $C_{12}EO_2$ and $C_{16}EO_8$ show significant partitioning.

Values of K for the $(C_nN)_2(OH)_2$ in H_2O and $(C_nN)_2OH$ in 0.1 M NaCl show the expected increase with n. It must be stressed that these values of K are small. Introduction of 0.1 M NaBr into the $(C_nN)_2(OH)_2$ results in a value of K=0.

Table 6: Approximate Partition Coefficient Values, K, at 25°C.

SURFACTANT	SYSTEM	K (=C_H/C_W)
$(C_{12}N)_2O$	Hexadecane/H_2O	3×10^1
$(C_{14}N)_2O$	Hexadecane/H_2O	1×10^2
$(C_{16}N)_2O$	Hexadecane/H_2O	5×10^1
$(C_{18}N)_2O^*$	Hexadecane/H_2O	6×10^3
$(C_{10}N)_2(OH)_2$	Hexadecane/H_2O	2×10^1
$(C_{12}N)_2(OH)_2$	Hexadecane/H_2O	4×10^1
$(C_{14}N)_2(OH)_2$	Hexadecane/H_2O	8×10^1
$(C_{10}N)_2(OH)_2$	Hexadecane/0.1 M NaBr	~0
$(C_{12}N)_2(OH)_2$	Hexadecane/0.1 M NaBr	~0
$(C_8N)_2OH$	Hexadecane/0.1 M NaCl	2×10^1
$(C_{10}N)_2OH$	Hexadecane/0.1 M NaCl	3×10^1
$(C_{12}N)_2OH$	Hexadecane/0.1 M NaCl	5×10^1
$C_8C_1C_8$	Hexadecane/0.1 M NaCl	3×10^1
$C_{10}C_1C_{10}$	Hexadecane/0.1 M NaCl	2×10^1
$C_{10}C_8C_{10}$	Hexadecane/0.1 M NaCl	6×10^1
$C_{12}EO_2$	Hexadecane/H_2O	6×10^3
$C_{12}EO_7$	Hexadecane/0.1 M NaCl	1×10^1
$C_{12}EO_8$	Hexadecane/0.1 M NaCl	~0
$C_{16}EO_8$	Hexadecane/H_2O	4×10^2
$C_{14}N(CH_3)_2O$	Hexadecane/0.1 M NaCl	~0

IV.1.6 Dynamic Interfacial Properties of Cationic and Anionic Geminis

Dynamic interfacial tension data for the anionic and cationic gemini surfactants were collected by the drop volume method, and fit to the equations known to describe dynamic surface tension data obtained by the maximum bubble pressure method (45-50). Data were fit to both the linear and exponential forms of the equations; residuals and coefficients of variation show that the equations adequately describe the dynamic interfacial as well as dynamic surface phenomena. Coefficients of variation of 5-10% for n_d indicate that this parameter is better fit to the empirical equations than the t_i parameter. The coefficient of variation for t_i is in the range 10-30%, with poorest fit at very short times.

It has been demonstrated (45) that the t_i parameter decreases rapidly with surfactant concentration, while n_d remains relatively invariant. For the anionic gemini surfactant, C_{10}-O-C_{10}, the results are shown in Table 7. The dynamic interfacial tension curve for this compound is Figure 10.

Table 7. Dynamic Interfacial Tension Parameters for C_{10}-O-C_{10} in Hexadecane/ 0.1 M NaCl at 25°C.

C_s (M)	t_i (s)	n_d
2.0 x 10-5	12.7	1.20
1.0 x 10-4	1.2(0.29)	1.30(1.08)
1.0 x 10-3	0.13	1.32

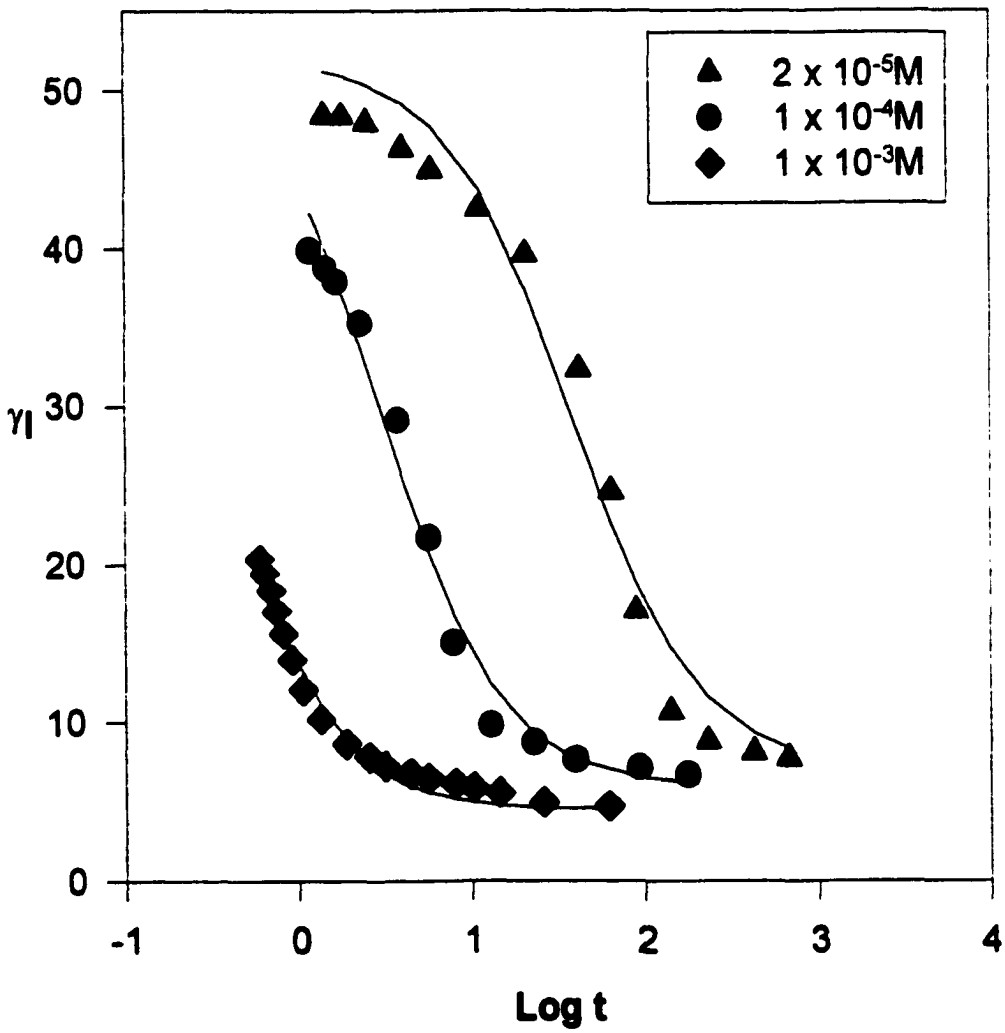

Figure 10. Dynamic interfacial tension vs Log t of C_{10}-O-C_{10} in hexadecane/0.1 M NaCl at 25°C. Solid lines fit to equation [10].

Values shown in parentheses in Table 7 are for the aqueous solution/air interface (46). The values are within experimental error and do not indicate any difference between the surface and interfacial systems.

The n_d and t_i parameters for the cationic gemini surfactant $(C_{12}N)_2(OH)_2$ as a function of surfactant concentration are listed in Table 8 The corresponding dynamic interfacial curve is Figure 11.

Table 8. Dynamic Interfacial Tension Parameters for $(C_{12}N)_2(OH)_2$ in Hexadecane/ H_2Oat 25°C.

C_s (M)	t_i (s)	n_d
2.0×10^{-5}	6.0	1.21
8.0×10^{-5}	4.4	1.02
3.0×10^{-4}	0.052	0.73
1.0×10^{-3}	0.00041	0.54

As with the C_{10}-O-C_{10} surfactant, there is a rapid decrease in t_i with concentration; the $(C_{12}N)_2(OH)_2$, however, shows a linear decrease of n_d with increase in C_s.

The n_d parameter is a measure of energy differences between adsorption and desorption and increases with the hydrophobic character of the surfactant (46).

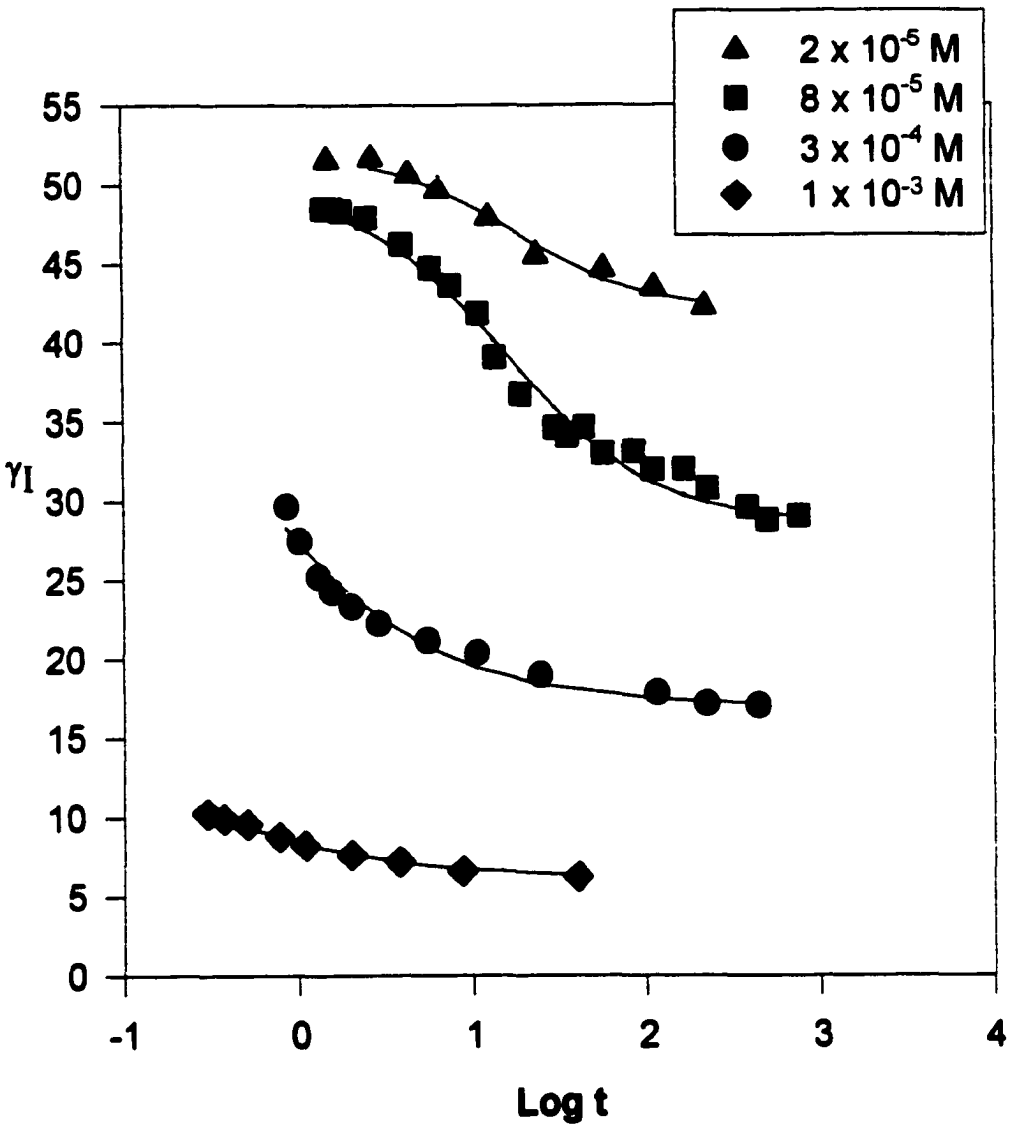

Figure 11. Dynamic interfacial tension vs Log t of $(C_{12}N)_2(OH)_2$ in hexadecane/H_2O at 25°C. Solid lines fit to equation [10].

For the $(C_nN)_2(OH)_2$ series it increases from 0.26 to 2.15 as the number of alkyl carbon atoms increases from 10 to 14. A concurrent increase in t_i with hydrophobicity is the result of tighter packing at the interface. Data for this series are shown in Table 9. Figure 12 is the corresponding interfacial tension curve.

Table 9. Dynamic Interfacial Tension Parameters for $(C_nN)_2(OH)_2$ at $C_s = 3.0 \times 10^{-4}$ M in Hexadecane/ H_2O at 25°C.

n	t_i (s)	n_d	A_{eq}
10	0.0094	0.26	179
12	0.052	0.73	199
14	2.85	2.15	209

At the air/aqueous interface, area per molecule, A, is inversely proportional to t_i.(46) This is explained on the basis that A decreases with the same factors which increase hydrophobic character, i.e., increase in alkyl carbon chain length. However, in the hexadecane/H_2O system, A is found to increase with the number of carbons, reflecting increased intercalation of the hexadecane at the interface. Hence, t_i can be expected to increase as well. In Table 9, area per molecule, A_{eq}, is the equilibrium value obtained by the spinning drop technique.

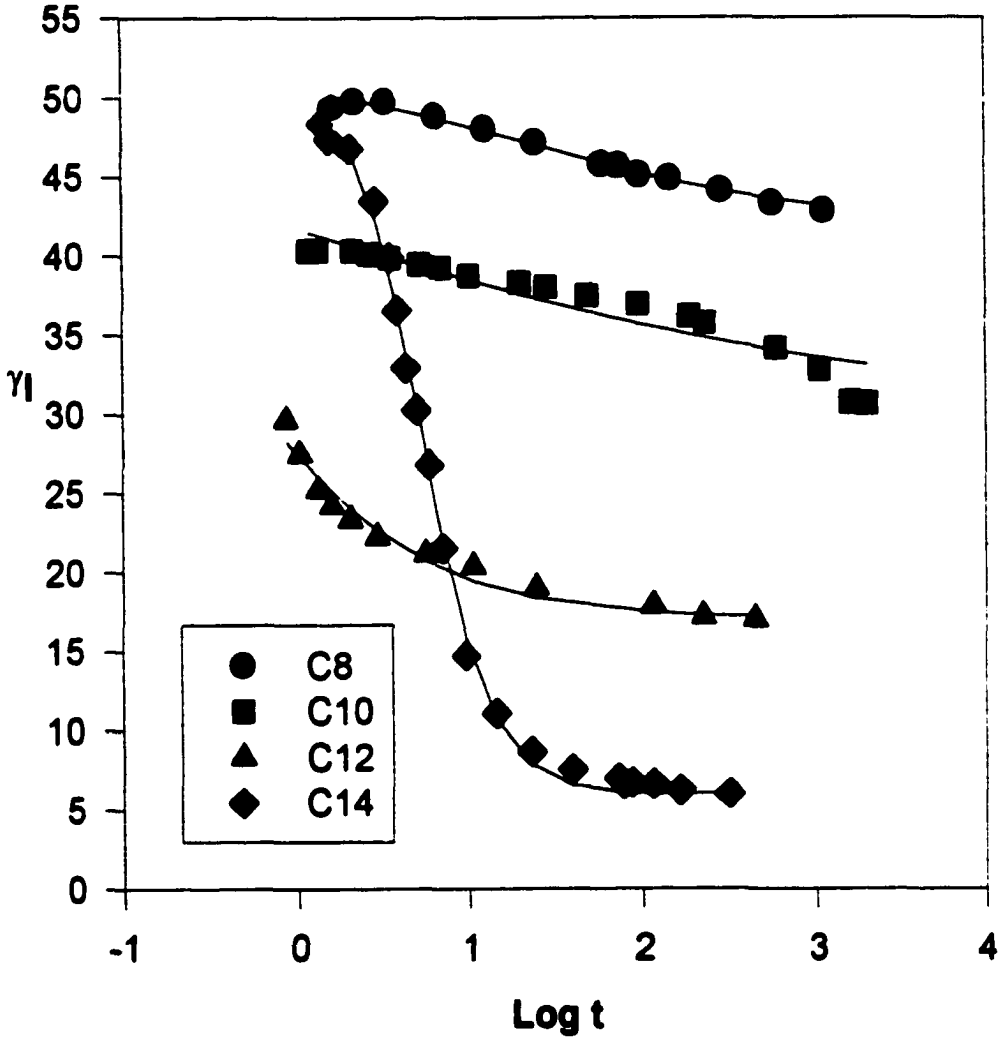

Figure 12. Dynamic interfacial tension vs Log t of $(C_nN)_2(OH)_2$ at C_s=3.0 x 10^{-4} M in hexadecane/H_2O at 25°C. Solid lines fit to equation [10].

It was noted earlier that a particular instrumental limitation of this system prevents a complete dynamic surface tension curve (Scheme II.1) from being obtained at some surfactant concentrations. Since n does not vary much with surfactant concentration, it should be possible to obtain a value of this parameter from a surfactant concentration which gives a full sigmoidal curve. One could then use this as a fixed parameter to synthesize the short-time portion of a non-sigmoidal curve and finally, obtain t_i for that system.

Again, it is possible to obtain meso-equilibrium using slow flow rates. Using the equilibrium values obtained by the spinning drop method, at a particular surfactant concentration, we may verify that the dynamic system has indeed approached equilibrium.

Having concluded that the dynamic equations and physical parameters derived for the aqueous solution/air interface are valid at the aqueous solution/hydrocarbon interface, we could use this dynamic system to study the aberrant behavior noted in long-chain cationic gemini surfactants. Studies of diffusion coefficients and t_i parameters for aberrant and non-aberrant systems, at various concentrations, should provide further evidence of pre-micellar aggregation. For example, molecules with small area per molecule pack more closely at the interface than larger molecules. These smaller molecules will have longer t_i. Does t_i change significantly where the A_{min} trend reverses, i.e., when an aberrant cmc is observed? It should therefore be possible to explain discrepancies in dynamic parameters on the basis of aberrant aggregation behavior.

IV.2 Aggregation Behavior of Cationic Gemini Surfactants

In an effort to confirm the cmc values obtained by surface tension techniques and to elucidate the morphology of these compounds, we have employed steady-state and dynamic fluorescence techniques.

IV.2.1 Steady State Fluorescence

The fluorescence probes pyrene and pyrene-3-carboxaldehyde exhibit emission behavior that is influenced by the polarity of their environment (39,41,42,85). Emission spectra may be used to speculate on the probe's environment, i.e., on the morphology of the surfactant aggregate, as well as for cmc determination.

cmc determinations with pyrene and pyrene-3-carboxaldehyde validate those from interfacial tension experiments and show that the probe does not influence the cmc; hence, those concentration regions considered to be pre-micellar aggregation areas are not shifted by the presence of the probe.

For pyrene-3-carboxaldehyde, a plot of maximum wavelength of emission (λ_{max}) versus log surfactant concentration displays a break at the cmc. Figure 13 shows such plots for the $(C_nN)_2O$ series; some members of the series have been omitted for clarity. All curves show λ_{max} = 470 nm at low surfactant concentration indicating that the monomeric form does not interact with the probe. A sigmoidal shape for the curves is evident, although the $(C_{20}N)_2O$ curve is incomplete due to loss of solubility at higher concentrations. The $(C_{12}N)_2O$ and $(C_{18}N)_2O$ plots level off at wavelengths of 443nm and 435 nm respectively; the blue-shifted value for

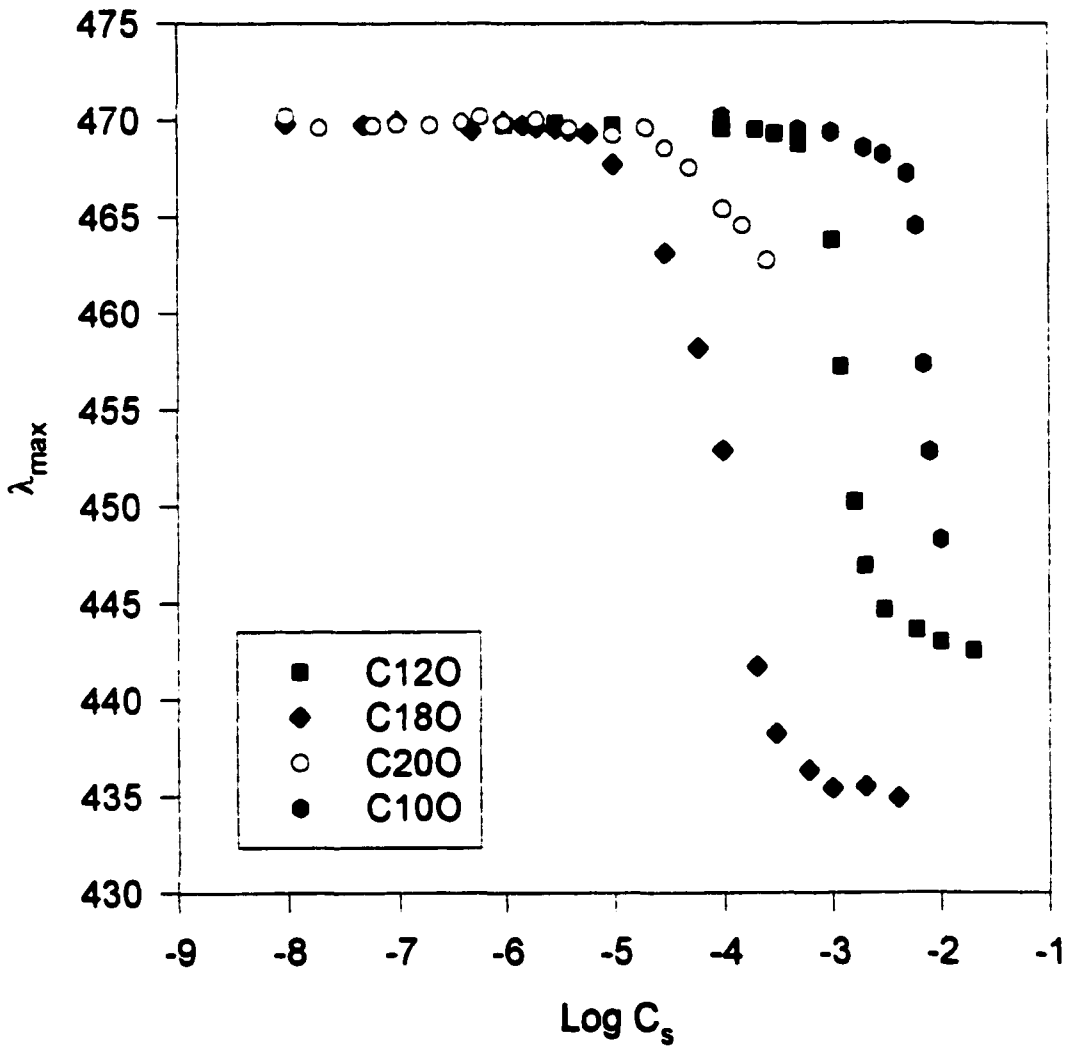

Figure 13. Wavelength of maximum fluorescence emission of pyrenecarboxaldehyde vs Log C_s of $(C_nN)_2O$ in H_2O at 25°C.

the $(C_{18}N)_2O$ representing the more hydrophobic nature inside the micelles with longer alkyl chains. Even for the long-chain compounds, the interior of the micelles is more polar than a pure hydrocarbon solvent such as heptane which has peaks around 400-420 nm (41).

The decrease in CMC values with alkyl chain length repeats the pattern seen with surface tension data, i.e., the $(C_{18}N)_2O$ CMC is somewhat larger than expected and the $(C_{20}N)_2O$ is much larger, having its break point occurring between the $(C_{12}N)_2O$ and $(C_{18}N)_2O$ compounds.

The slope of the sigmoidal curves becomes progressively more gentle as the alkyl chain length increases. It may be useful to consider the physical significance of this trend. We have plotted the λ_{max} versus log C curves for the conventional trimethylamonium bromide surfactants for comparison (Figures 14, 15 and 16). Note that the data for $C_{16}(CH_3)_3Br$ (CTAB) were taken from the literature (39), whereas data for $C_{12}(CH_3)_3Br$ (DTAB) and $C_{14}(CH_3)_3Br$ (TTAB) are from our laboratory.

At low surfactant concentration, the conventional and gemini surfactants show the same λ_{max} plateau at 470 nm indicative of the pyrene-3-carboxaldehyde in an aqueous environment. The second plateau, at which the probe is entirely within the micelle, is reached at slightly lower λ_{max}, i.e., is blue-shifted, for the gemini surfactants. This reflects the more hydrophobic character inside the two-chained gemini micelle. The extent of curvature between the two plateaus is quite different for the conventional and gemini series. While the slope at the inflection point remains relatively constant for the DTAB, TTAB and CTAB series,

it becomes progressively smaller for $(C_{12}N)_2O$, $(C_{14}N)_2O$ and $(C_{16}N)_2O$. In order to compare the slope at the inflection point for a $(C_nN)_2O$ surfactant and its monoquaternary analogue, it is necessary to consider that the concentration change (ΔC) is occurring in different concentration regions, i.e., the CMC's for the two compounds differ by two orders of magnitude. Division of ΔC by the CMC value yields a normalized slope which permits comparison. In Figure 17 a plot of the normalized slope versus n for the $(C_nN)_2O$ geminis shows a decreasing (less negative) slope which appears to level off as n reaches 16 carbons.

The more gradual slopes represent a greater surfactant concentration range between the two plateaus. The probe is experiencing a variety of environments between totally aqueous at low concentration and totally hydrophobic (micellar) at high concentrations. Possibly the number, and/or types, of submicellar structures is increasing with chain length until a maximum is reached. This would explain the leveling off at n = 18; the length at which aberrant surface tension behavior is encountered. Conversely, the conventional surfactants exhibit slopes that are independent of the alkyl chain length (Table 10). Further, for short alkyl chain lengths, the gemini slopes are in the same range as for conventional compounds.

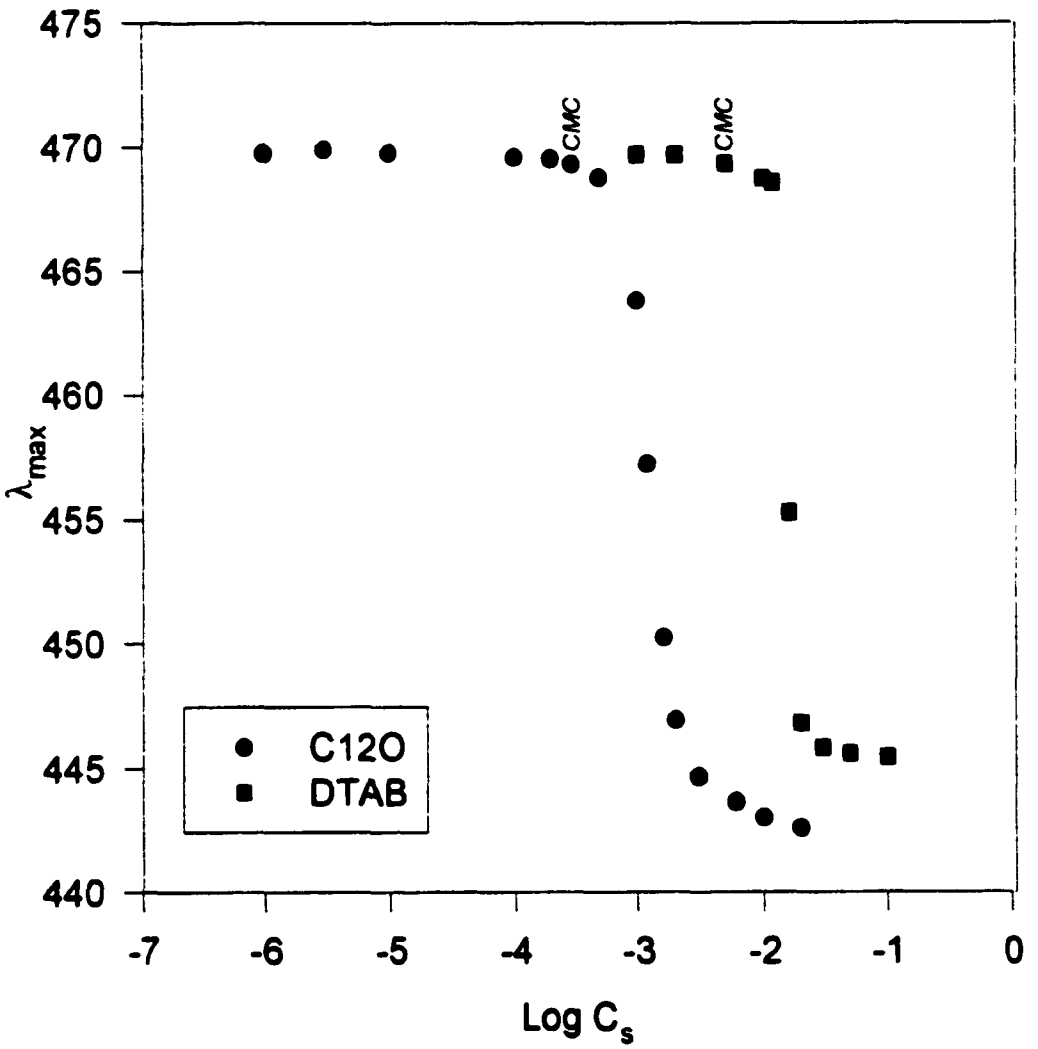

Figure 14. Wavelength of maximum fluorescence emission of pyrenecarboxaldehyde vs Log Cs in H2O at 25°C.

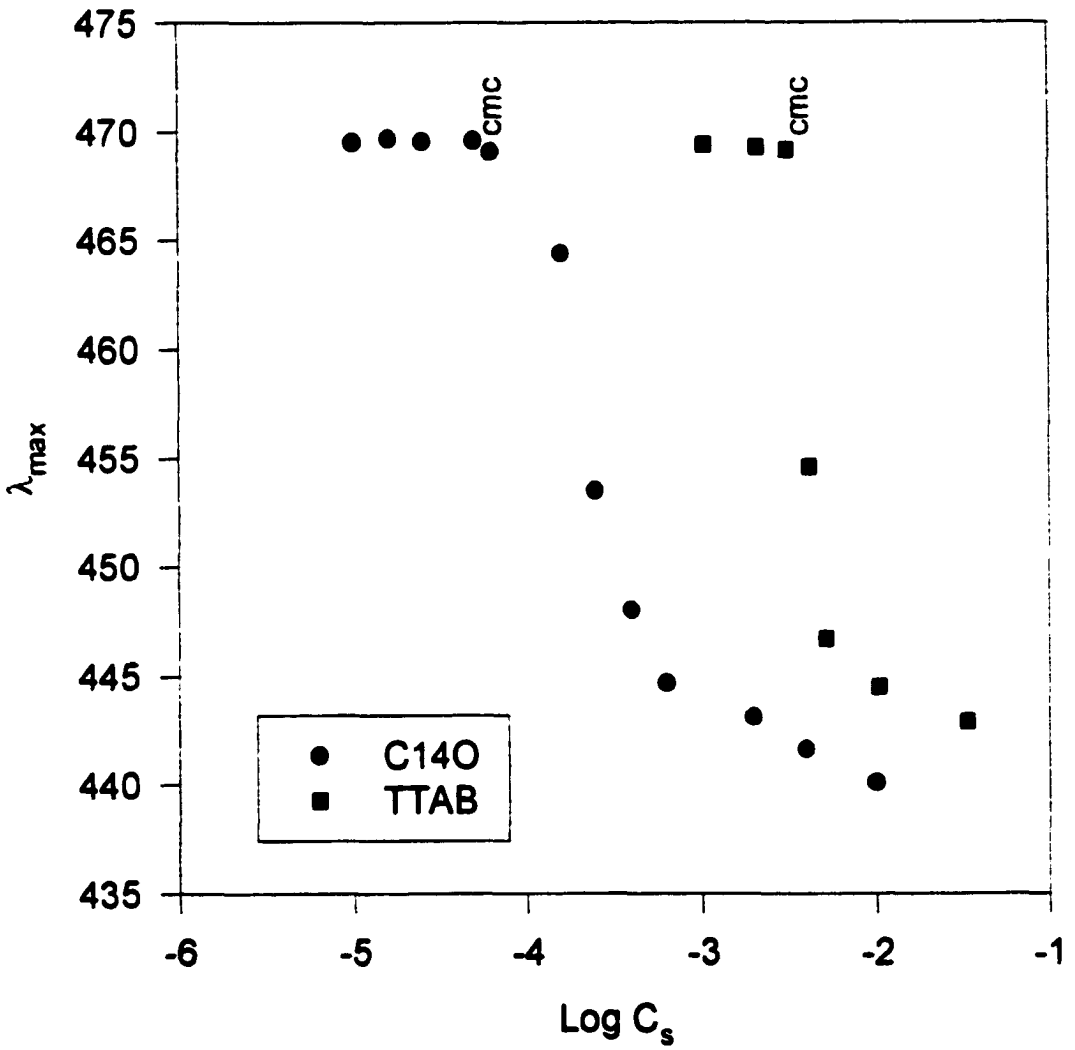

Figure 15. Wavelength of maximum fluorescence emission of pyrenecarboxaldehyde vs Log C_s in H_2O at 25°C.

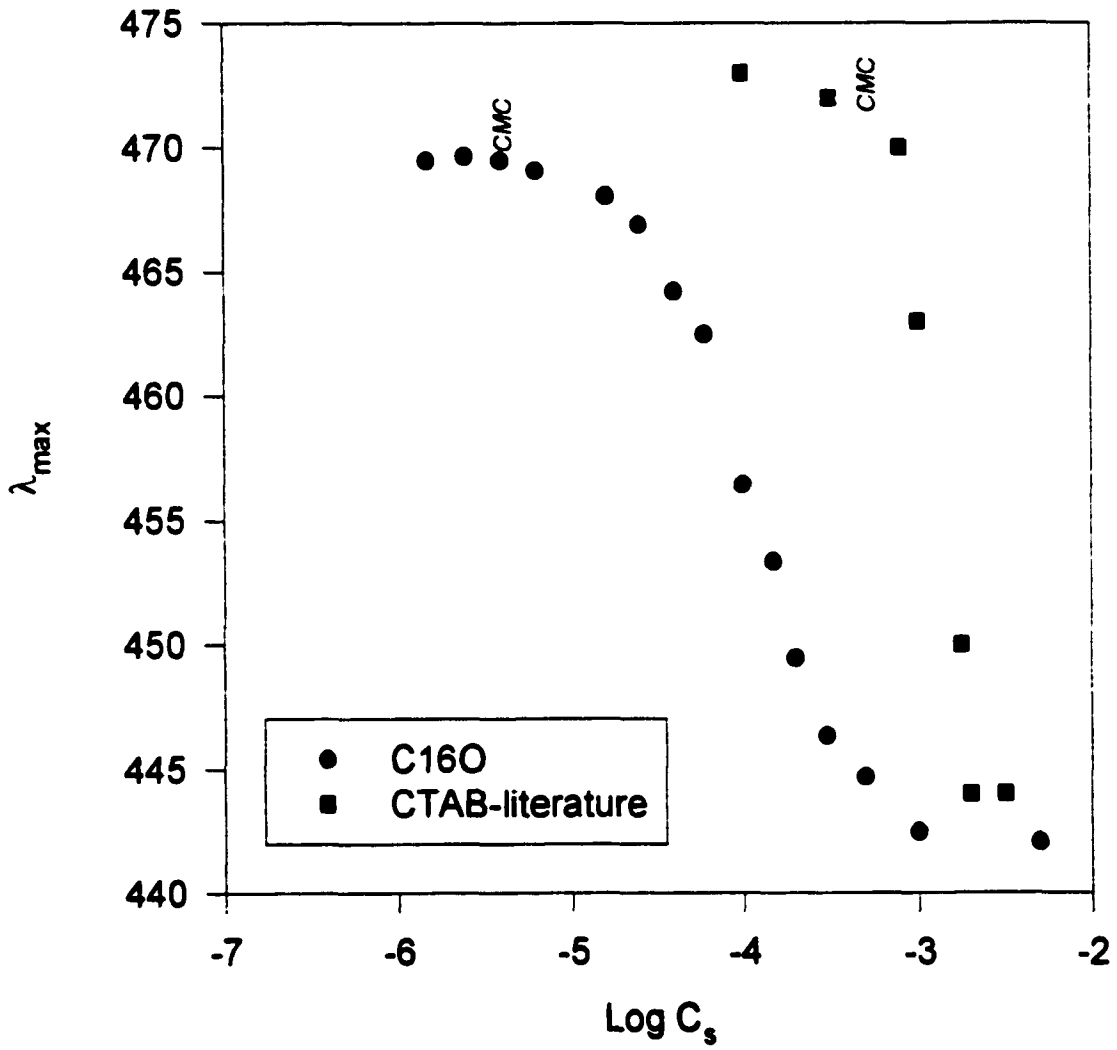

Figure 16. Wavelength of maximum fluorescence emission of pyrenecarboxldehyde vs Log C_s in H_2O at 25°C.

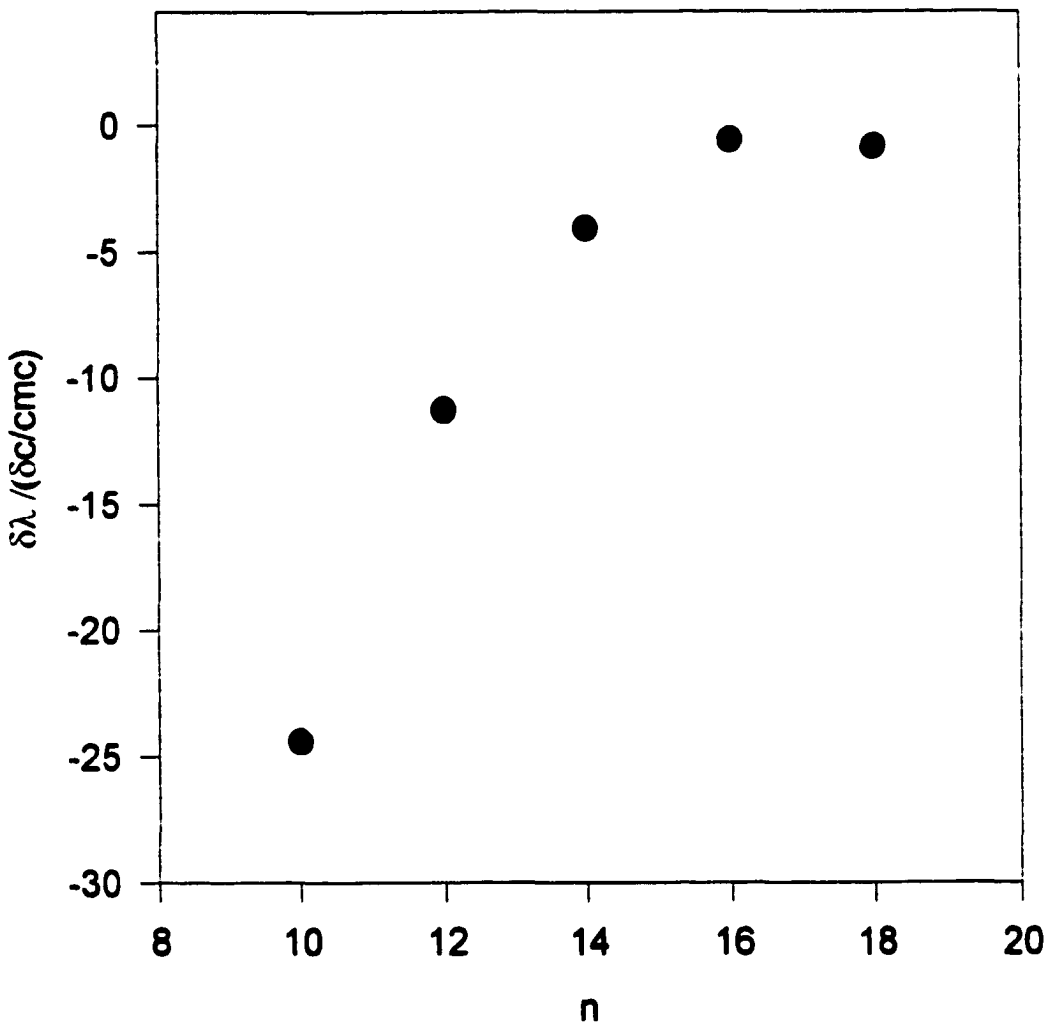

Figure 17. Normalized slope of fluorescence emission maxima versus surfactant concentration curves vs alkyl carbon number of $(C_nN)_2O$ in H_2O at 25^0C. Slope is taken at inflection point.

Table 10. Normalized slopes of λ_{max} vs log C_s curves for Gemini and Conventional surfactants

n=# OF CARBONS	GEMINI $(C_nN)_2O$	CONVENTIONAL $C_n(CH_3)_3Br$
10	-24.4	
12	-11.3	-32
14	-4.1	-41
16	-0.61	-24
18	-0.88	

The quantum yield of pyrene-3-carboxaldehyde emission is also influenced by the polarity of its environment (41). The fluorescence intensity is greatest in polar environments and may be expected to drop at the cmc. Plotting intensity versus surfactant concentration therefore provides an alternative parameter to λ_{max} for monitoring the environment.

Figures 18, 19 and 20 show plots of the fluorescence intensity at the maximum of the emission peak versus gemini surfactant concentration. The wavelength position, λ_{max}, is plotted on an additional y-axis for reference.

The non-aberrant $(C_{12}N)_2O$ compound in Figure 18 shows a linear decrease of fluorescence intensity with increasing surfactant concentration until the cmc, (as indicated by the break-point in the λ_{max} curve) is reached. At that surfactant concentration, the intensity drops sharply and levels off. The level plateau at high surfactant concentrations indicates a totally micellized probe when either the peak position or peak intensity is used as the polarity parameter.

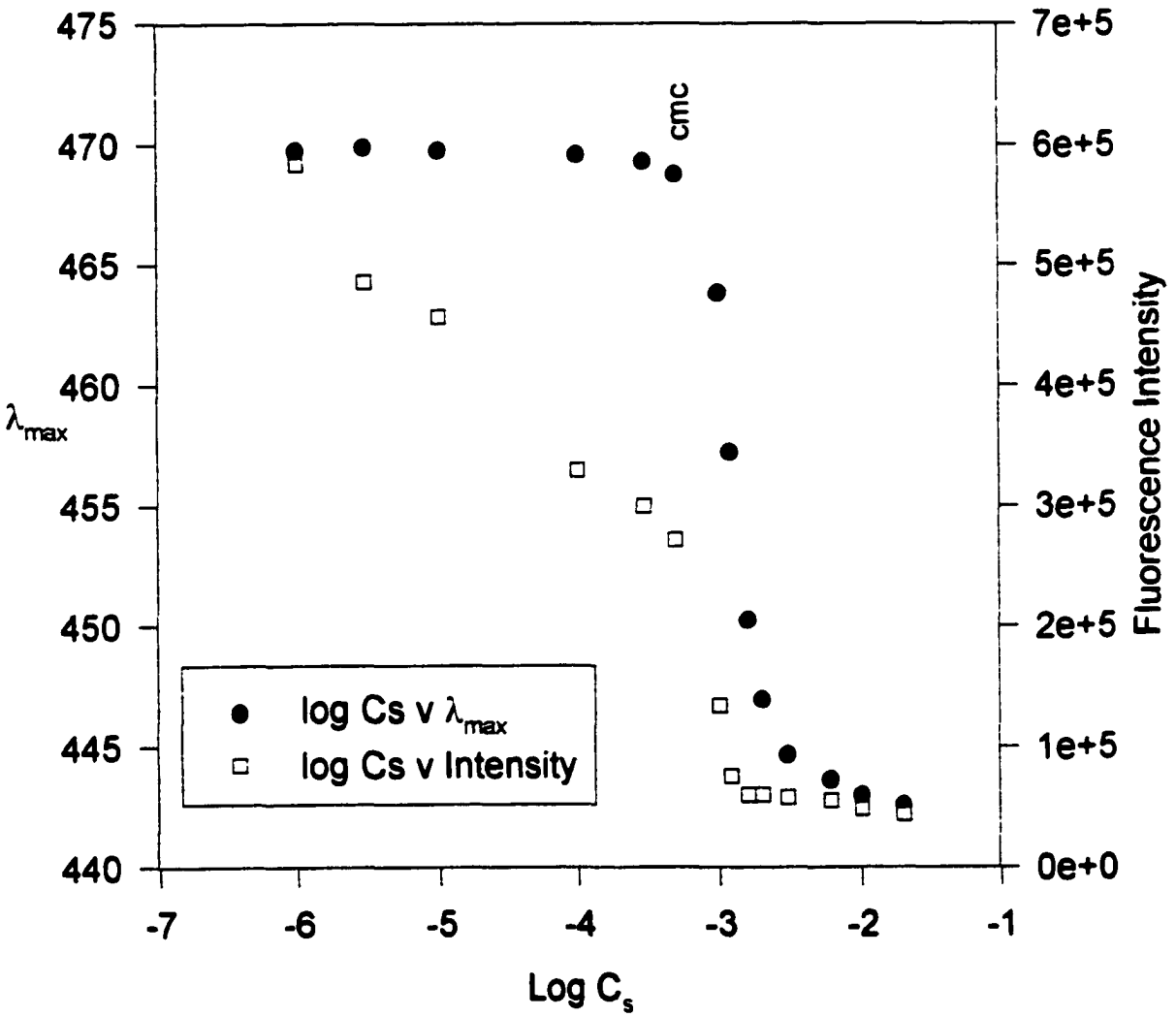

Figure 18. Wavelength of maximum fluorescence emission and fluorescence intensity of pyrenecarboxaldehyde vs Log C_s of $(C_{12}N)_2O$ in H_2O at 25^0C.

The $(C_{18}N)_2O$ and $(C_{20}N)_2O$ compounds (Figures 19 and 20) have displaced cmc values and are suspected of forming pre-micellar aggregates between the expected and observed cmc's. Both compounds show a sudden sharp drop in fluorescence intensity at the expected (theoretical) cmc. Considerable fluctuation in the intensity occurs in the surfactant concentration range between the expected and observed cmc's. The fluctuations in intensity come to an end, and the intensity begins a smooth decline at the surfactant concentration corresponding to the cmc value as determined by the λ_{max} parameter. Note also that the decline in intensity is gradual for these aberrant compounds compared with the sharp decline in the $(C_{12}N)_2O$ compound.

It appears, therefore, that the intensity of pyrenecarboxaldehyde fluorescence emission is more sensitive to the probe environment than is the position of that emission. The intensity parameter senses an environment, in the concentration region between the expected and observed cmc, which is intermediate between that of aqueous solution and a micelle, e.g. a dimer.

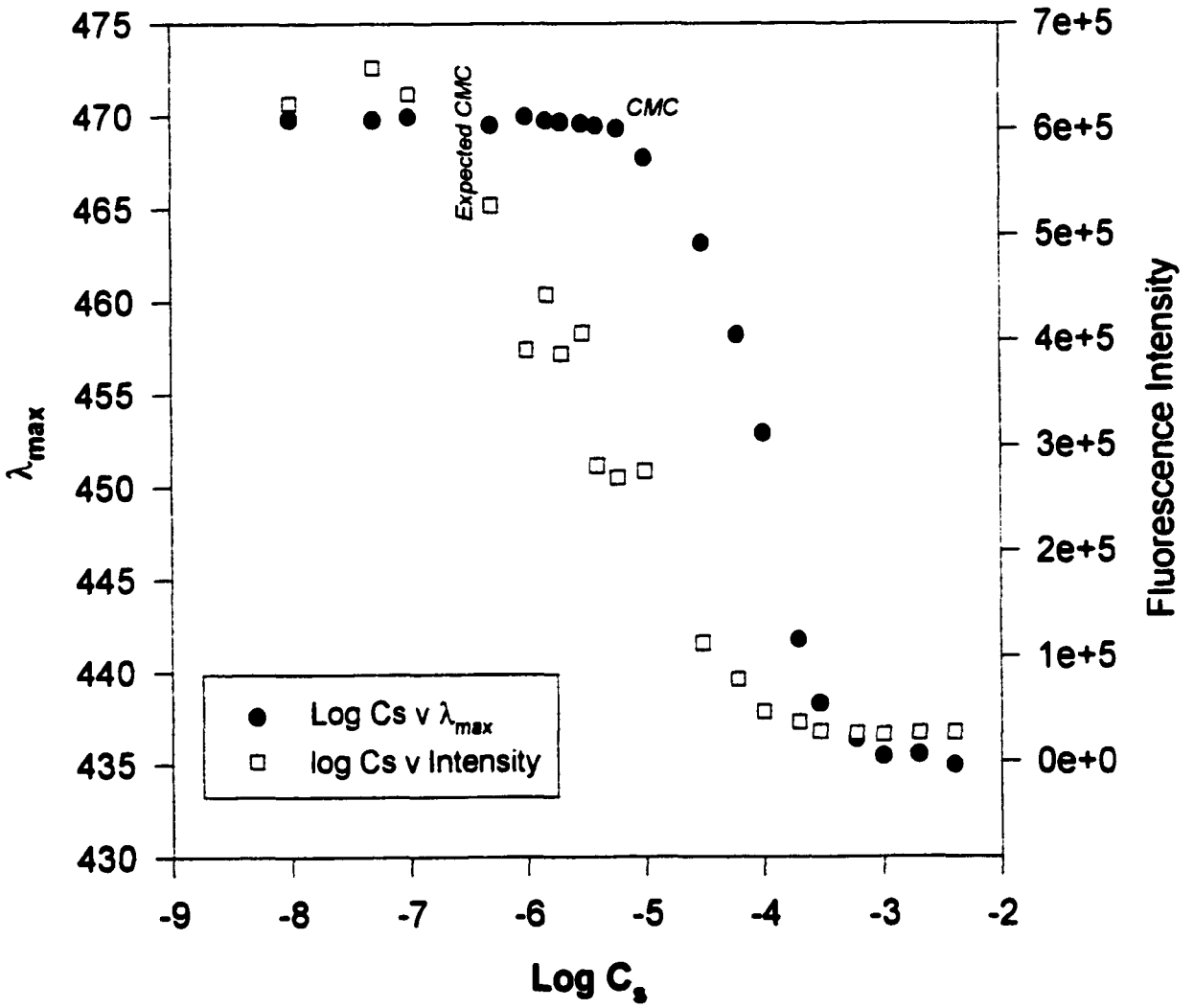

Figure 19. Wavelength of maximum fluorescence emission and fluorescence intensity of pyrenecarboxaldehyde vs Log Cs of $(C_{18}N)_2O$ in H_2O at 25°C.

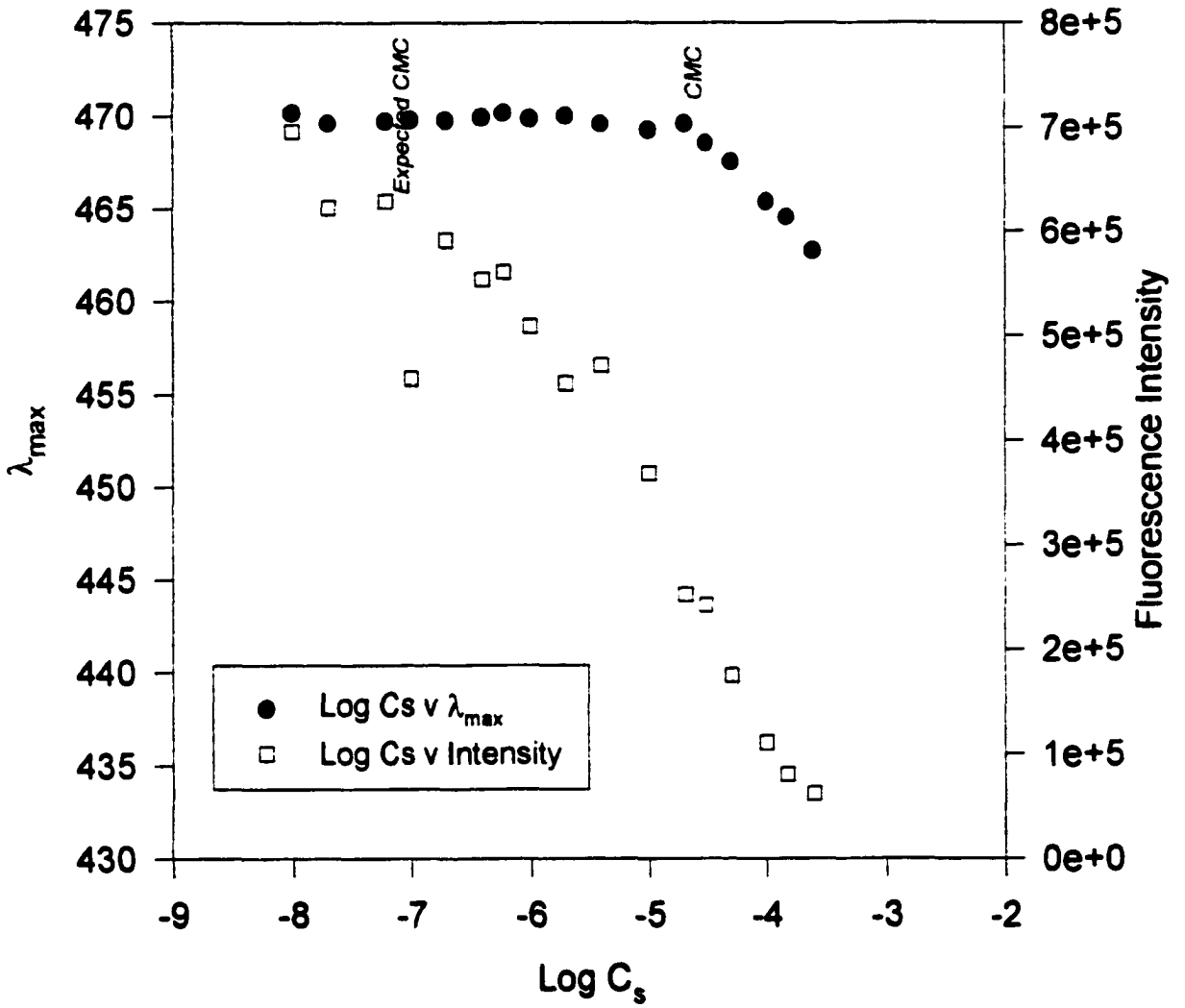

Figure 20. Wavelength of maximum fluorescence emission and fluorescence intensityof pyrenecarboxaldehyde vs Log Cs of $(C_{20}N)_2O$ in H_2O at 25^0C.

For pyrene monomer fluorescence emission, a plot of I_1/I_3 versus log surfactant concentration displays a break at the cmc. Figure 21 displays these plots for the $(C_nN)_2O$ series from n = 12 to 18. At low surfactant concentration, where the pyrene is in an aqueous environment, the I_1/I_3 value for the series is 1.57 ± 0.3. The literature value for pyrene in water is 1.59 (85). The second plateau, where pyrene is solubilized inside the micelle, has an I_1/I_3 value of 1.33 ± 0.3 for the series, which is the same as the literature value for pyrene in methanol (85). While this method provided excellent confirmation of cmc values obtained by surface tension experiments, it did not provide the subtle clues to the probe environment, which were seen with pyrenecarboxaldehyde.

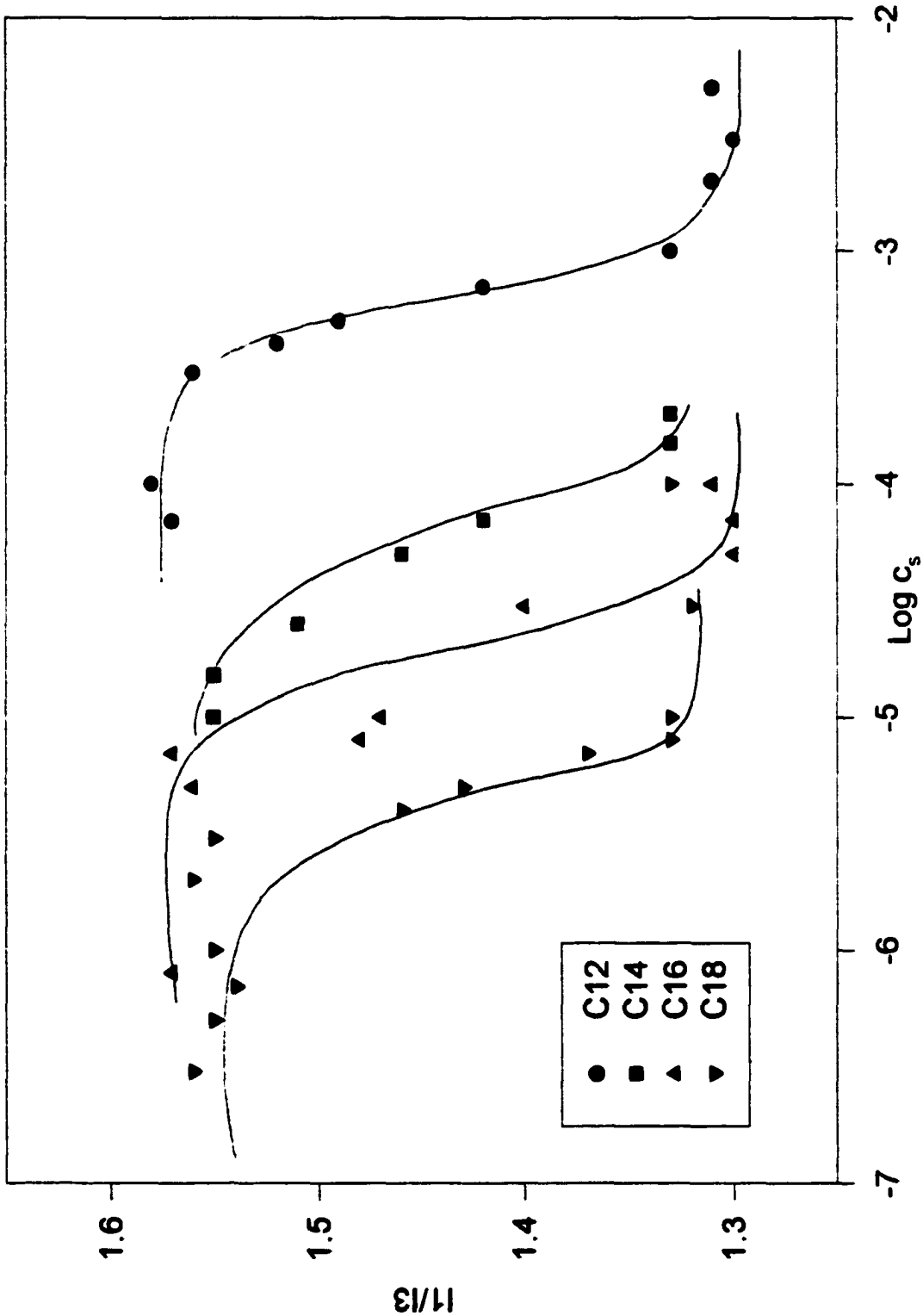

Figure 21. I1/I3 ratio of pyrene fluorescence emission vs Log Cs of $(C_nN)_2O$ in H_2O at 25°C.

Correlation between cmc values obtained by interfacial tension and fluorescence methods for $(C_nN)_2O$ compounds is demonstrated in Figure 22. The solid line is a linear regression (r^2 = 0.9995) for surface tension data on surfactants n = 10 to 16. For non-aberrant compounds, pyrenecarboxaldehyde determinations coincide with those from surface tension, while pyrene determinations are slightly lower for $(C_{12}N)_2O$ and $(C_{14}N)_2O$. For $(C_{18}N)_2O$ and $(C_{20}N)_2O$, pyrenecarboxaldehyde, following the λ_{max} parameter, gives a higher, more aberrant cmc value than either surface tension or pyrene determinations. Since the $(C_{18}N)_2O$ and $(C_{20}N)_2O$ surfactants are experiencing dynamic formation of small aggregates in the region between the expected and observed cmc, it is not surprising that different fluorescent probes would judge the critical micelle concentration differently. Indeed, even following different parameters using pyrenecarboxaldehyde detects this concentration differently. Finally, the pyrenecarboxaldehyde is sensing the environment at the interface while the pyrene is solubilized deeper, in the palisades layer.

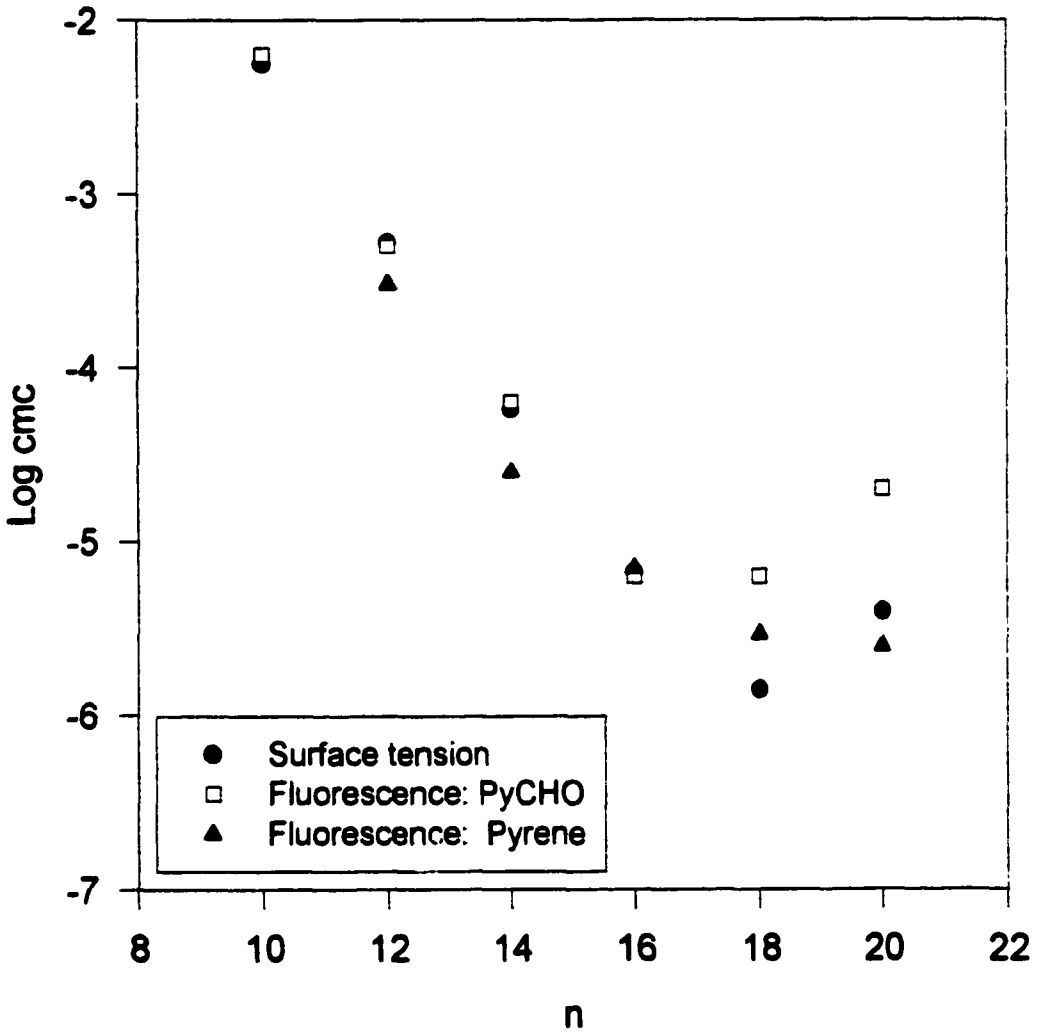

Figure 22. Log cmc vs alkyl chain carbon number of $(C_nN)_2O$ in H_2O at 25°C; determinations with various methods.

Table 11. CMC Determination of $(CnN)_2O$ by Surface Tension and Fluorescence Methods in H_2O at 25°C

COMPOUND	SURFACE TENSION (MOL/L)	FLUORESCENCE PYRENE (I1/I3) (MOL/L)	FLUORESCENCE PYCHO λ_{MAX} (MOL/L)
$(C_{10}N)_2O$	5.6×10^{-3}		6×10^{-3}
$(C_{12}N)_2O$	5.2×10^{-4}	3.0×10^{-4}	5×10^{-4}
$(C_{14}N)_2O$	5.8×10^{-5}	2.5×10^{-5}	6×10^{-5}
$(C_{16}N)_2O$	6.6×10^{-6}	7.0×10^{-6}	6×10^{-6}
$(C_{18}N)_2O$	1.4×10^{-6}	2.9×10^{-6}	6×10^{-6}
$(C_{20}N)_2O$	4.0×10^{-6}	2.5×10^{-6}	2×10^{-5}

IV.2.2 Dynamic Fluorescence

Four series of dimethyl alkyl ammonium bromide gemini surfactants have been studied in a effort to define the structure-performance relationship. That relationship, between alkyl chain length and physico-chemical parameters such as cmc and A_{min}, follows theoretically established guidelines for the shorter chain compounds, regardless of the chemical identity of the spacers investigated here. Aberrant behavior is observed to begin in aqueous solutions when n reaches 18 carbons and in 0.1 M NaCl solution at 16 carbons. cmc values for the aberrant compounds are one to two orders of magnitude greater than expected in all systems. Hexadecane/aqueous and hexadecane/0.1 M NaCl results parallel those in air/aqueous and air/0.1 M NaCl. A measure of degree of aberration for these surfactants is calculated as a new parameter, cmc/cmc*. The expected (theoretical) critical micelle concentration (cmc*) is determined from cmc and pC_{20} values as in Figure 2.

Table 12: Degree of aberration, cmc/cmc*, in cationic gemini surfactants

n	C_nO (H_2O/25°C)	$C_n(OH)_2$ (H_2O/25°C)	$C_n(OH)$ (0.1 NaCl/50°C)	C_nAr (0.1 NaCl/50°C)
12	1	1	1	1
14		1	6.1	3.6
16		1.8	158	34
18	4			420
20	31			

From Table 12 we see that, regardless of system conditions (temperature and addition of electrolyte) or chemical nature of the spacer, compounds with n = 12 do not exhibit aberrant behavior. Without added electrolyte, very slight deviation begins at n = 16. Addition of electrolyte causes much greater deviation, beginning at n = 14. Comparing the behavior of the $(C_nN)OH$ and CnAr series, which were investigated under the same system conditions, there is a greater tendency toward pre-micellar aggregation for the compounds with the flexible hydroxy spacer than with the rigid aryl spacer. Closer packing of the hydrophobic groups in compounds with a hydroxy spacer may facilitate dimer formation more so than in groups with rigid spacers.

Steady state fluorescence techniques provided an alternate method of study. Literature confirmations of cmc values for gemini surfactants (usually conductivity) have proven erratic. Here, steady state methods, using pyrene-3-carboxaldehyde and pyrene as the probe, have shown excellent correlation with conventional surface tension methods. Further, the shapes of emission maxima versus concentration curves for the shorter-chain geminis indicate a simple two-step process, similar to the shape of their mono-quaternary analogues. In contrast, those compounds displaying unusual physico-chemical properties have sigmoidal curves indicative of a multi-step process.

Dynamic fluorescence techniques are employed to determine aggregation numbers of these cationic gemini surfactants. Of particular interest is the region between the expected and observed cmc. When using equation [19] to determine aggregation number, we use the expected cmc value.

Initially, steady state determination of aggregation number was attempted, as it is a simpler method than dynamic determination. For the $(C_{18}N)_2O$ compound in water at 25°C, steady state determination returned a value for N of 13 ± 3 gemini molecules per micelle. (Note that aggregation numbers will be given as geminis/micelle; comparison of aggregation number with conventional surfactants requires multiplication of this number by 2.) For these experiments, probe and quencher to micelle ratios were according to literature protocols, and the data were well-fit to a straight line. The probe/quencher pair in this case was pyrene/dimethylbenzophenone (DMBP). This pair has frequently been cited for use in the literature for determination of aggregation number.

Static quenching, a fundamental assumption in steady state determination of N, was tested by dynamic experiments. From Table 13 we see that the average lifetime ,$<\tau>$, decreases with increasing quencher concentration, [Q]. This implies dynamic quenching. The aggregation numbers in Table 13, calculated by the dynamic method, are equal to 33 ± 5.

Use of pyrene/DMBP is obviously not suitable to our purposes. Further, this method proved problematic, for any probe/quencher pair, at low surfactant concentrations.

TABLE 13: $(C_{18}N)_2O$/Pyrene/DMBP/H_2O/25°C
Time-Resolved Fluorescence Data at various quencher concentrations.
$C_s = 1.0 \times 10^{-3}$; $C_{py} = 1.0 \times 10^{-6}$.

Data file	*[Q] x 10^6 (M)*	*n*	*$K_0^{(a)}$ x 10^3 (ns^{-1})*	*$K_0^{(b)}$ x 10^3 (ns^{-1})*	*τ_{avg} (ns)*	*N (± 5)*
ttagg016	0.0	0.06	7.6	7.9	122.7	33
ttagg020	2.0	0.15	7.9	8.1	120.0	36
ttagg023	4.0	0.25	7.9	8.1	114.8	31
ttagg026	6.0	0.39	8.3	8.6	110.4	32

(a) reciprocal of lifetime of monomer component obtained from fitdec program.
(b) slope of decay curve from linear regression on channels 600-→ 1023.

Time-resolved fluorescence quenching (dynamic quenching) using pyrene monomer/excimer (62,63,90,91) was employed for conventional surfactants of known aggregation numbers. Results are listed in Table 14. The major experimental consideration is that the decay curve displays a well-developed tail (63). Additionally, the pyrene concentration must be low enough to avoid inner-filter effects. Within these guidelines, and under stable lamp conditions, this method produces excellent results.

TABLE 14: Aggregation Numbers for Conventional Surfactants using Pyrene.

SURFACTANT	SYSTEM	C_S (M)	C_S/CMC	τ_I (ns)	F_I	$\langle\tau\rangle$ (ns)	N	N_{LIT}
DTAB	H_2O/25°C	0.16	10	47.02 122.26	16 84	110	70±5	65[a]
TTAB	H_2O/25°C	0.034	9.4	54.87 118.96	4 96	116	80±10	97[a] 70[b]
CTAB	0.1M NaCl/ 50°C	5.0×10^{-4}	3.3	36.83 128.12	9 91	120	106±10	89[a] (in H_2O)
SDS	H_2O/25°C	0.080	10	33.37 177.63	1 99	176	72±5	75[a]
SDS	H_2O/25°C	0.024	3.0	21.99 156.85	6 94	149	72±5	75[a]
SDS	H_2O/25°C	0.016	2.0	29.19 169.87	5 95	163	78±5	75[a]
SDS	H_2O/25°C	0.080	10	36.40 164.7	1 99	163	72±5	75[a]

(a) ref (109)
(b) ref (91)

Aggregation numbers for cationic gemini surfactants are listed in Appendix B. Variation of aggregation number as a function of total surfactant concentration is often of interest. A normalized surfactant concentration, C_s/cmc, is useful.

In virtually all experiments, the dynamic fluorescence decay data were well-fit to the sum of two exponentials. The shorter lifetime, τ_1 corresponds to the excimer decay, while τ_2 corresponds to monomer decay. These lifetimes, the fractional contribution of each, f_i, and the calculated average lifetime, $<\tau>$, are listed in Table B1 through Table B11.

It has been shown that average fluorescence lifetime increases sharply at the cmc (85), and this fact has been used as the basis of a method for cmc determination. When using an excimer-forming probe such as pyrene, this method requires that the concentration of fluorescent probe be held constant as the surfactant concentration is varied. As the concentration of pyrene increases, the amount of excimer also increases, and the average lifetime is shortened. Consequently, a meaningful comparison of $<\tau>$ requires that the experiments have equal concentrations of pyrene.

Aggregation numbers for the four homologous series of cationic gemini surfactants versus normalized surfactant concentration are plotted in Figures 23-26. A value of Cs/cmc between 0 and 1 indicates the region between the expected and observed cmc, i.e., the pre-micellar region.

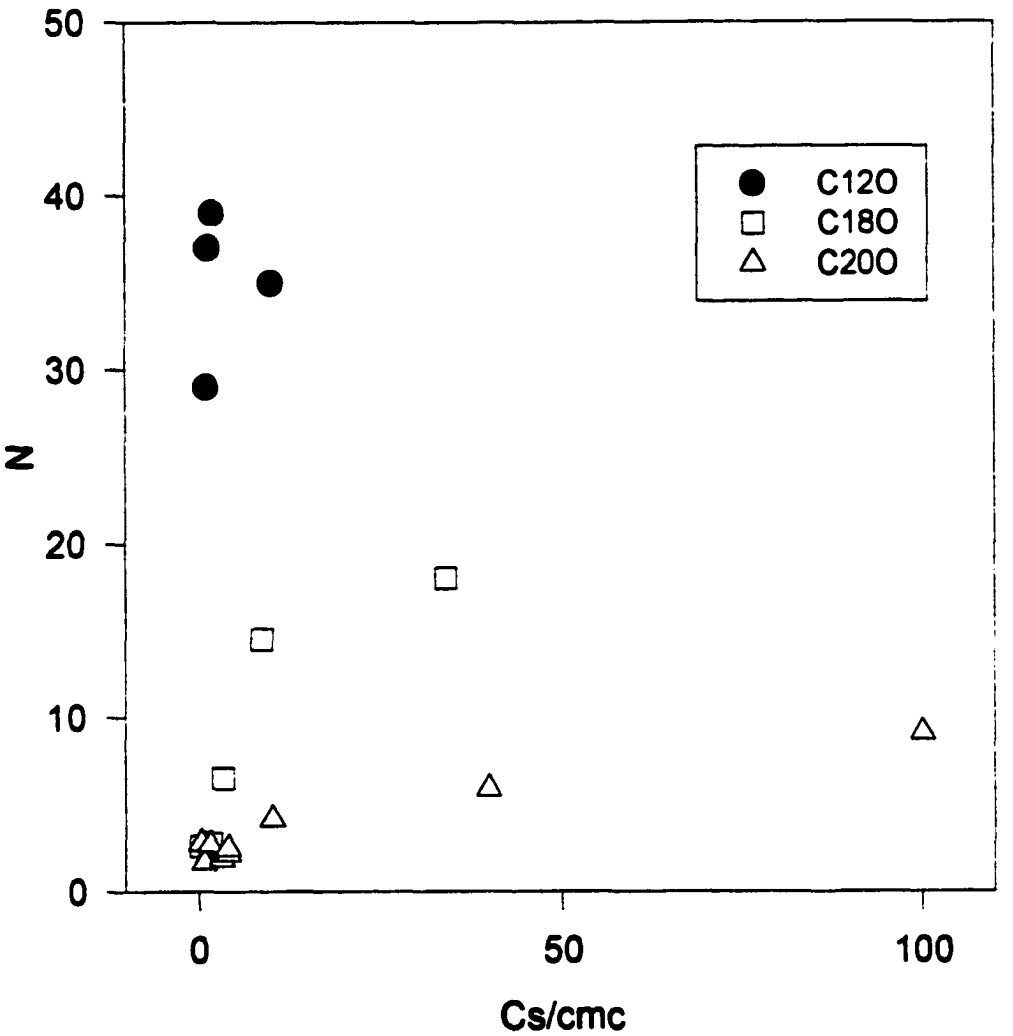

Figure 23: Aggregation Number, N v Normalized surfactant concentration for $(C_nN)_2O$ surfactants in aqueous solution at 25°C.

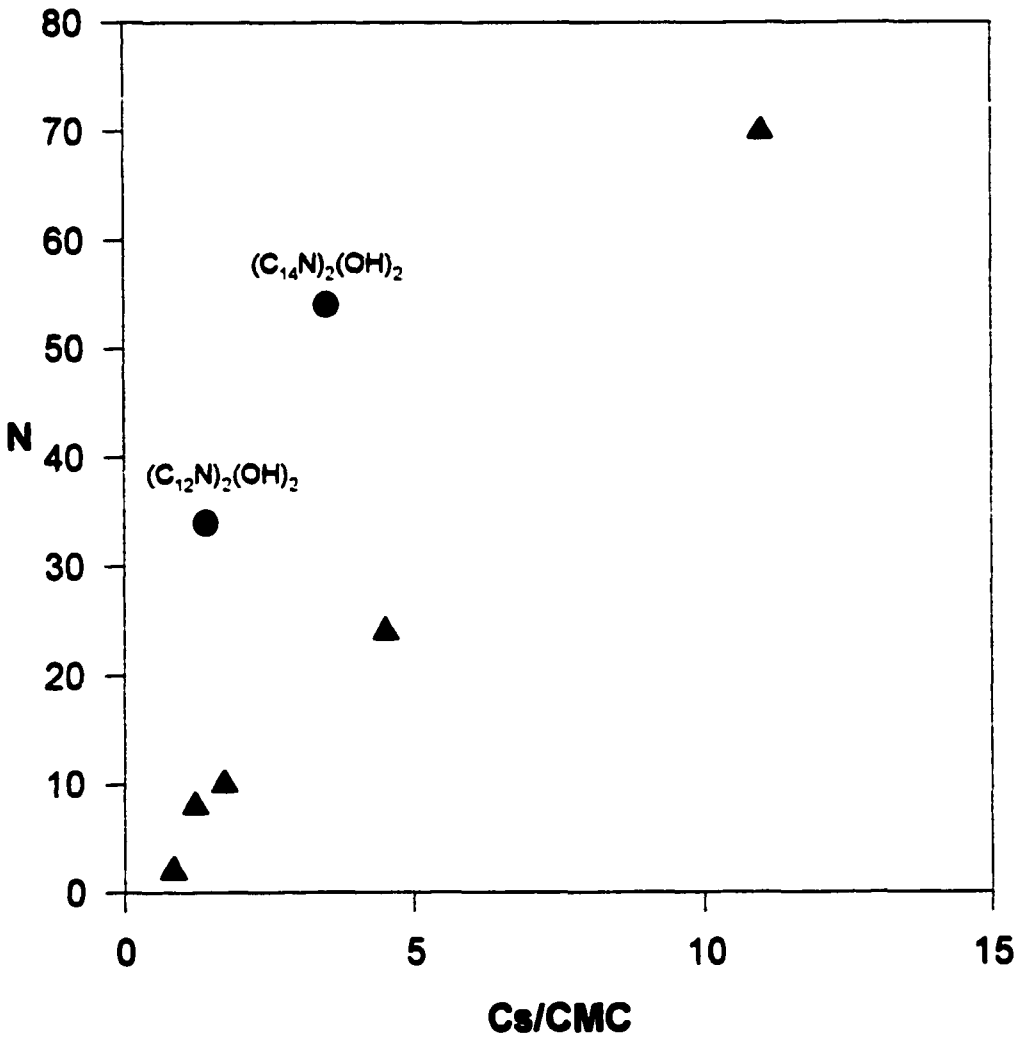

Figure 24. Aggregation number, N, vs normalized surfactant concentration for $(C_{16}N)_2(OH)_2$ in H_2O at 25°C.

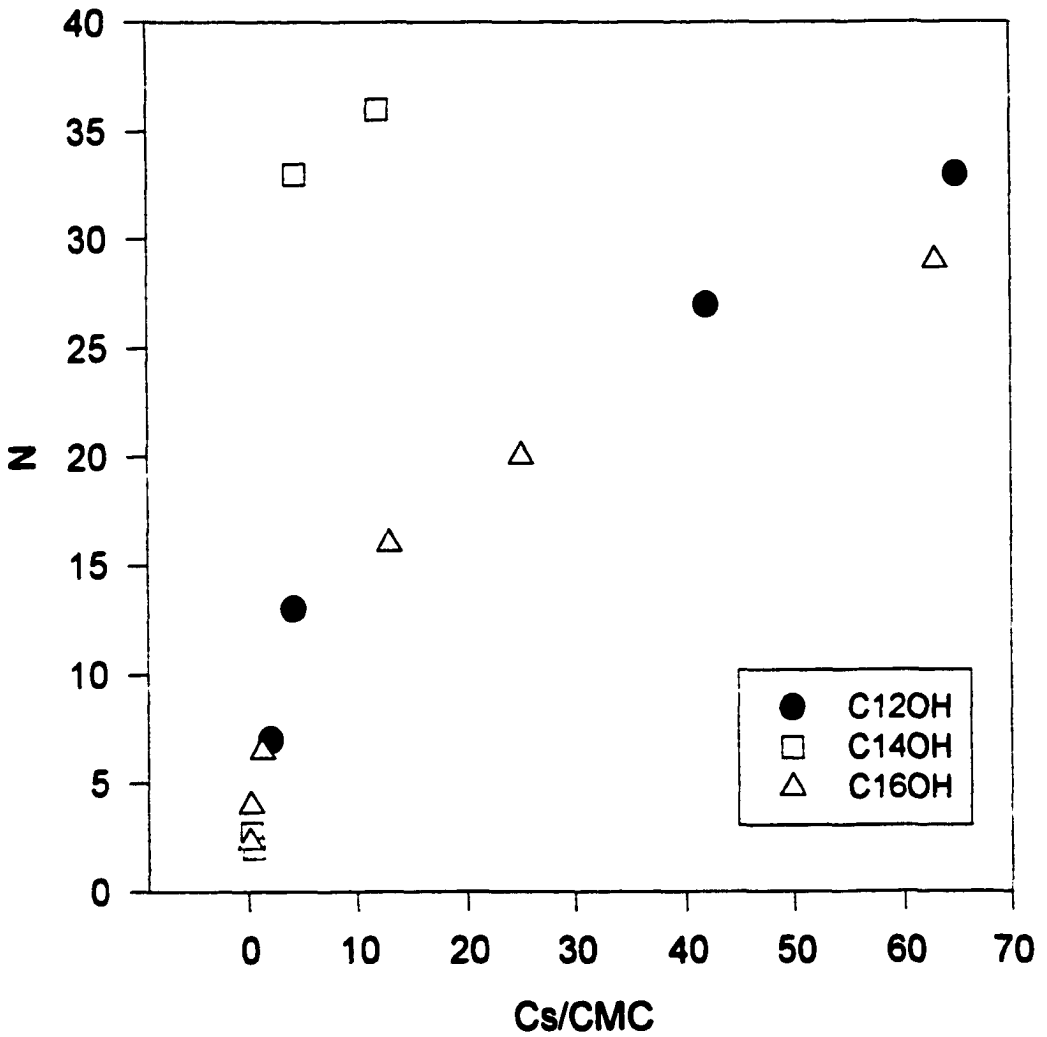

Figure 25. Aggregation number, N, vs Normalized surfactant concentration for $(C_nN)_2OH$ in 0.1 M NaCl at 50°C.

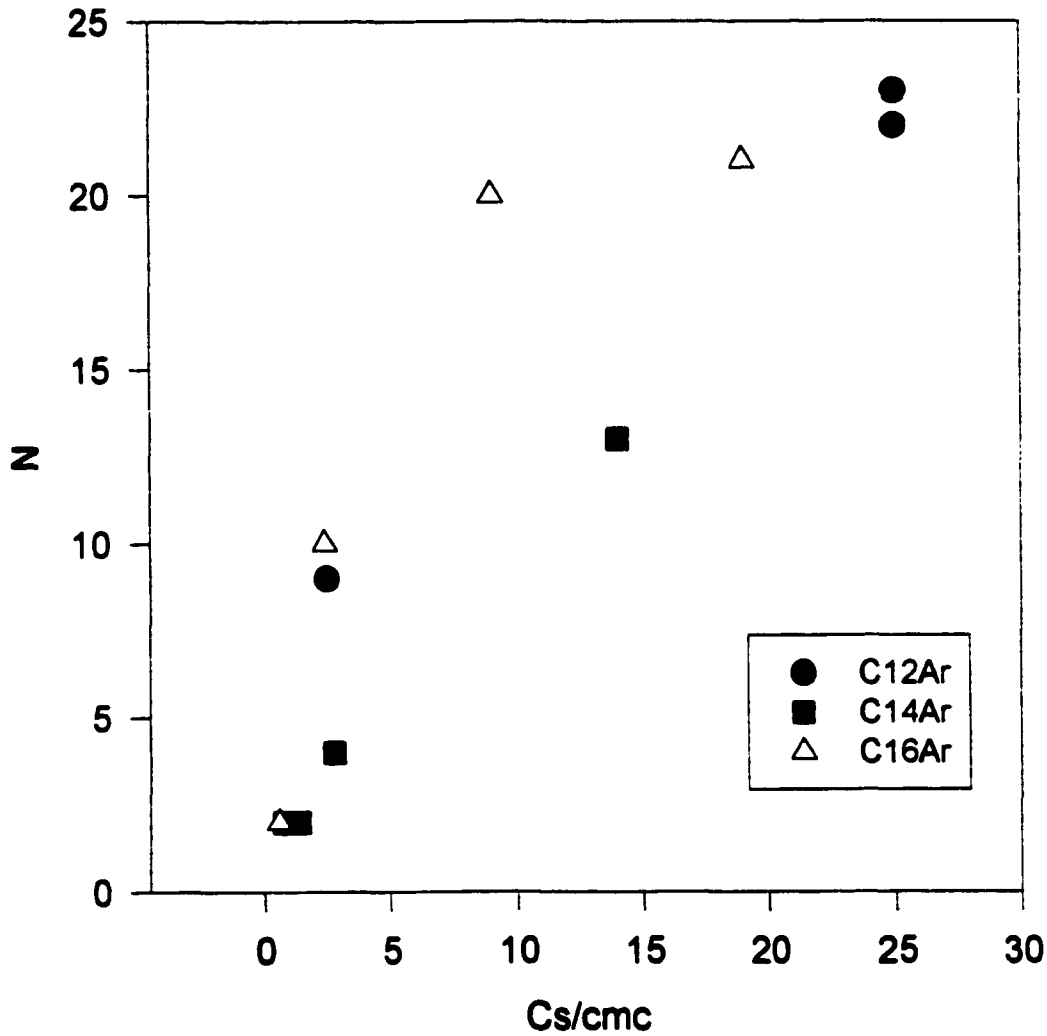

Figure 26. Aggregation Number, N, vs Normalized surfactant concentration for $(C_nN)_2Ar$ surfactants in 0.1 M NaCl at 50°C.

The non-aberrant compounds $(C_{12}N)_2O$ and $(C_{12}N)_2(OH)_2$, in water at 25°C and Cs/cmc = 1.4, have aggregation numbers of 37 and 34 respectively. A spherical micelle formed from C12, single-chain monomers, under the same system conditions, has an aggregation number ≈ 70. Specifically, DTAB has a literature value of 65 (109). (Recall, divide by 2 for comparison with gemini micelle). The distribution of aggregation numbers for the $(C_{12}N)_2O$ compound, within one order of magnitude of the cmc, is 35 with a standard deviation of ± 4. For spherical micelles, the spread (standard deviation) in the Gaussian distribution is equal to the square root of N (32). The data therefore indicate that for $(C_{12}N)_2O$ and $(C_{12}N)_2(OH)_2$, we have spherical, monodisperse micelles near the critical micelle concentration. Relatively little has been published on aggregation numbers for gemini surfactants. Zana (29) has reported on C12 geminis with methylene spacers of various lengths, and reports spherical, monodisperse micelles at surfactant concentration near the cmc.

The $(C_{14}N)_2(OH)_2$ is also a non-aberrant compound. Its aggregation number is 54 near the cmc. TTAB, its single-chain analogue, has N = 97 under the same conditions (109). $(C_{16}N)_2(OH)_2$ shows a very small degree of aberration in water at 25°C. with a narrow concentration range between the expected and observed cmc. An aggregation number of 2, indicating dimers, was found in this region. Linear increase in N begins at the observed cmc with a value of N = 70 achieved within an order of magnitude increase in the normalized surfactant concentration (Figure 24).

The $(C_{18}N)_2O$ and $(C_{20}N)_2O$ compounds in water at 25 °C both show the presence of dimers between the expected and observed cmc. Aggregation numbers begin a linear increase at the observed cmc for both. A reversal of the "expected" pattern is seen as the surfactant concentration increases. The $(C_{20}N)_2O$ aggregation numbers lie below those for the $(C_{18}N)_2O$ (Figure 23). For conventional, non-aberrant surfactants, aggregation number increases with alkyl chain length. It is likely that this is related to the relative degree of aberration for these compounds. The reversed pattern is repeated for the aberrant compounds $(C_{14}N)_2OH$ and $(C_{16}N)_2OH$ in 0.1 M NaCl at 50°C. Dimers are again seen in the pre-micellar region; aggregation numbers for the $(C_{16}N)_2OH$ compound lie below those for the $(C_{14}N)_2OH$ (Figure 25).

Figure 27 shows aggregation as a function of reduced surfactant concentration for three aberrant compounds with n = 16 and differing spacers. All three have aggregation numbers indicating dimers in the region between expected and observed cmc. As surfactant concentration increases, the least aberrant compound, $(C_{16}N)_2(OH)_2$, attains an aggregation number comparable to its conventional analogue. $(C_{16}N)_2OH$, the most aberrant compound, has relatively small aggregation numbers at high surfactant concentration.

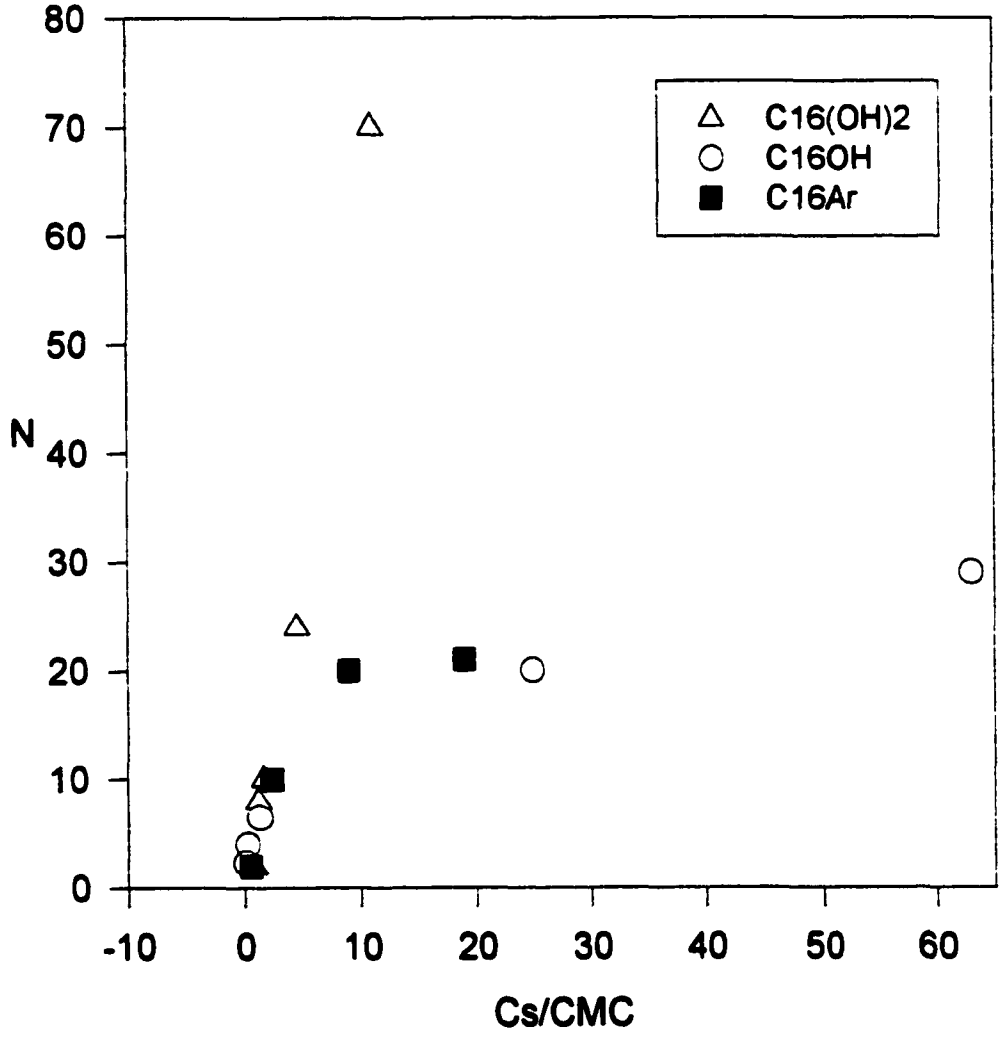

Figure 27. Aggregation number, N, vs normalized surfactant concentration for $(C_{16}N)_2(OH)_2$ in H_2O at 25°C and $(C_{16}N)_2Ar$ and $(C_{16}N)_2OH$ in 0.1 M NaCl at 50°C.

Figures 28-30 show aggregation numbers of $(C_{12}N)_2O$, $(C_{18}N)_2O$ and $(C_{20}N)_2O$ and I1/I3 values as a function of surfactant concentration. The non-aberrant $(C_{12}N)_2O$ has values of N beginning at the observed cmc (the initial drop off of the I1/I3 curve) and quickly level off to a number comparable to a conventional C12 surfactant, indicating spherical, monodisperse micelles. The $(C_{18}N)_2O$ shows dimers in the region between the expected and observed cmc, with linear increase in N at the observed cmc. The I1/I3 curve for the $(C_{20}N)_2O$ indicates the presence of two observed cmc's, the first at 2.5 x 10-6 M and the second at 8.0 x 10-6 M. The aggregation numbers fluctuate between 1.7 and 2.8 in the region between the expected cmc and the second cmc, where they begin a linear increase.

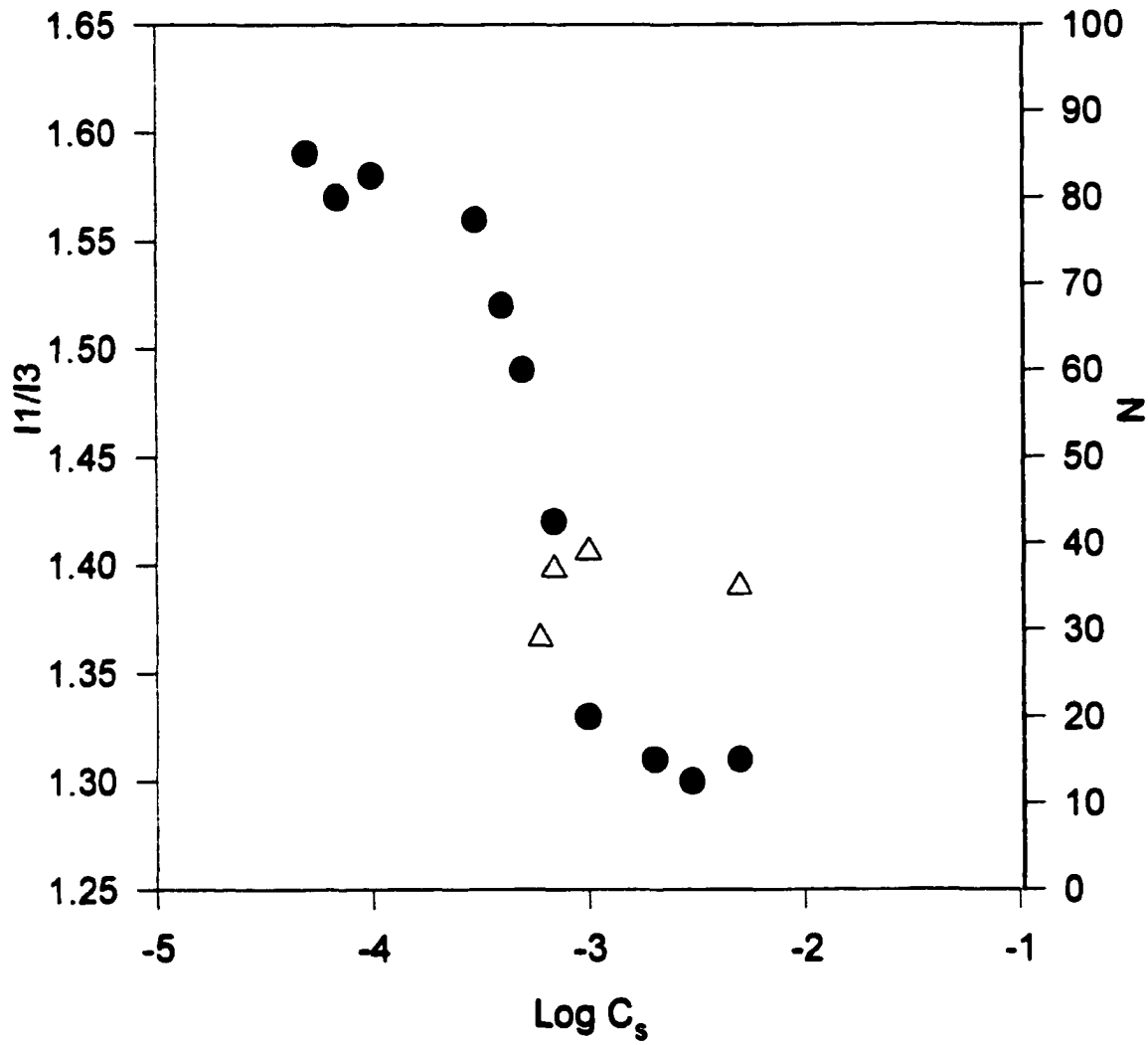

Figure 28. I_1/I_3 and N vs Log C_s for $(C_{12}N)_2O$ in aqueous solution using Pyrene at 25°C.

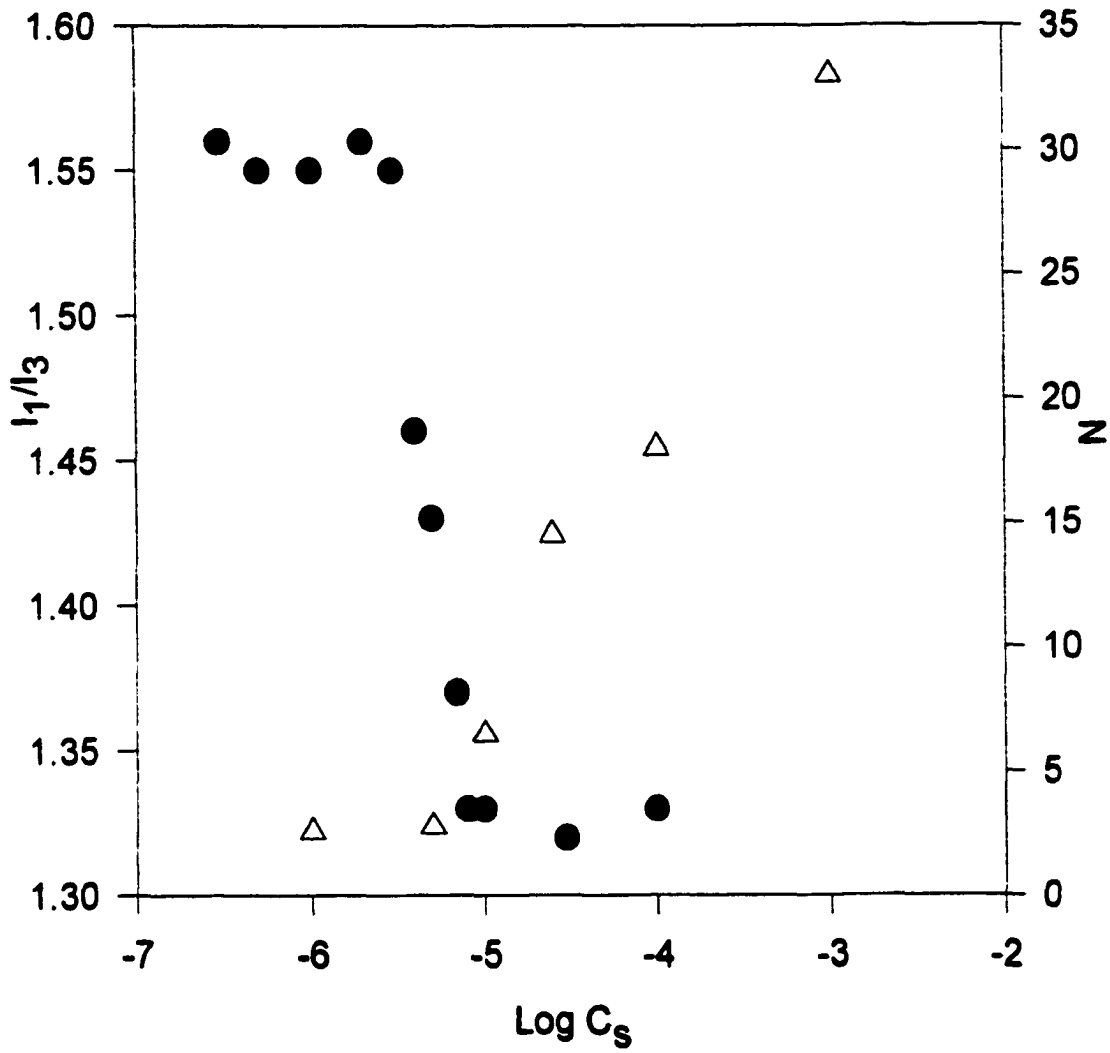

Figure 29. I_1/I_3 and N v Log C_s for $(C_{18}N)_2O$ in aqueous solution using Pyrene at 25^0C.

● I_1/I_3

△ N

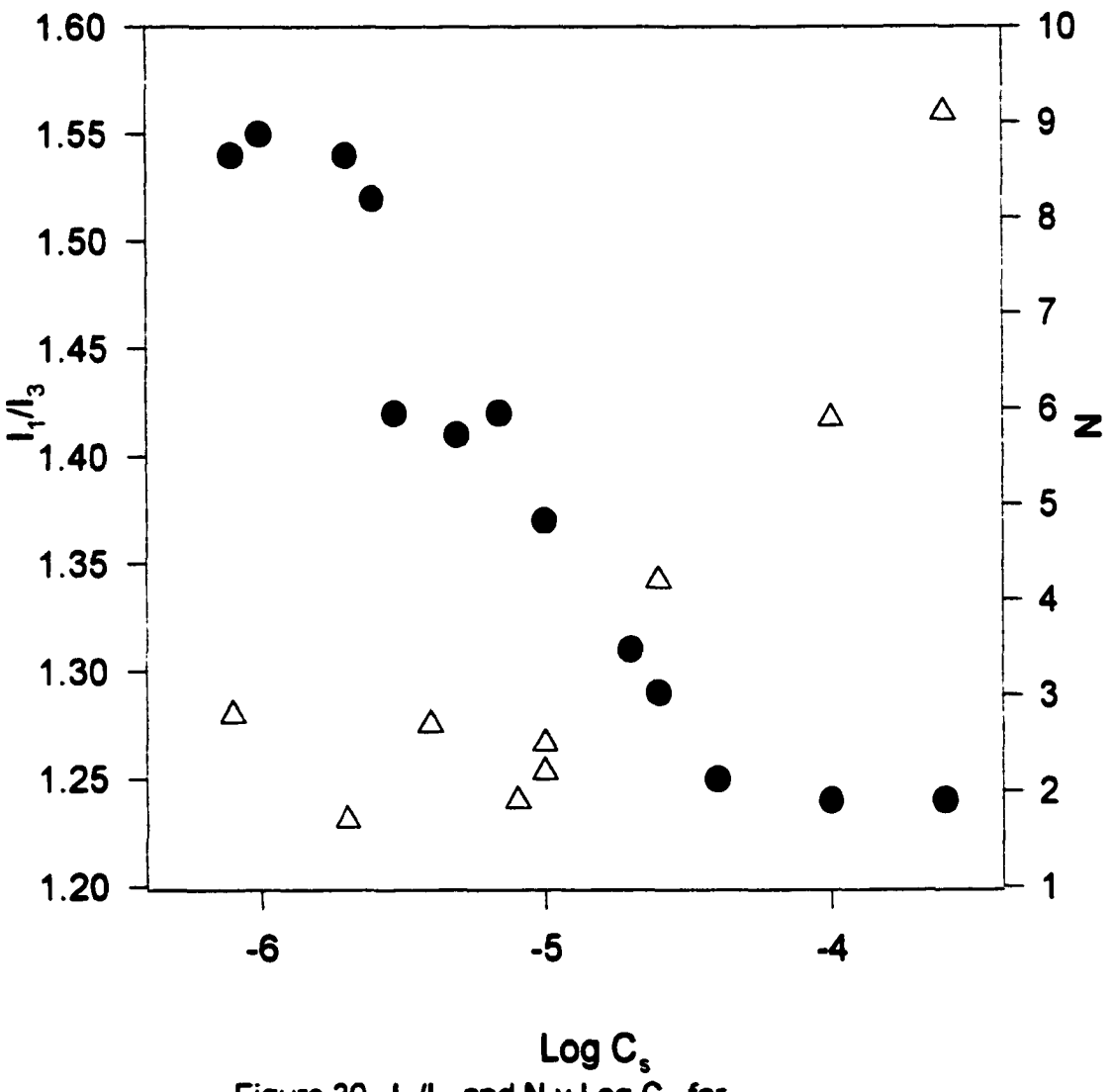

Figure 30. I_1/I_3 and N v Log C_s for $(C_{20}N)_2O$ in aqueous solution using Pyrene at 25^0C

● I_1/I_3
△ N

For the $(C_nN)_2Ar$ series, the aggregation numbers indicate dimers in the pre-micellar concentration region for the $(C_{14}N)_2Ar$ and $(C_{16}N)_2Ar$ compounds with increasing N at the observed cmc. The surface tension curve for the (C18N)2Ar indicates the presence of two cmc's, the first at 2.1 x 10-6 M and the second at 7.6 x 10-5 M. The expected cmc is 5.0 x 10-9 M. Aggregation numbers for this compound are shown in Figure 31. Between the expected cmc and first cmc there are dimers which begin to grow rapidly and reach an aggregation number of 62 at 9 x 10-6 M surfactant concentration. There is a precipitous drop in N to a value of 1.9 (dimer) at Cs = 1 x 10-5 M. An I1/I3 ratio of 1.46 at Cs = 1 x 10-5 M confirms its hydrophilic environment. At Cs = 9 x 10-6 M , I1/I3 is 1.13 indicating a hydrophobic (micellar) environment. The dimers begin to grow as surfactant concentration increases and the second cmc is reached. A value of N = 63 is attained at the solubility limit of Cs = 3.8×10^{-4} M.

Figure 32 is an overlay of aggregation numbers onto the surface tension plot. The symmetry between the two is evident. As noted earlier, the size of an aggregate is a thermodynamic balance between energy and entropy factors. A shift in this balance, causing entropy to become the overwhelming consideration might account for the sudden re-formation of dimers between 9×10^{-6} M and 1×10^{-5} M surfactant concentration.

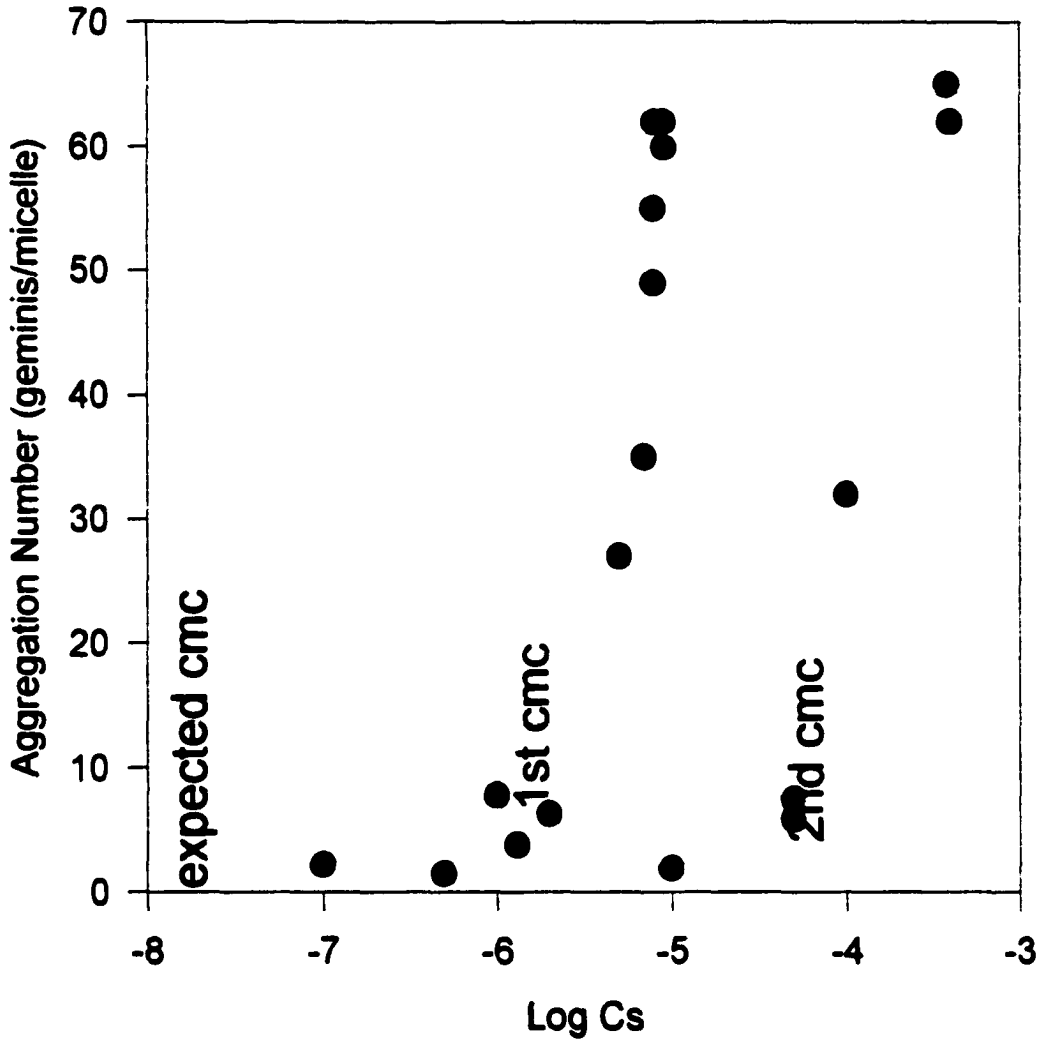

Figure 31. $(C_{18}N)_2Ar$ / Pyrene / 0.1 M NaCl / 50C

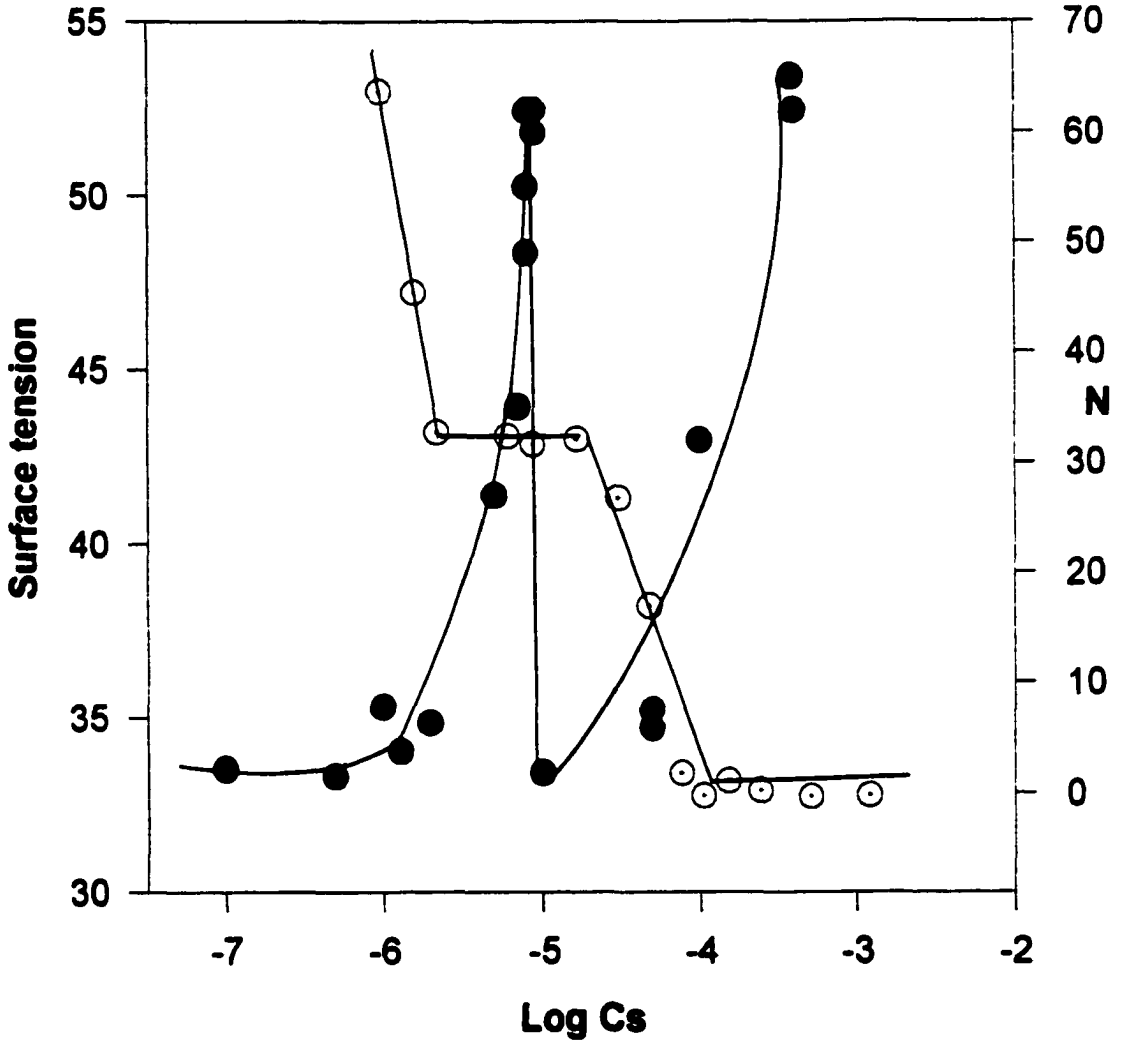

Figure 32. Surface tension and Aggregation number vs Log Cs for $(C_{16}N)_2Ar$ in 0.1 M NaCl at 50°C.

Studies of the aggregation behavior of gemini surfactants is in a relatively early stage. To date, aggregation numbers have been collected mainly on the shorter chain compounds where aberrant behavior is not an issue. A recent small angle neutron study on the ortho isomer of (C8N)2Ar detected the presence of two cmc values (57). In the region between the first and second cmc, they found aggregation numbers of 3 – 7 indicating the formation of pre-micelles and subsequent formation of normal micelles after the second cmc. The existence of such aberrant behavior in a short chain gemini is likely due to conformation as the para isomer was non-aberrant.

As the alkyl chain length increases to the point where aberrant surface tension behavior is observed, i.e., there is non-linear behavior between the cmc and the number of carbon atoms, n, spherical, monodisperse micelles are no longer observed at low surfactant concentration. Aggregation numbers from dynamic fluorescence measurements indicate the presence of dimers between the expected and observed cmc's, followed by growth patterns which depend of surfactant structure as well as system conditions.

The morphology of aberrant gemini micelles at concentrations well-above the observed cmc would be fascinating to investigate, but is experimentally unfeasible due to loss of solubility for these long-chain compounds.

The wider range of structures for gemini aggregates versus conventional surfactant aggregates suggests new applications. For example, the presence of

thread-like aggregates results in increased viscoelasticity. This presents a possible way to control the rheology of solutions.

Finally, the existence of synergism between gemini and conventional surfactants (33-36) suggests use of geminis for more effective detergent formulation. As the degree of synergism depends highly on the structure of the gemini, understanding of the relationship between nature of the surfactant and aggregation behavior is necessary.

Appendix A

Interfacial Tension Data

Table A1: Equilibrium Surface Tension of $(C_{12}N)_2O$ in H_2O at 25°C

Log C_s (M)	γ_S (mN/m)
-3.000	39.98
-3.222	40.00
-3.398	42.18
-3.699	47.94
-4.000	50.85
-3.523	43.30
-3.301	40.70

Table A2: Equilibrium Surface Tension of $(C_{14}N)_2O$ in H_2O at 25°C

Log C_s (M)	γ_S (mN/m)
-4.002	39.10
-3.701	40.06
-3.525	39.79
-4.303	41.79
-4.701	48.70
-4.525	44.90
-4.400	43.50
-4.099	39.30

Table A3: Equilibrium Surface Tension of $(C_{16}N)_2O$ in H_2O at 25°C

Log C_s (M)	γ_S (mN/m)
-5.000	37.15
-5.222	38.71
-4.699	38.00
-5.398	43.70
-5.301	40.40
-4.495	37.64

Table A4: Equilibrium Surface Tension of $(C_{18}N)_2O$ in H_2O at 25°C

Log C_s (M)	γ_s (mN/m)
-5.222	40.20
-5.620	40.00
-6.000	44.70
-6.097	48.20
-5.886	41.30

Table A5: Equilibrium Surface Tension of $(C_{18}N)_2O$ in H_2O at 25°C (Theoretical)

Log C_s (M)	γ_s (mN/m)
-6.125	38.00
-6.750	52.00

Table A6: Equilibrium Surface Tension of $(C_{20}N)_2O$ in H_2O at 25°C

Log C_s (M)	γ_s (mN/m)
-5.000	56.00
-6.000	61.30
-5.796	59.60
-5.398	54.70

Table A7: Equilibrium Surface Tension of $(C_{12}N)_2O$ in 0.1 M NaCl at 25°C.

-Log C_s (M)	γ_S (mN/m)
-3.000	38.90
-4.000	38.70
-4.222	38.80
-4.699	40.30
-5.000	43.00
-5.222	44.20
-5.398	47.00
-5.699	48.50

Table A8: Equilibrium Surface Tension of $(C_{14}N)_2O$ in 0.1 M NaCl at 25°C.

-Log C_s (M)	γ_S (mN/m)
-4.292	36.10
-4.690	36.50
-4.991	36.00
-5.292	36.40
-5.991	37.40
-5.690	35.60
-6.292	40.40

Table A9: Equilibrium Surface Tension of $(C_{16}N)_2O$ in 0.1 M NaCl at 25°C.

-Log C_s (M)	γ_S (mN/m)
-6.000	32.70
-6.398	46.70
-4.000	34.10
-5.301	34.50
-6.301	41.70
-6.201	40.00

Table A10: Equilibrium Surface Tension of $(C_{18}N)_2O$ in 0.1 M NaCl at 25°C.

-Log C_s (M)	γ_S (mN/m)
-5.000	30/00
-6.000	29.70
-6.097	29.70
-6.222	37.80
-6.523	57.90
-6.699	64.40

Table A11: Equilibrium Interfacial Tension of $(C_{12}N)_2O$ in Hexadecane/ H_2O at 25°C

Log C_s (M)	γ_s (mN/m)
-3.000	8.45
-3.301	12.85
-3.155	9.73
-3.222	11.49
-2.301	7.47
-2.824	8.27
-2.602	7.89
-3.398	14.82

Table A12: Equilibrium Interfacial Tension of $(C_{14}N)_2O$ In Hexadecane/ H_2O at 25°C

Log C_s (M)	γ_s (mN/m)
-3.292	7.66
-3.594	7.97
-3.815	7.93
-3.893	7.91
-4.000	9.31
-4.222	11.50
-4.301	13.30

Table A13: Equilibrium Interfacial Tension of $(C_{16}N)_2O$ in Hexadecane/H_2O at 25°C

Log C_s (M)	γ_s (mN/m)
-4.301	7.32
-4.699	7.24
-4.000	7.32
-5.000	7.24
-5.301	9.95
-5.523	12.90
-5.824	15.08

Table A14: Equilibrium Interfacial Tension of $(C_{18}N)_2O$ in Hexadecane/H_2O at 25°C

Log C_s (M)	γ_s (mN/m)
-4.000	15.00
-3.523	16.00
-4.301	22.30
-3.000	15.60
-4.398	23.40
-4.222	19.10

Table A15: Equilibrium Interfacial Tension of $(C_8N)_2(OH)_2$ in Hexadecane/H_2O at 25°C

Log C_s (M)	γ_S (mN/m)
-1.775	7.17
-2.076	13.36
-1.903	10.34
-2.000	11.42
-1.301	6.30
-1.699	6.30

Table A16: Equilibrium Interfacial Tension of $(C_{10}N)_2(OH)_2$ in Hexadecane/H_2O at 25°C

Log C_s (M)	γ_S (mN/m)
-2.000	5.62
-2.097	5.54
-2.523	9.03
-2.699	11.98
-2.398	6.62

Table A17: Equilibrium Interfacial Tension of $(C_{12}N)_2(OH)_2$ in Hexadecane/H_2O at 25°C

Log C_s (M)	γ_S (mN/m)
-3.000	5.38
-3.301	9.11
-3.523	13.18
-2.801	5.40
-2.277	4.83

Table A18: Equilibrium Interfacial Tension of $(C_{14}N)_2(OH)_2$ in Hexadecane/H_2O at 25°C

Log C_s (M)	γ_S (mN/m)
-3.301	4.46
-4.301	12.16
-4.000	7.72
-3.824	5.25
-3.602	4.96
-4.125	9.24

Table A19: Equilibrium Interfacial Tension of $(C_{16}N)_2(OH)_2$ in Hexadecane/H_2O at 25°C

Log C_s (M)	γ_S (mN/m)
-4.523	5.24
-4.921	7.42
-4.745	6.01
-4.046	4.64
-4.268	5.03
-5.268	10.92

Table A20: Equilibrium Interfacial Tension of $(C_8N)_2OH$ in Hexadecane/H_2O at 25°C

Log C_s (M)	γ_S (mN/m)
-1.780	2.09
-1.955	2.31
-2.080	3.81
-2.257	6.27
-2.400	8.14
-2.558	10.87

Table A21: Equilibrium Interfacial Tension of $(C_{10}N)_2OH$ in Hexadecane/H_2O at 25°C

Log C_s (M)	γ_S (mN/m)
-3.000	6.36
-3.222	6.33
-3.398	8.50
-3.699	10.93
-3.301	6.38
-3.523	9.07
-4.000	13.46

Table A22: Equilibrium Interfacial Tension of $(C_{12}N)_2OH$ in Hexadecane/H_2O at 25°C

Log C_s (M)	γ_S (mN/m)
-4.000	3.36
-5.000	4.57
-4.398	3.40
-5.301	7.74
-5.194	6.57

Table A23: Equilibrium Interfacial Tension of $(C_{14}N)_2OH$ in Hexadecane/H_2O at 25°C

Log C_s (M)	γ_S (mN/m)
-5.222	2.65
-5.398	2.70
-5.699	5.34
-5.824	7.62
-5.523	2.66

Table A24: Equilibrium Interfacial Tension of $(C_{16}N)_2OH$ in Hexadecane/H_2O at 25°C

Log C_s (M)	γ_S (mN/m)
-4.955	16.19
-3.955	5.07
-3.478	4.55
-4.478	4.25
-4.654	7.42
-4.779	10.84

Table A25: Equilibrium Interfacial Tension of $C_8C_1C_8$ in Hexadecane/0.1 M NaCl at 25°C

Log C_s (M)	γ_s (mN/m)
-2.703	5.24
-3.004	5.20
-3.180	5.20
-3.418	5.92
-3.745	11.43
-4.025	13.12
-4.195	14.27

Table A26: Equilibrium Interfacial Tension of $C_{10}C_1C_{10}$ in Hexadecane/0.1 M NaCl at 25°C

Log C_s (M)	γ_s (mN/m)
-4.699	8.04
-4.860	8.10
-4.959	8.06
-5.270	11.64
-5.366	12.77

Table A27: Equilibrium Interfacial Tension of $C_{10}C_8C_{10}$ in Hexadecane/0.1 M NaCl at 25°C

Log C_s (M)	γ_s (mN/m)
-4.122	1.49
-4.298	1.52
-4.599	1.53
-4.775	1.49
-4.863	2.25
-5.025	4.01

Table A28: Equilibrium Interfacial Tension of $C_{12}EO_2$ in Hexadecane/H_2O at 25°C

Log C_s (M)	γ_s (mN/m)
-1.920	2.30
-2.137	2.77
-2.312	3.50
-2.438	6.27
-2.614	7.09
-2.738	9.19

Table A29: Equilibrium Interfacial Tension of $C_{12}EO_7$ in Hexadecane/0.1 M NaCl at 25°C

Log C_s (M)	γ_s (mN/m)
-3.207	2.16
-3.507	2.19
-3.684	2.16
-3.983	3.16
-4.052	3.88
-4.161	5.91
-4.248	6.17
-4.320	8.24

Table A30: Equilibrium Interfacial Tension of $C_{12}EO_8$ in Hexadecane/0.1 M NaCl at 25°C

Log C_s (M)	γ_s (mN/m)
-3.533	3.17
-3.710	3.35
-3.833	3.19
-4.010	3.96
-4.135	5.66
-4.312	8.60

Table A31: Equilibrium Interfacial Tension of $C_{16}EO_8$ in Hexadecane/H_2O at 25°C

Log C_s (M)	γ_s (mN/m)
-3.538	1.30
-3.839	1.50
-4.140	1.72
-4.578	6.32
-4.860	8.11
-5.150	10.90
-5.323	14.32

Table A32: Equilibrium Interfacial Tension of $C_{14}N(CH_3)_2O$ in Hexadecane/0.1 M NaCl at 25°C

Log C_s (M)	γ_s (mN/m)
-3.060	2.18
-3.237	2.19
-3.538	2.18
-3.839	2.18
-4.102	3.42
-4.383	8.42
-4.674	14.7

Table A33: Dynamic Interfacial Tension of $C_{10}OC_{10}$ at Cs = 2×10^{-5} M in Hexadecane/0.1 M NaCl at 25°C.

time (s)	log t	γ_t(mN/m)
673.2000	2.8280	7.7170
425.4000	2.6280	8.1270
230.3500	2.3620	8.8010
139.9000	2.1460	10.6930
89.2600	1.9510	17.0520
64.3100	1.8080	24.5720
42.2700	1.6260	32.2990
20.7300	1.3160	39.5900
11.1100	1.0460	42.4490
5.8770	0.7690	44.9100
4.0400	0.6060	46.3080
2.5070	0.3990	47.8940
1.8060	0.2570	48.3030
1.4070	0.1480	48.3830

Table A34: Dynamic Interfacial Tension of $C_{10}OC_{10}$ at Cs = 1×10^{-4} M in Hexadecane/0.1 M NaCl at 25°C.

time (s)	log t	γ_t(mN/m)
176.0700	2.2460	6.7270
93.5980	1.9710	7.1520
40.0170	1.6020	7.6450
22.8750	1.3590	8.7400
12.8840	1.1100	9.8460
7.8750	0.8960	15.0450
5.6770	0.7540	21.7140
3.8120	0.5810	29.1300
2.3070	0.3630	35.2590
1.6550	0.2190	37.9410
1.4480	0.1610	38.7280
1.1620	0.0652	39.8890

Table A35: Dynamic Interfacial Tension of $C_{10}OC_{10}$ at Cs = 1 x 10^{-3} M in Hexadecane/0.1 M NaCl at 25°C.

time (s)	log t	γ_t(mN/m)
62.2000	1.7940	4.7530
26.0760	1.4160	4.9820
14.5910	1.1640	5.5750
10.3340	1.0140	5.9230
8.0570	0.9060	6.1570
5.6670	0.7530	6.4960
4.4540	0.6490	6.8070
3.1780	0.5020	7.2860
2.5650	0.4090	7.8400
1.8910	0.2770	8.6700
1.3380	0.1260	10.2250
1.0540	0.0228	12.0810
0.9150	-0.0386	13.9840
0.8190	-0.0867	15.6460
0.7450	-0.1280	17.0790
0.6870	-0.1630	18.3740
0.6360	-0.1970	19.4400
0.5920	-0.2280	20.3570

Table A36: Dynamic Interfacial Tension of $(C_{12}N)_2(OH)_2$ at Cs = 8 x 10^{-5} M in Hexadecane/H_2O at 25°C.

time (s)	log t	γ_t(mN/m)
757.7800	2.8800	29.0000
501.6000	2.7000	28.7480
386.9800	2.5880	29.5720
229.8500	2.3610	30.7380
167.4100	2.2240	31.9780
111.3600	2.0470	31.9110
86.6540	1.9380	33.1090
57.5760	1.7600	32.9980
45.2940	1.6560	34.6120
35.6980	1.5526	34.0990
30.2120	1.4800	34.6300
19.2060	1.2830	36.6910
13.6310	1.1350	39.0610
10.9470	1.0390	41.8270
7.6080	0.8810	43.6030
5.8510	0.7670	44.7110
4.0320	0.6060	46.2170
2.5070	0.3990	47.8940
1.8075	0.2570	48.3430
1.5860	0.2000	48.4790
1.4090	0.1490	48.4520

Table A37: Dynamic Interfacial Tension of $(C_{12}N)_2(OH)_2$ at Cs = 2 x 10^{-5} M in Hexadecane/H_2O at 25°C.

time (s)	log t	γ_t(mN/m)
220.7500	2.3440	42.1730
113.5700	2.0550	43.3940
58.3350	1.7660	44.5780
23.8080	1.3770	45.4830
12.5370	1.0980	47.9020
6.4970	0.8130	49.6480
4.4170	0.6450	50.6300
2.7040	0.4320	51.6580
1.4990	0.1760	51.5470

Table A38: Dynamic Interfacial Tension of $(C_{12}N)_2(OH)_2$ at Cs = 3×10^{-4} M in Hexadecane/H_2O at 25°C.

time (s)	log t	γ_t(mN/m)
445.1800	2.6490	17.0100
224.4800	2.3510	17.1540
116.7700	2.0670	17.8460
24.8400	1.3950	18.9850
10.6600	1.0280	20.3650
5.5420	0.7437	21.1750
2.9120	0.4642	22.2530
2.0370	0.3090	23.3490
1.3200	0.1206	25.2170
1.5880	0.2009	24.2700
1.0270	0.0116	27.4680
0.8620	-0.0645	29.6420

Table A39: Dynamic Interfacial Tension of $(C_{12}N)_2(OH)_2$ at Cs = 1×10^{-3} M in Hexadecane/H_2O at 25°C.

time (s)	log t	γ_t(mN/m)
40.8900	1.6120	6.2500
8.6700	0.9380	6.6250
3.9730	0.5790	7.2460
2.0070	0.3030	7.6680
1.0840	0.0351	8.2840
0.7700	-0.1140	8.8260
0.5030	-0.2980	9.6090
0.3720	-0.4290	9.9490
0.2990	-0.5240	10.2820

Table A40: Dynamic Interfacial Tension of $(C_8N)_2(OH)_2$ at Cs = 3.0 x 10^{-4}M in Hexadecane/H_2O at 25°C.

time (s)	log t	γ_t(mN/m)
1121.1000	3.0500	42.8350
566.9700	2.7540	43.3260
288.7600	2.4610	44.1320
146.9000	2.1670	44.9020
98.4110	1.9930	45.1210
74.7460	1.8740	45.6950
59.9130	1.7780	45.7840
24.6840	1.3920	47.1570
12.5750	1.1000	48.0470
6.3930	0.8060	48.8530
3.2570	0.5130	49.7780
2.1710	0.3370	49.7700
1.6150	0.2080	49.3650

Table A41: Dynamic Interfacial Tension of $(C_{10}N)_2(OH)_2$ at Cs = 3.0 x 10^{-4}M in Hexadecane/H_2O at 25°C.

time (s)	log t	γ_t(mN/m)
2003.5000	3.3020	30.6200
1606.4000	3.2060	30.6890
1071.5000	3.0300	32.7520
595.4400	2.7750	34.1260
233.7600	2.3690	35.7260
189.2800	2.2770	36.1610
96.6810	1.9850	36.9400
49.0540	1.6910	37.4850
28.4100	1.4540	37.9920
20.0690	1.3030	38.3020
10.1330	1.0060	38.7160
6.8520	0.8360	39.2710
5.1640	0.7130	39.4620
3.4800	0.5420	39.8890
2.6250	0.4190	40.1190
2.1100	0.3240	40.3100
1.3210	0.1210	40.3790
1.1720	0.0689	40.3020

Table A42: Dynamic Interfacial Tension of $(C_{12}N)_2(OH)_2$ at Cs = 3.0 x 10^{-4}M in Hexadecane/H_2O at 25°C.

time (s)	log t	γ_t(mN/m)
445.1800	2.6490	17.0100
224.4800	2.3510	17.1540
116.7700	2.0670	17.8460
24.8400	1.3950	18.9850
10.6600	1.0280	20.3650
5.5420	0.7437	21.1750
2.9120	0.4642	22.2530
2.0370	0.3090	23.3490
1.3200	0.1206	25.2170
1.5880	0.2009	24.2700
1.0270	0.0116	27.4680
0.8620	-0.0645	29.6420

Table A43: Dynamic Interfacial Tension of $(C_{14}N)_2(OH)_2$ at Cs = 3.0 x 10^{-4}M in Hexadecane/H_2O at 25°C.

time (s)	log t	γ_t(mN/m)
316.5000	2.5000	6.0470
163.8900	2.2150	6.2620
116.0100	2.0650	6.6490
88.0740	1.9450	6.7300
78.2840	1.8940	6.6710
75.0060	1.8750	6.8780
73.1720	1.8640	6.9890
39.6300	1.5980	7.5710
22.7200	1.3650	8.6810
14.4770	1.1610	11.0630
9.6240	0.9830	14.7090
7.0510	0.8480	21.5530
5.8490	0.7670	26.8180
4.9540	0.6950	30.2850
4.3080	0.6340	32.9200
3.8270	0.5830	36.5560
3.4810	0.5420	39.9010
2.8430	0.4540	43.4510
2.0410	0.3100	46.7900
1.5500	0.1900	47.3780
1.4060	0.1480	48.3490

Appendix B

Time-Resolved Fluorescence Data

TABLE B1: $(C_{12}N)_2O$/Pyrene/H_20/25°C
Time-Resolved Fluorescence Data

DATA FILE	C_S X 10^3 (M)	C_{PY} X 10^6(M)	F_i	τ_i	<τ>	C_S/CMC	N±5
ssagg117	0.60	0.78	8 92	22.60 130.76	122	1.2	29
ttagg107	0.70	0.46	1 7 92	8.99 36.06 132.08	124	1.4	37
ssagg107	1.0	7.0	7 52 41	20.22 48.09 118.75	76	2.0	39
ttagg112	5.0	45	18 82	60.63 113.00	103	10	35

TABLE B2: $(C_{18}N)_2O$/Pyrene/H_2O/25°C
Time-Resolved Fluorescence Data

DATA FILE	C_S X 10^6(M)	C_{PY} X 10^6(M)	F_i	τ_i	$<\tau>$	C_S/CMC	N
ssagg132	1.0	0.067	2 98	24.87 129.59	127	0.34	2.6±0.2
ssagg137	5.0	0.36	10 90	37.64 127.02	118	1.7	2.8±0.4
ttagg137	10	0.50	23 77	37.01 122.59	103	3.4	6.5±1.0
ssagg142	25	0.47	17 83	43.80 112.65	101	8.6	14.5±1.5
ttagg142	100	0.78	8 92	53.16 114.06	109	34	18±3
ttagg012	1000	1.0	17 83	74.71 131.81	122	345	33±3
ttagg016	1000	1.0	16 84	72.79 132.05	123	345	33±3

TABLE B3: $(C_{20}N)_2O$/Pyrene/H_2O/25°C
Time-Resolved Fluorescence Data

DATA FILE	C_S X 10^6(M)	C_{PY} X 10^6(M)	F_i	τ_i	$\langle\tau\rangle$	C_S/CMC	N
ttagg098	0.80	0.063	3 97	47.13 133.48	131	0.32	2.8±0.2
ssagg082	2.0	0.14	1 99	11.04 128.75	127	0.80	1.7±0.2
ttagg077	4.0	0.10	4 96	9.49 127.71	123	1.6	2.7±0.1
ssagg102	8.0	0.31	3 97	31.84 129.30	127	3.2	1.9±0.2
ttagg082	10	0.36	5 95	34.60 130.68	126	4.0	2.2±0.5
ttagg031	10	1.0	9 91	27.25 128.33	119	4.0	2.5±0.5
ssagg092	25	1.2	10 90	23.80 126.52	116	10	4.2±0.2
ssagg087	100	4.4	2 11 87	9.71 44.03 183.61	165	40	5.9±0.3
ttagg087	250	13	7 20 72	11.72 41.16 176.48	137	100	9.1±0.2

TABLE B4: $(C_{12}N)_2OH$/Pyrene/0.1 M NaCl/50°C
Time-Resolved Fluorescence Data

DATA FILE	C_S X 10^3(M)	C_{PY} X 10^6(M)	F_i	τ_i	$\langle\tau\rangle$	C_S/CMC	N
ttmic472	0.048	0.96	2 37 61	25.83 151.88 100.71	118	2.1	7±2
ssmic472	0.096	1.9	5 18 77	21.38 61.13 132.54	114	4.2	13±2
ttmic522	0.96	17	6 25 69	18.72 43.45 140.79	110	42	27±2
ttagg147	1.5	0.67	3 97	51.23 147.33	145	65	33±10
ssagg147	3.0	0.52	2 98	50.12 136.73	135	130	43±14

TABLE B5: $(C_{14}N)_2OH$/Pyrene/0.1 M NaCl/50°C
Time-Resolved Fluorescence Data

DATA FILE	C_S X 10^6(M)	C_{PY} X 10^6(M)	F_i	τ_i	$\langle\tau\rangle$	C_S/CMC	N
ttagg157	2.0	0.10	2 98	26.65 110.65	109	0.25	2.7±0.5
ttmic452	3.5	0.32	2 98	40.43 111.23	110	0.44	2.0±0.5
ssmic452	35	0.32	1 30 69	18.40 82.62 129.08	114	4.4	33±3
ssmic532	98	1.0	16 84	51.93 108.71	100	12	36±5

TABLE B6: $(C_{16}N)_2OH$/Pyrene/0.1 M NaCl/50°C Time-Resolved Fluorescence Data

DATA FILE	C_S X 10^6(M)	C_{PY} X 10^6(M)	F_i	τ_i	$\langle\tau\rangle$	C_S/CMC	N
ssmic444	1.0	0.10	7 93	102.64 151.84	116	0.13	2.3±0.4
ssagg157	2.0	0.10	13 87	81.66 123.67	118	0.25	4.0±1.0
ttmic444	10	0.49	11 89	43.66 105.95	99	1.3	6.5±1.0
ssmic512	100	7.8	21 43 36	17.95 36.56 118.50	62	13	16±2
ssagg152	200	0.99	4 96	38.96 120.04	117	25	20±5
ttagg152	500	1.1	2 98	36.68 138.14	136	63	29±5

TABLE B7: $(C_nN)_2(OH)_2$/Pyrene/H_2O/25°C
Time-Resolved Fluorescence Data

DATA FILE	n	C_S X 10^3(M)	C_{PY} X 10^6(M)	F_i	τ_i	<τ>	C_S/CMC	N
ssmic102	12	1.0	1.7	14 86	46.06 124.84	114	1.4	34±3
ssmic052	14	0.30	0.52	8 92	57.63 139.66	134	3.5	54±5
jjagg122	16	0.015	0.31	4 96	33.94 131.11	128	0.83	2.0±0.4
ttagg127	16	0.021	0.24	9 91	33.63 121.23	113	1.2	8.0±1.0
ssmic432	16	0.030	0.50	5 95	55.54 137.97	134	1.7	10±1
ssmic421	16	0.030	0.50	11 89	21.79 134.45	133	1.7	10±1
ssagg122	16	0.090	0.71	10 90	50.50 127.90	120	4.5	24±3
uumic102	16	0.20	0.33	5 95	38.37 126.78	123	11	70±5

TABLE B8: $(C_{12}N)_2Ar$/Pyrene/0.1 M NaCl/50°C
Time-Resolved Fluorescence Data

DATA FILE	C_S X 10^3(M)	C_{PY} X 10^6(M)	F_i	τ_i	$\langle\tau\rangle$	C_S/CMC	N
ttmic482	0.10	2.1	13 87	34.27 119.02	108	2.5	9.0±1.0
ssmic482	1.0	2.1	5 95	52.88 137.44	134	25	23±2
ssmic522	1.0	1.5	19 81	38.63 135.31	117	25	22±2

TABLE B9: $(C_{14}N)_2Ar$/Pyrene/0.1 M NaCl/50°C
Time-Resolved Fluorescence Data

DATA FILE	C_S X 10^6(M)	C_{PY} X 10^6(M)	F_i	τ_i	$\langle\tau\rangle$	C_S/CMC	N
ssmic464	5.5	0.55	1 99	22.52 114.29	114	0.76	2.0±0.5
ttmic464	10	1.0	1 1 98	5.41 18.61 113.91	111	1.4	2.0±0.5
jjmic464	20	2.0	1 14 85	5.58 31.29 111.18	99	2.8	4.0±0.5
ttmic512	100	7.0	22 35 43	19.23 46.17 119.68	72	14	13±1

TABLE B10: $(C_{16}N)_2Ar$/Pyrene/0.1 M NaCl/50°C
Time-Resolved Fluorescence Data

DATA FILE	C_S X 10^6(M)	C_{PY} X 10^6(M)	F_i	τ_i	$\langle\tau\rangle$	C_S/CMC	N
ssmic439	3.2	0.32	2 98	48.70 120.01	119	0.60	2.0±0.5
ttmic439	13	0.32	16 84	62.57 117.85	109	2.4	10±2
ttmic435	50	0.80	21 79	54.11 117.22	104	9	20±5
ttmic532	100	2.0	27 73	55.41 124.10	106	19	21±3

TABLE B11: $(C_{18}N)_2Ar$/Pyrene/0.1 M NaCl/50°C
Time-Resolved Fluorescence Data

DATA FILE	C_S X 10^6(M)	C_{PY} X 10^6(M)	F_i	τ_i	$\langle\tau\rangle$	C_S/CMC	N
jjagg172	0.10	0.01	0.1 99.9	9.51 106.05	106	0.05	2.2±0.4
kkagg172	0.50	0.07	5 95	87.61 110.66	110	0.24	1.5±0.5
ssagg162	1.0	0.05	12 88	78.60 124.95	119	0.48	7.8±0.3
ssmic232	1.3	0.19	4 96	36.16 103.34	101	0.62	3.8±0.2
ttagg162	2.0	0.10	4 96	49.65 114.04	111	0.95	6.3±0.2
ssagg187	5.0	0.10	2 98	39.41 113.39	112	2.4	27±1
ttagg187	7.0	0.10	1 99	16.67 106.60	106	3.3	35±2
ssmic312	7.9	0.070	13 87	52.49 108.13	101	3.8	49±3
ssmic222	7.9	0.070	5 95	30.77 101.70	98	3.8	55±5
ssagg181	8.0	0.046	5 95	65.10 121.90	119	3.8	62±2

TABLE B11(continued): $(C_{18}N)_2Ar$/Pyrene/0.1 M NaCl/50°C
Time-Resolved Fluorescence Data

DATA FILE	C_S X 10^6(M)	C_{PY} X 10^6(M)	F_i	τ_i	$\langle\tau\rangle$	C_S/CMC	N
ssagg197	9.0	0.085	1 99	20.72 110.38	110	4.3	62±2
ttagg197	9.0	0.085	1 99	33.56 111.18	111	4.3	60±2
ssagg167	10	0.24	2 98	39.83 115.18	114	4.8	1.9±0.5
ttagg202	10	0.69	2 98	32.81 112.42	111	4.8	1.9±0.6
ssmic202	50	0.98	11 89	53.25 129.56	122	24	5.9±1.0
ssmic321	50	1.0	8 92	47.93 109.40	105	24	7.5±2.0
ttagg167	100	1.0	11 89	54.36 128.68	121	48	32±5
ssmic212	380	1.7	14 86	47.64 101.05	94	181	62±5
ssmic331	380	0.69	3 97	43.28 161.45	158	181	65±10

References

1. *World Book Encyclopedia Dictionary*, Doubleday, Chicago, 1963.
2. Traube, J., *Ann.*, **1891**, *265*, 27
3. Langmuir, I., *J. Am. Chem. Soc.*, **1917**, *39*, 1848.
4. Tanford, C., *Proc. Nat. Acad. Sci. U.S.A.*, **1979**, *76*.
5. McBain, J. W. and Martin, H. E., *J. Chem. Soc.*, **1914**, *105*, 957.
6. Clint, J. H., in *Surfactant Aggregation*, Chapman and Hall, New York, **1992**; p. 82.
7. Menger, F. M., *Accts. Chem. Res.*, **1979**, *12(4)*, 111.
8. McBain, J. W. and Hoffmann, O. A., *J. Phys. Colloid Chem.*, **1949**, *53*, 39.
9. McBain, J. W. and Harkins, W. D., *J. Chem. Phys.*, **1949**, *16*, 156.
10. Hartley, G. S., *Trans. Faraday Soc.*, **1935**, *31*, 31.
11. Hartley, G. S., *Q. Rev., Chem. Soc.*, **1948**, *2*, 152.
12. Abbott, A. D. and Tartar, H. V., *J. Phys. Chem.*, **1955**, *59*, 1195.
13. Schott, H., *J. Pharm. Sci.*, **1971**, *60*, 1594.
14. Tanford, C., *J. Phys. Chem.*, **1972**, *76*, 3020.
15. Debye, P. and Anacker, E. W., *J. Phys. Colloid Chem.*, **1951**, *55*, 644.
16. Kalyanasundaram, K. and Thomas, J. K., *J. Phys. Chem.*, **1976**, *80*, 1462.
17. Eastoe, J., Rogueda, P. *et al. Langmuir*, **1994**, *10*, 4429.
18. Israelachvili, J. et al. *J. Chem. Soc. Faraday Trans. 1*, **1976**,*72*,1525.
19. Rosen, M.J. *Chemtech* **1993**, *23*, 30.
20. Karabomi, S.; Esselink, K.; Hilbers, P.A.J.; Smit, B.; Karthauser, J.; VanOs, N.M.; Zana, R. *Science* **1994**, *266*, 254.

21. Zhu, Y-P; Masuyama, A.; Okahara, M.J. *J.Am.Oil Chem.Soc.* **1990**, *67*, 459.

22. Zhu, Y-P.; Masuyama, A.; Kobata, Y.; Nakatsuji, Y.; Okahara, M. Rosen, M.J. *J.Colloid Interface Sci.* **1993**, *158*, 40.

23. Bunton, C.A.; Robinson, J.; Schaak, J.; Stam, M.F. *J.Org.Chem.* **1971**, *36*, 2346.

24. Devinsky, F.; Lacko, I.; Mlynarcik, D.; Racansky, V.; Krasnec, L. *Tenside Deterg.* **1985**, *22*, 10.

25. Parreira, H.C.; Lukenbach, E.R.; Lindemann, M.K.O. *J.Am.Oil Chem.Soc.* **1979**, *56*, 1015.

26. Menger, F.M.; Littau, C.A. *J.Am.Chem.Soc.* **1993**, *115*, 10083.

27. Song, Li D.; Rosen, M.J. *Langmuir* **1996**, *12*, 1149.

28. Rosen, M.J.; Liu, Letian *J.Am.Oil Chem.Soc.* **1996**, *73*, 885.

29. Danino, D.; Talmon, Y. and Zana, R. *Langmuir* **1995**, *11*, 1448.

30. Zana, R. and Talmon, Y. *Nature* **1993**, *362*, 228.

31. Danino. D.; Kaplun, A. et al. In: Herb, C.A. and Prud'homme, R. K. (eds.) *Structure and flow in surfactant solutions*. ACS Symp. Ser. No. 578, American Chemical Society, Washington, D.C., **1994**.

32. Israelachvili, J.N. Physical principles of surfactant self-association into micelles, vesicles and microemulsion droplets, in *Surfactants in Solution*; Mittall and Bothorel (eds.), Plenum; New York, Vol.4, **1986**, p3.

33. Rosen, M.J.; Zhu, Z; Gao, T. *.J. Colloid Interface Sci.* **1993**, *157*, 224.

34. Rosen, M.J.; Gao, T.; Nakatsuji, Y.; Masuyama, A. *Colloids Surf. A Physicochem. Eng. Asp.* **1994**, *88*, 1.

35. Liu, L. and Rosen, M.J. *J. Colloid Interface Sci.* **1996**, *179*, 454.

36. Rosen, M.J.; Zhu, Z.; Hua, X.Y. *J. Am. Oil Chemists Soc.* **1992**, *69*, 30.

37. Gibbs, J.W. *The Collected Works of J.W. Gibbs*; Longmans, Green: London, 1928; vol.1, p.119.

38. Rosen, M.J. in *Surfactants and Interfacial Phenomena*; 2nd ed.; Wiley-Interscience: New York, **1989**; p.68.

39. Ananthapadmanabhan, K.P.; Goddard, E.D.; Turro, N.J.; Kuo, P.L. *Langmuir* **1985**, *1*, 352.

40. Frindi, M.; Michels, B.; Levy, H.; Zana, R. *Langmuir* **1994**, *10*, 1140.

41. Kalyanasundaram, K.; Thomas, J.K. *J.Phys.Chem.* **1977**, *81*, 2176.

42. Turro, N.J.; Okubo, T. *J.Phys.Chem.* **1982**, *86*, 159.

43. Rosen, M.J.; Murphy, D.S. *Langmuir* **1991**, *7*, 2630.

44. Murphy, D.S.; Rosen, M.J. *J.Phys.Chem.* **1988**, *92*, 2870.

45. Gao, T. and Rosen, M.J. *J. Am. Oil Chem. Soc.* **1994**, *71*, 771.

46. Gao, T. and Rosen, M.J. *J. Colloid Interface Sci.*, **1995**, *172*, 242.

47. Rosen, M.J. and Song, Li D. *J. Colloid Interface Sci.*, **1996**, *179*, 261.

48. Hua, X. Y. and Rosen, M.J. *J.Colloid Interface Sci.* **1988**, *124(2)*, 652.

49. Rosen, M.J. and Hua, X.Y. *J.Colloid Interface Sci.* **1990**, *139(2)*, 397.

50. Hua, X. Y. and Rosen, M.J. *J.Colloid Interface Sci.* **1991**, *141(1)*, 180.

51. Boucher, E.A.; Grinchuk, T.M.; Zettlemoyer, A.L. *J.Colloid Interface Sci.* **1967**, *23*, 600.

52. Cordes, E.H. in *Reaction Kinetics in Micelles*; Plenum Press: New York, **1973**; p.127.

53. Allen, M.; Evans, D.F.; Mitchell. D.J.; Ninham, B.W. *J. Phys. Chem.* **1987**, *91*, 2320.

54. Huisman, H.F. *Proc. Kon. Ned. Akad. Wetensch.* **1964**, *B-67*, 367, 376, 388, 407.

55. Rohde, A. and Sackmann, E. *J. Coll. Interface Sci.* **1979**, *70*, 494.

56. Chevalier, Y. and Zemb, T. *Rep. Prog. Phys.* **1990**, *53*, 279.

57. Hattori, N.; Hirata, H.; Okabayashi, H.; O'Connor, C.. *Colloid Polym. Sci.* **1999**, *277*, 361.

58. Doughty, D.A. *J. Phys. Chem.* **1979**, *83*, 2621.

59. Turro, N.J. and Yekta, A. *J. Amer. Chem. Soc.*, **1978**, *100*, 5951.

60. Infelta, P. *Chem. Phys. Letters* **1979**, *61(1)*, 88.

61. Kalyansundaram, K. in *Microheterogeneous Systems*; Academic Press: Orlando, FL; **1987.**

62. Almgren, M. and Lofroth, J.E. *J. Coll. Interface Sci.* **1981**, *81*, 486.

63. Almgren, M. *Adv. Coll. Interface Sci.* **1992**, *41*, 9.

64. Maestri, M.; Infelta, P.; Gratzel, M. *J. Chem. Phys.* **1978**, *69*, 1522.

65. Atik, S. and Thomas, J.K. *Chem. Phys. Lett.* **1981**, *79*, 351.

66. Malliaris, A.; Lang, J.; Zana, R. *J. Phys. Chem.* **1986**, *90*, 655.

67. Almgren, M. and Lofroth, J.E. *J. Chem. Phys.* **1982**, *76*, 2734.

68. Warr, G.G. and Grieser, F. *J. Chem. Soc., (Faraday Trans. I)*, **1986**, *82*, 1813.

69. Rosen, M.J. *J. Colloid Interface Sci.* **1976**, *56*, 320.

70. Rosen, M.J. *J. Am. Chem. Soc.* **1974**, *51*, 461.

71. Rosen, M.J. and Aronsen, S. *Colloids Surf.* **1981**, *3*, 201.

72. Klevens, H.B. *J. Am. Oil Chem. Soc.* **1953**, *30*,74.

73. Joos, P. and Rillaerts, E. *J. Coll. Interface Sci.* **1981**, *79*, 96.

74. Pierson, F.W. and Whitaker, S. *J. Coll. Interface Sci.* **1976**, *54(2)*, 203.

75. Lakowicz, J.R. in *Principles of Fluorescence Spectroscopy*; Plenum: New York, **1983**; p.1.

76. Hartley, G.S. *Trans. Faraday Soc.*, **1934**, *30*, 444.

77. Shinitzky, A.C.; Dianoux, C.; Gitler, C.; Weber, G. *Biochemistry*, **1971**, *10*, 2106.

78. Hautala, R.; Schore, N.; Turro, N.J. *J. Am. Chem. Soc.*, **1973**, *95*, 5508.

79. Infelta, P.; Gratzel, M.; Thomas, J.K. *J. Phys. Chem.*, **1974**, *78*, 190.

80. Zana, R. in *Surfactant Solutions: New Methods of Investigation*; Marcel Dekker: New York, **1987**, p.241.

81. Lakowicz, J.R. in *Principles of Fluorescence Spectroscopy*; Plenum: New York, **1983**; p.44.

82. Vonnegut, B. *Rev. Sci. Inst.* **1942**, *13*, 6.

83. Gratzel, M.; Kalyansundaam, K.; Thomas, J.K. *J. Am. Chem. Soc.* **1974**, *96*, 7869.

84. Erikkson, J.C. and Gilberg, G. *Acta. Chem. Scand.* **1966**, *20*, 2019.

85. Kalyansundaam, K.; Thomas, J.K. *J. Am. Chem. Soc.* **1977**, *99(7)*, 2039.

86. Lakowicz, J.R. in *Principles of Fluorescence Spectroscopy*; Plenum: New York, **1983**; p.58.

87. Marquardt, D.W. *J. Soc. Ind. Appl. Math.* **1963**, *II(2)*, 431.

88. Lakowicz, J.R. in *Principles of Fluorescence Spectroscopy*; Plenum: New York, **1983**; p.68.

89. Tachiya, M. *Chem. Phys. Lett.* **1975**, *33(2)*, 289.

90. Atik, S.; Nam, M.; Singer, L. *Chem Phys. Lett* **1979**, *67(1)*, 75.

91. Lianos, P. and Zana, R. *J. Phys. Chem.* **1980**, *84*, 3339.

92. Rosen, M.J. in *Surfactants and Interfacial Phenomena*; 2nd ed.; Wiley-Interscience: New York, **1989**; p.120.

93. Rosen, M.J. in *Surfactants and Interfacial Phenomena*; 2nd ed.; Wiley-Interscience: New York, **1989**; pp 87, 135..

94. Zhu, Y-P; Masuyama, A.; Kiroto, Y.; Okahara, M.; Rosen, M.J. *J. Am. Oil Chem. Soc.* **1992**, *69*, 626.

95. Zana, R. in *Novel Surfactants*; ed. Krister Holmberg; M. Dekker: New York **1998**; p.250.

96. Venable, R.L.; Nauman, R.V. *J. Phys. Chem.* **1964**, *68*, 3498.

97. Van Os, N.M.; Haak, J.R.; Rupert, L.A.M. in *Physical Chemical Properties of Selected Anionic, Cationic and Nonionic Surfactants*; Elsevier, **1993**.

98. Devinsky, F.; Lacko, I.; Bitterova, F.; Tomeckova, L. *J. Coll. Interface Sci.* **1986**, *114*, 314.

99. Nagarajan, R. in *Structure-Performance Relationships in Surfactants*; eds. K. Esumi; M. Ueno; M. Dekker: New York; **1997**; p.39.

100. Kim, T-S; Kida, T.; Nakatsuji, Y.; Hirao, T.; Ikeda, I. *J. Am. Oil Chem. Soc.* **1996**, *73*, 907.

101. Rosen, M.J. in *Surfactants and Interfacial Phenomena*; 2nd ed.; Wiley-Interscience: New York, **1989**; p.10.

102. Shinoda, K. *J. Phys. Chem.* **1955**, *59*, 432.

103. Zhu, Y-P; Masuyama, A.; Okahara, M.J. *J.Am.Oil Chem.Soc.* **1991**, *68*, 268.

104. Song, L.D. PhD Thesis; CUNY, **1996.**

105. Dahanayake, M.; Cohen, A.W.; Rosen, M.J. *J. Phys. Chem.* **1986**, *90*, 2413.

106. Rosen, M.J.; Zhu, Z.H.; Gu, B.; Murphy, D.S. *Langmuir*, **1988**, *4*, 1273.

107. Rosen, M.J.; Cohen, A. W.; Dahanayake, M.; Hua, X.Y. *J. Phys. Chem.* **1982**, *86*, 541.

108. Elworthy, P.H.; MacFarlane, C.B. *J. Pharm. Pharmacol. Suppl.* **1962**, *14*, 100.

109. Malliaris, A.; Le Moigne, J.; Sturm, J.; Zana, R. *J. Phys. Chem.* **1985**, *89*, 2709.